1-1-2000

The geology and geochemistry of volcanic rocks in the Lava Mountains, California: Implications for Miocene development of the Garlock Fault

Deborah L Keenan
University of Nevada, Las Vegas

INFORMATION TO USERS

This manuscript has been reproduced from the microfilm master. UMI films the text directly from the original or copy submitted. Thus, some thesis and dissertation copies are in typewriter face, while others may be from any type of computer printer.

The quality of this reproduction is dependent upon the quality of the copy submitted. Broken or indistinct print, colored or poor quality illustrations and photographs, print bleedthrough, substandard margins, and improper alignment can adversely affect reproduction.

In the unlikely event that the author did not send UMI a complete manuscript and there are missing pages, these will be noted. Also, if unauthorized copyright material had to be removed, a note will indicate the deletion.

Oversize materials (e.g., maps, drawings, charts) are reproduced by sectioning the original, beginning at the upper left-hand corner and continuing from left to right in equal sections with small overlaps.

Photographs included in the original manuscript have been reproduced xerographically in this copy. Higher quality 6" x 9" black and white photographic prints are available for any photographs or illustrations appearing in this copy for an additional charge. Contact UMI directly to order.

ProQuest Information and Learning
300 North Zeeb Road, Ann Arbor, MI 48106-1346 USA
800-521-0600

THE GEOLOGY AND GEOCHEMISTRY OF VOLCANIC ROCKS IN THE LAVA MOUNTAINS, CALIFORNIA: IMPLICATIONS FOR MIOCENE DEVELOPMENT OF THE GARLOCK FAULT

by

Deborah L. Keenan

Bachelor of Science
Old Dominion University
1996

A thesis submitted in partial fulfillment
of the requirement for the

Master of Science Degree
Department of Geoscience
College of Sciences

Graduate College
University of Nevada, Las Vegas
December 2000

UNLV

Thesis Approval

The Graduate College
University of Nevada, Las Vegas

November 5, 20 00

The Thesis prepared by

Deborah L. Keenan

Entitled

The Geology and Geochemistry of Volcanic Rocks in the Lava Mountains, California: Implications for Miocene Development of the Garlock Fault

is approved in partial fulfillment of the requirements for the degree of

Master of Science in Geology

Examination Committee Chair

Dean of the Graduate College

Examination Committee Member

Examination Committee Member

Graduate College Faculty Representative

PR/1017-53/1-00

ABSTRACT

The Geology and Geochemistry of Volcanic Rocks in the Lava Mountains, California: Implications for Miocene Development of the Garlock Fault

by

Deborah L. Keenan

Dr. Eugene I. Smith, Examination Committee Chair
Professor of Geology
University of Nevada, Las Vegas

The Lava Mountains are located in the Mojave Desert, southern California along the Garlock Fault, a major continental strike-slip fault that separates the southwestern Basin and Range to the north from the Mojave block to the south. Chemical similar dacitic lava and pyroclastic flows erupted from the 9-km diameter Western Lava Mountains volcano. Dacites with limited chemical variability reflect interaction of mantle derived basalt with both metabasalt and graywacke of the Mesozoic Rand Schist and Cretaceous "Atolia-type" granitoids. Geophysical data suggests a low angle contact between these lithologies at a depth of about 20 km. This boundary may have served as a density barrier to rising magma. Magma trapped at this barrier could not ascend until it evolved by fractional crystallization and assimilation to a density less than that of the host rock. This density was achieved as soon as SiO_2 evolved to values greater than about 63 wt. %; the resulting magma corresponds to the composition of Lava Mountains dacite. Both geochemistry and stratigraphy were used to develop correlations of volcanic units across the Garlock Fault between the Lava Mountains to the south and the El Paso

Mountains to the north of the fault. This work demonstrated a total of 32-40 km movement of the fault since 10.3 Ma, which indicates a displacement rate of 3.1-3.8 mm/yr.

TABLE OF CONTENTS

LIST OF FIGURES

ACKNOWLEDGMENTS

I thank my committee composed of Gene Smith (committee chair), Terry Spell and Michael Wells from the Department of Geoscience and Steven Lepp, the Graduate College representative from the Department of Physics for their help. I thank Wanda Taylor for her help and support. This project was funded by the U.S. Navy's Geothermal Project Office. I especially thank Frank Monastero for his interest and support. Also, special thanks to Alex Sánchez for sharing his observations and data on the geology and geochemistry of the Lava Mountains.

CHAPTER 1

INTRODUCTION

This thesis is based on research and field work in and about the Lava Mountains, located in the Mojave Desert, southern California (Fig. 1). Volcanism in the Lava Mountains began at about 11.7 Ma and ended at 6.4 Ma. The Lava Mountains lie along and to the south of the Garlock Fault, a major northeast striking, left lateral strike-slip fault with about 64 km of sinistral displacement and some localized dip-slip movement (Smith, 1962; Smith and Ketner, 1970; Davis and Burchfiel, 1973; Dibblee, 1995; Monastero et al., 1997). The Garlock Fault, extending 250 km from the San Andreas Fault to the Avawatz Mountains south of Death Valley, separates the southwestern Basins and Range to the north from the Mojave block to the south. Other areas sampled for geochemical and geochronological studies are in the Summit Hills to the northwest of the Lava Mountains and in the El Paso Mountains 20 km west of the Lava Mountains to the north of the Garlock Fault.

The Lava Mountains volcanic field is unique in the Mojave Desert area because it is the only area along the Garlock Fault where volcanism and strike-slip faulting were coeval. This study, therefore, provides the opportunity to characterize the style of volcanism and petrogenesis of a volcanic section produced during a period of strike-slip faulting. Additionally, the close proximity of volcanic centers in the Lava Mountains to the Garlock Fault and the potential for locating units that were transported across the fault

provide the opportunity to more fully understand the development of the Garlock Fault during Tertiary time. Units coeval and geochemically identical to those in the Lava Mountains occur north of the Garlock Fault in the El Paso Mountains in the Miocene Dove Spring Formation (Loomis and Burbank, 1988). Furthermore, lithologies characteristic of the El Paso Mountains occur as conglomerate clasts in the eastern Lava Mountains (Carter, 1982, 1987, 1994). Specifically, the important problems addressed by this thesis are: (1) the identification of volcanic vents in the western Lava Mountains, (2) the origin of compositionally similar dacitic lavas and pyroclastic rocks, and (3) the Miocene displacement history of the Garlock Fault. Addressing these problems involved detailed mapping at a scale of 1:12,000 of 40 km^2 in the western Lava Mountains, substantially revising the stratigraphy of the Lava Mountains volcanic section and completing geochemical analysis of 71 samples in the Lava and El Paso Mountains. Six new $^{40}Ar/^{39}Ar$ dates were also completed to support this study.

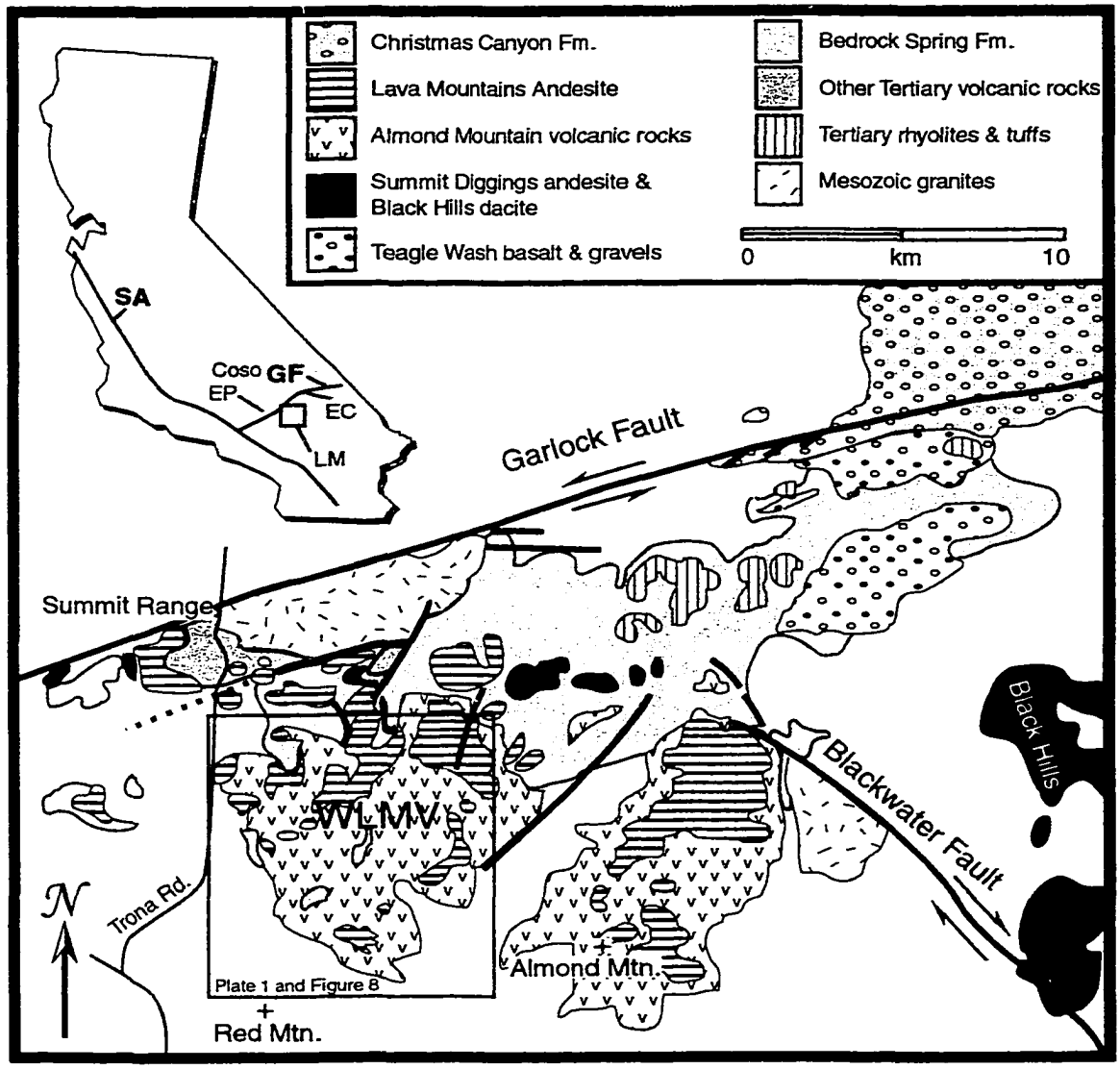

Figure 1. Index map of the Lava Mountains showing the location of the Western Lava Mountains volcano (WLMV). Box indicates approximate area covered by Plate 1 and Figure 8. Inset map shows the Lava Mountains (LM), Eagle Crags volcanic field (EC), El Paso Mountains (EP), Garlock Fault (GF), San Andreas Fault (SA) and the Coso Range.

CHAPTER 2

STRATIGRAPHY

Lava Mountains

Volcanic rocks in the Lava Mountains lie on a basement composed of the Rand Schist. Outcrops of the schist border the Lava Mountains to the southwest. Composed mainly of metamorphosed and deformed graywacke, basalt, chert, limestone and ultramafic rock (for example, Jacobson, 1990), the Rand Schist is of Mesozoic age, probably Cretaceous; 72 Ma, by $^{40}Ar/^{39}Ar$ (Jacobson, 1990). Intruding Rand Schist are Cretaceous (70 Ma) quartz monzonite to granodiorite plutons mapped as Atolia Quartz Monzonite by Smith (1964). More detailed descriptions of these basement lithologies are presented in Chapter 4. Atolia quartz monzonite to granodiorite (70 Ma) comprise much of the Mesozoic granitoids in the vicinity of the Lava Mountains (Smith, 1964).

Smith (1964) developed a detailed stratigraphy of the Lava Mountains based on reconnaissance mapping. The units were given ages varying from Pre-Middle Pliocene to Quaternary based on paleontological and stratigraphic observations. Revision of this stratigraphy was required based on new evidence from field observations, geochemistry and geochronology. From this evidence I determined that volcanic activity in the Lava Mountains occurred in three episodes spanning roughly 5 Ma in the mid- to late-Miocene (Fig. 2).

Episode 1

Units mapped by Smith (1964) as volcanic units older than the Bedrock Spring Formation represent the first episode of volcanism. Ranging in age from 10.7 to 11.7 Ma, these units are lithologically diverse and include (1) dacite (11.7 ± 0.2 Ma sanidine $^{40}Ar/^{39}Ar$ date (all dates are ± 2σ); Table 1) with large phenocrysts (2 cm) of plagioclase herein named the Summit Range dacite, (2) dacite containing quartz, hornblende, biotite and plagioclase dated at 10.73 ± 0.1 Ma (biotite $^{40}Ar/^{39}Ar$; Table 1), and (3) volcaniclastic rocks. A vent area for dacite is marked by a volcanic dome in the Summit Range (Fig. 3). Also included in episode 1 are pyroclastic flows mapped by Smith (1964) in the northeastern part of the Lava Mountains as "other upper Pliocene (?) volcanics (Tt)." The age of this unit is unclear. Smith (1964) indicated that it may overlie the Bedrock Springs Formation, but field relations are obscure. Geochemical similarities between these pyroclastic units and tuffs of member two of the Dove Spring Formation (11.8 to 15.1 Ma; Loomis and Burbank, 1988) support their assignment to episode one. These pyroclastic units either erupted from nearby domes of felsite (mapped as Tf by Smith, 1964) or from an unidentified source to the south of the Lava Mountains.

Episode 2

Rocks of the second episode (10.4 to 9.54 Ma) are volumetrically the most important and are separated from volcanic rocks of the first episode by the sandstones of the Bedrock Spring Formation (Fig. 2). The following units were produced during the second episode: (1) volcanic rocks in the uppermost part of the Bedrock Springs Formation, (2) "Quaternary" andesite (Smith, 1964) herein named the Summit Diggings

andesite, (3) the Almond Mountain volcanic section, and (4) the "Quaternary" basalt (Smith, 1964) herein named the Teagle Wash Basalt.

The Almond Mountain volcanic section erupted from the 9-km diameter western Lava Mountains volcano. This volcanic center was originally recognized by Smith (1964) and briefly described by Carter (1994), but detailed mapping, volcanology and geochemistry were accomplished as a part of this study (Chapter 3). Placing the Summit Diggings andesite, the Teagle Wash basalt and volcanic rocks of the Bedrock Springs Formation into the same time frame as the Almond Mountain volcanic section represents a major revision of Smith's (1964) stratigraphy (Fig. 2). Detailed justification for assigning these units to the second episode of volcanism follows. Smith (1964, p.44) based the Quaternary age of the Summit Diggings andesite on one contact where "...andesite rests on the upper part of a surface that was elsewhere covered by older gravels of early Quaternary age." A new $^{40}Ar/^{39}Ar$ date of 10.34 ± 0.69 Ma (Table 1) questions the field interpretation and places the Summit Diggings andesite stratigraphically below the Almond Mountain volcanic section. Field observation also supports this age assignment. A dome and several flows of the Summit Diggings andesite intrude and overlie the Bedrock Springs Formation. Resting on the flows are the lapilli tuff and breccia of the Almond Mountain volcanic section and flows of the Lava Mountains Andesite (Fig. 2).

Assignment of the Teagle Wash basalt to this episode is mainly based on field relationships. Smith (1964) assigned a Quaternary age to the basalt because he mapped it lying on and intruding the conglomerate facies of the Quaternary Christmas Canyon Formation. I do not question the age assignment of the Christmas Canyon Formation,

which appears to be firmly based on fossil evidence and a 620 ka K/Ar date from an interbedded tuff (Izett and Wilcox, 1982). Rather, I question the assignment of the conglomerate beneath the basalt to this formation. The conglomerate described by Carter (1982, 1987 and 1994) contains clasts of spotted Mesquite Schist, carbonate clasts of the Paleocene Goler Formation, weakly lineated hornblende quartz diorite and vesicular basalt that is chemically identical to basalt flows in member 4 of the Dove Springs Formation (Fig. 4). These clasts could only have been derived from the El Paso Mountains north of the Garlock Fault (Carter 1982, 1987 and 1994). The conglomerate probably represents part of a fanglomerate sheet that extended from drainages in the El Paso Mountains south into the Lava Mountains. It was then was cut and displaced by movement along the Garlock Fault (Carter, 1982). If it is assumed that the conglomerate belongs to the Christmas Canyon Formation and is Quaternary in age, as mapped by Smith (1964), at least 30 km of displacement must have occurred along the Garlock Fault in approximately 620 ka. This results in displacement rates as high as 5 cm/year; a value that is one-order of magnitude higher than the estimated average long-term slip rate of 7 mm/year (Carter, 1987, 1994). Therefore, the conglomerate and overlying basalt are interpreted here to be Tertiary in age. This agrees with Carter's (1982) statement that these conglomerates "appear to overlie beds of the Bedrock Springs Formation, and may represent slide blocks which slid across the fault from a high-standing area to the north during accumulation of the Bedrock Springs Formation...." This age assignment is strengthened by the geochemical correlation of 11.6 to 10.4 Ma basalt in the Dove Springs Formation with both the basalt boulders in the conglomerate and the Teagle Wash Basalt (Chapter 5).

Summary

In summary, volcanism of the Lava Mountains occurred in three episodes. The first episode is separated from the second by the Bedrock Springs Formation and about 500 ka of time. The period between episode two and three is no longer than 3 Ma. The period of quiescence may be shorter, considering that the younger date for the Almond Mountain volcanic section is from a bomb in the upper-middle part of the section.

El Paso Mountains

Basement rocks of the El Paso Mountains are the Paleozoic Garlock series, which include argillite, chert, hornfels and carbonates, and the Mesquite Schist which is probably of Precambrian age (Dibblee, 1952). Above the Garlock series lies the Goler Formation, a Middle Paleocene conglomerate, sandstone and mudrock assemblage (Loomis and Burbank, 1988). An angular unconformity forms the contact between the Goler Formation and the Ricardo Group (Loomis and Burbank, 1988).

Loomis and Burbank (1988) defined the Ricardo Group and separated it into the upper (Dove Spring Formation) and lower (Cudahy Camp Formation) formations (Fig. 7). New $^{40}Ar/^{39}Ar$ dates for the El Paso Mountains (Cudahy Camp Formation, member 5) (Monastero et al., 1997) range from 7.2 Ma in andesites in the upper part of the section to 17.9 Ma on basalts in the lower part. An angular unconformity forms the contact between the two formations (Loomis and Burbank, 1988). The Dove Spring Formation is further divided into six members. Member five includes a tuff that was dated at 10.4 Ma by the apatite fission track technique (Loomis and Burbank, 1988).

Monastero and Sabin (1997) correlated units of the lower part of the Ricardo

Group, (Cudahy Camp Formation) lithologically and temporally, to a volcanic section in the Eagle Crags Volcanic Field. Loomis and Burbank (1988) demonstrated with paleocurrent indicators that the source area for the Cudahy Camp Formation was probably to the southeast (where the Eagle Crags Volcanic Field was originally located with respect to the El Paso Mountains). Monastero and Sabin (1997) used this information along with their own data to correlate andesite and basaltic andesite flows (17.1-18.2 Ma) and tuff and tuff breccia (18.3 Ma) in the Eagle Crags field to andesite and basaltic andesite flows (15.1 to 17.9 Ma) and tuff and tuff breccia (18.5 Ma) of the Cudahy Camp Formation.

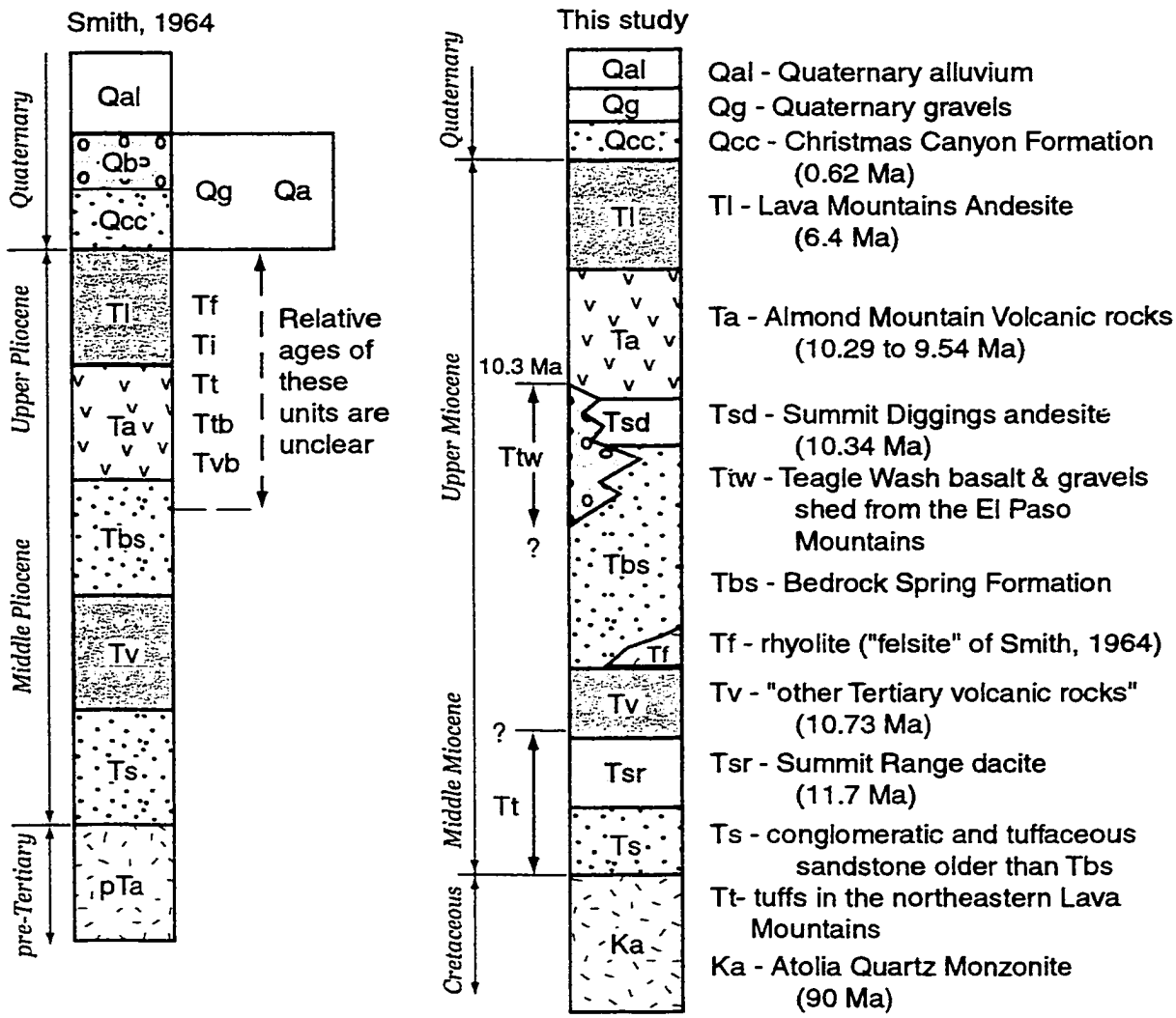

Figure 2. Stratigraphy of volcanic and sedimentary units in the Lava Mountains. The revised stratigraphy used in this thesis is compared to the stratigraphy of Smith (1964). Note that Qb of Smith (1964) was renamed Ttw in this thesis. Also, Qa of Smith (1964) was renamed Tsd. All dates are from this study.

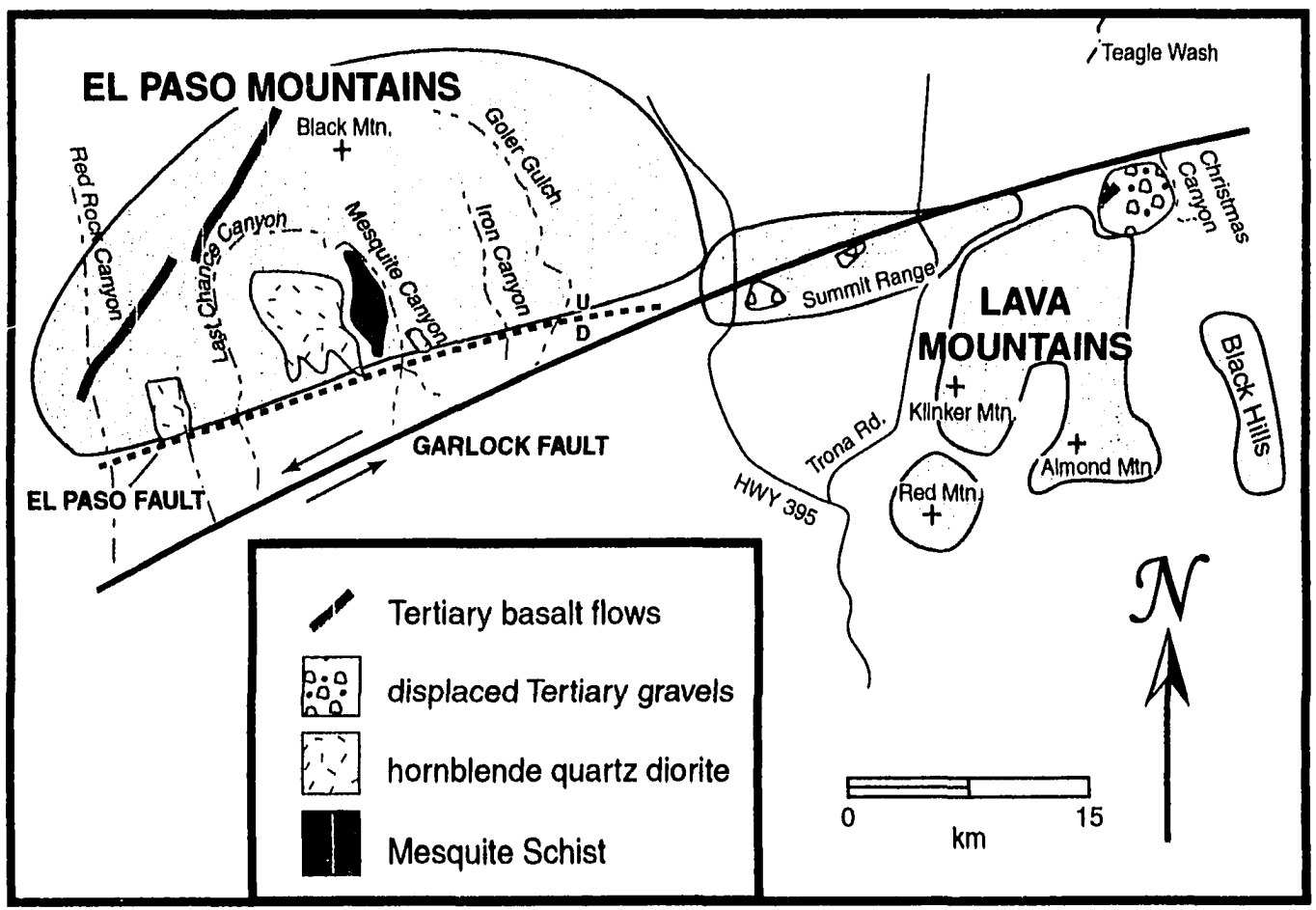

Figure 3. Location of the Lava Mountains, Summit Range and El Paso Mountains with respect to the Garlock Fault.

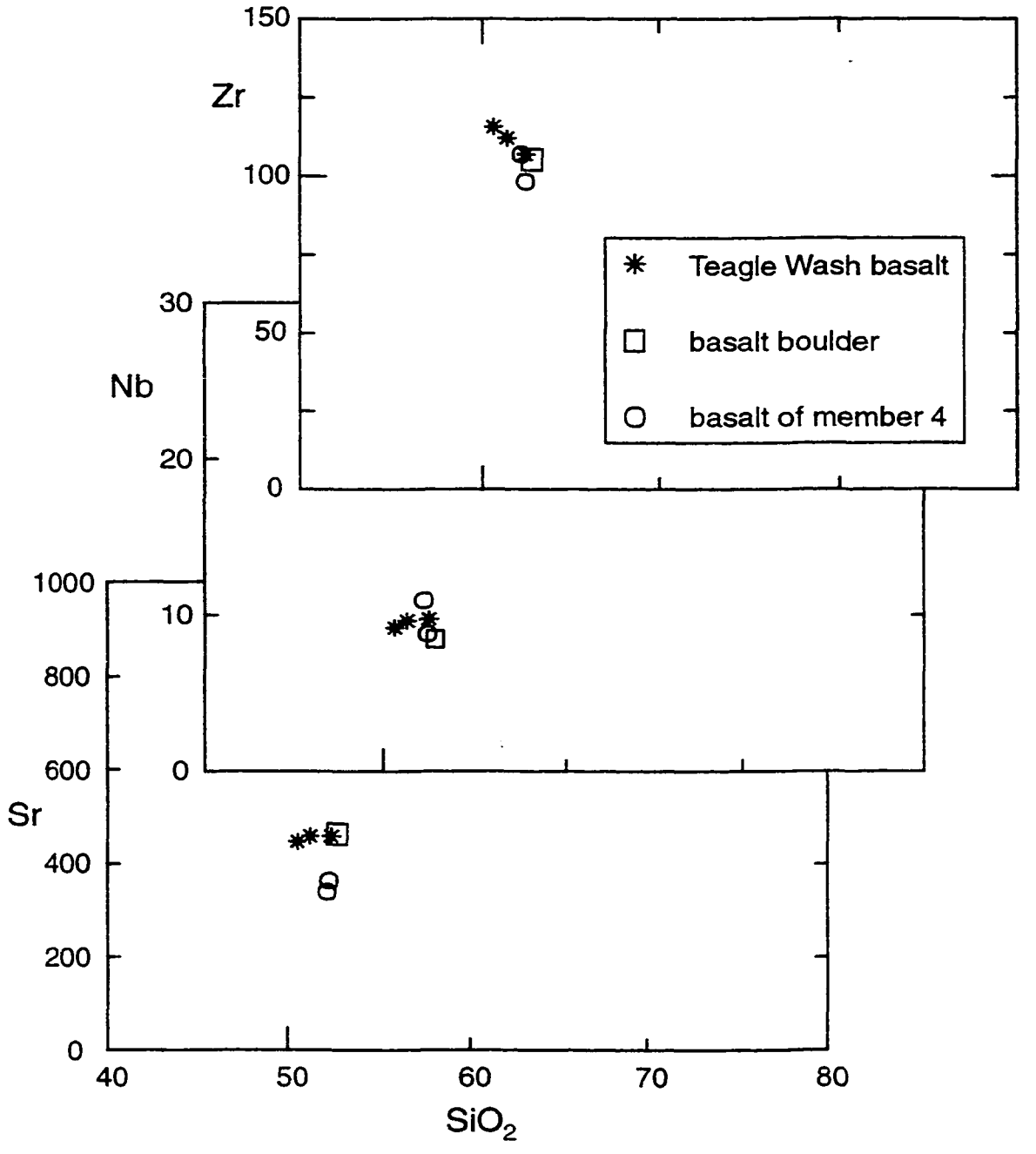

Figure 4. Chemical comparison of Teagle Wash basalt, basalt boulders and basalt of Member 4 of the Dove Spring Formation. Sr, Nb and Zr concentrations in ppm. SiO_2 concentration in weight percent.

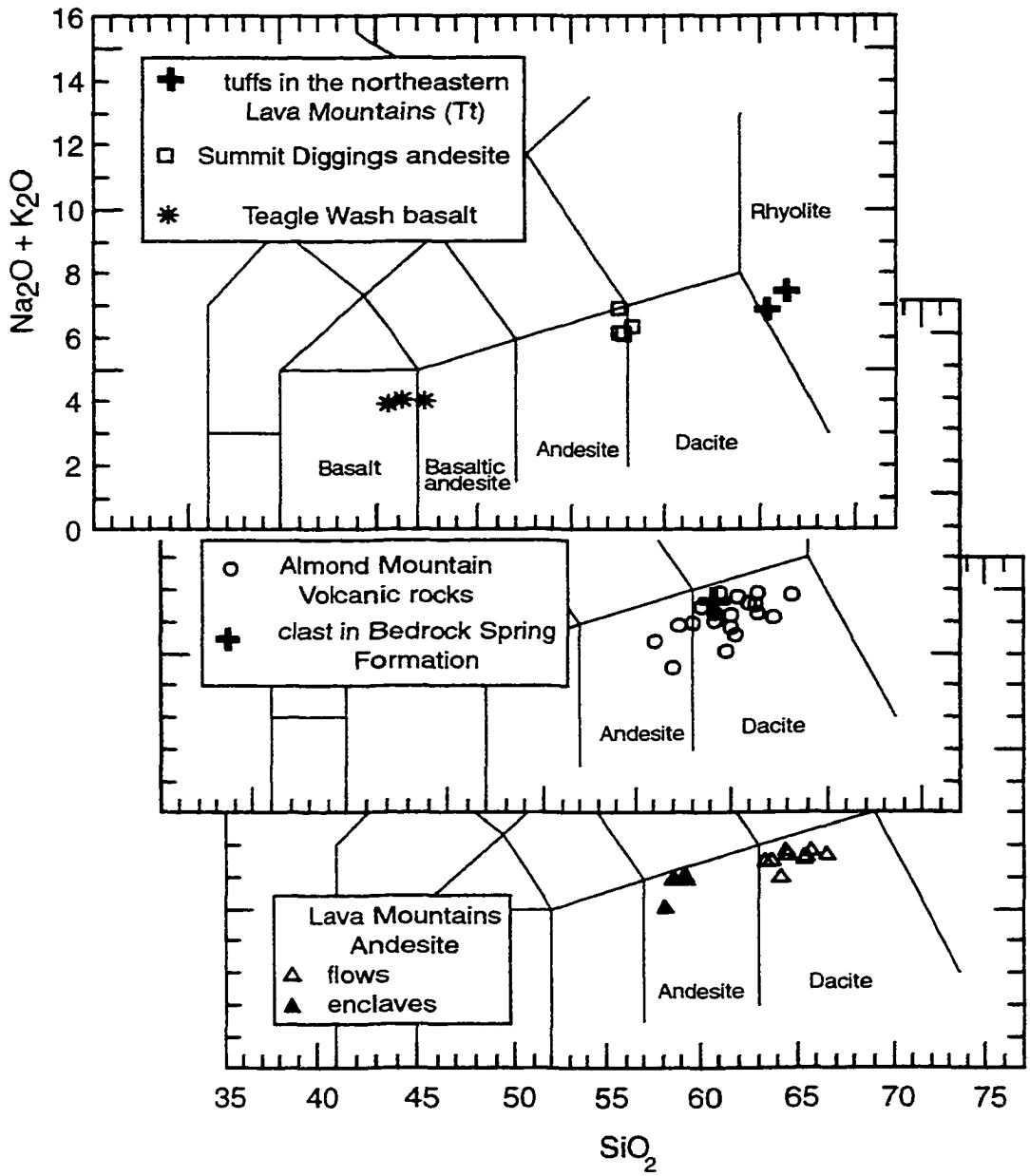

Figure 5. Total alkalis vs. SiO_2 rock classification diagrams (Le Bas et al., 1986) showing simliar composition for main group rocks (Almond Mountain volcanic section, Lava Mountains andesite and the Summit Diggings andesite) and other volcanic units in the Lava Mountains. Dacite clast in the Bedrock Spring Formation is shown by a filled cross. Concentrations in weight percent.

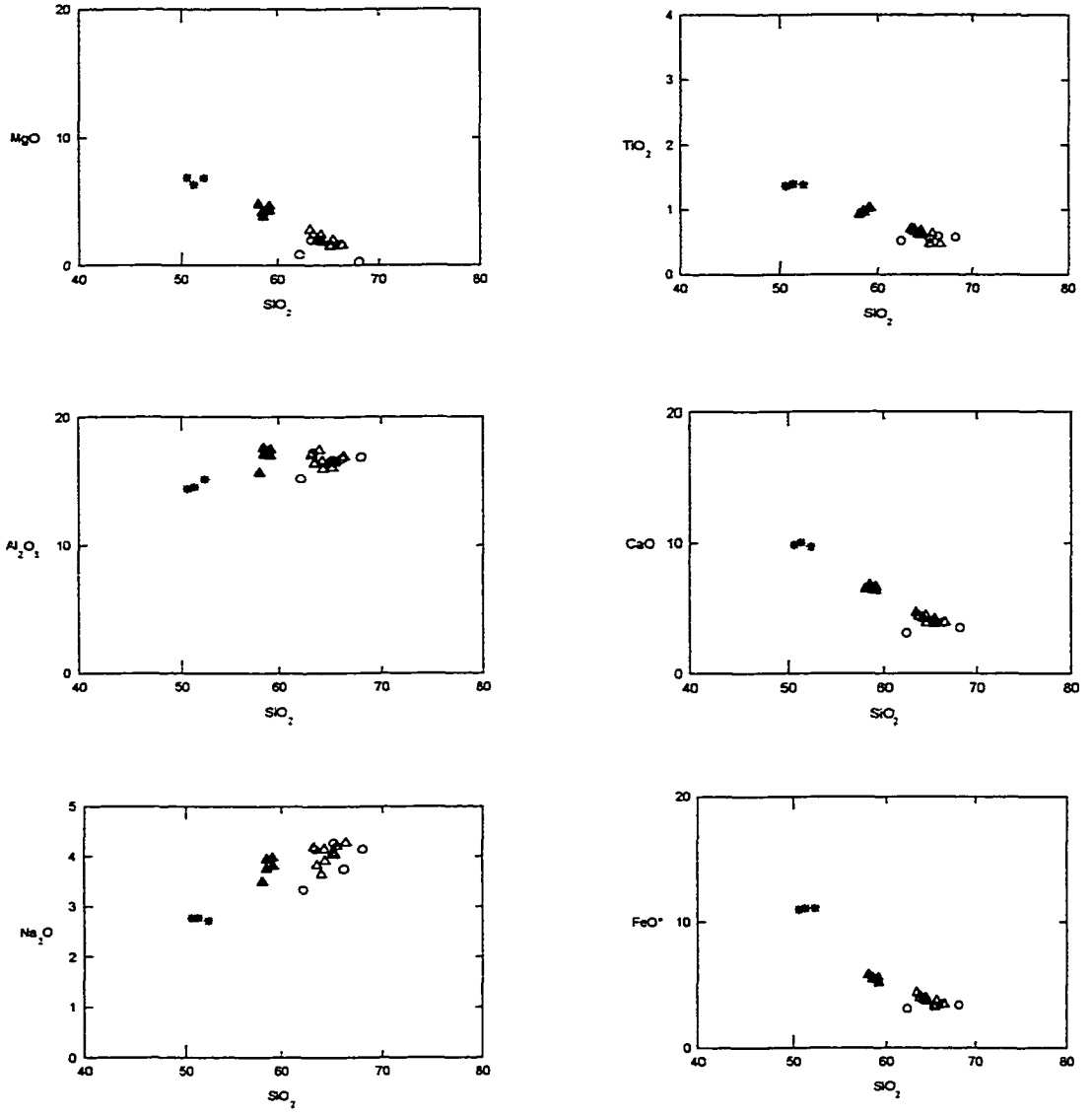

Figure 6. Selected Harker variation diagrams for volcanic rocks in the Lava Mountains. Symbols are defined in Figure 5. All concentrations in weight percent.

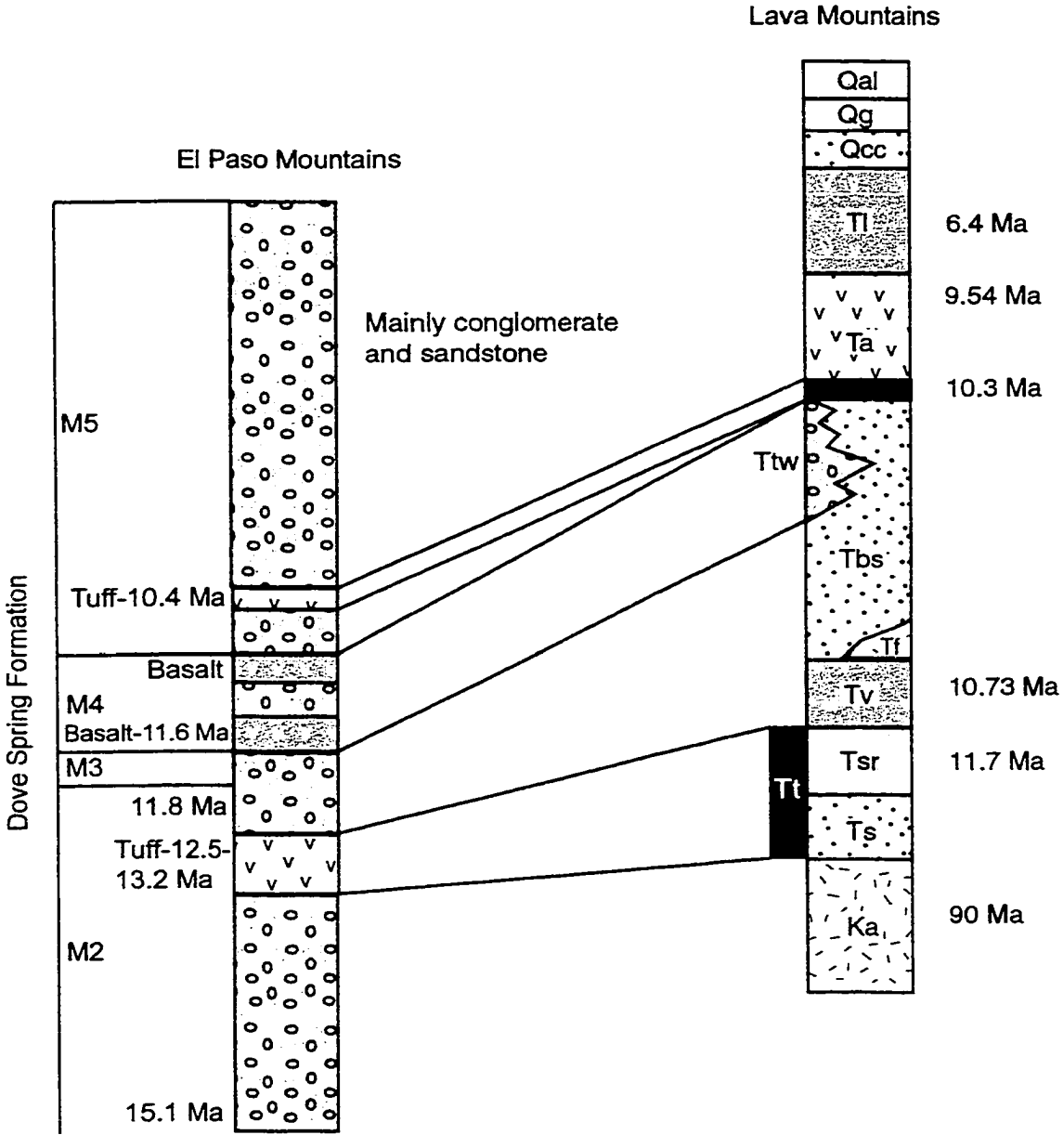

Figure 7. Correlation of a stratigraphic section in the El Paso Mountains (Loomis and Burbank, 1988) with the section in the Lava Mountains (this thesis). Dates from the El Paso Mountains from Loomis and Burbank (1988); dates for the Lava Mountains from this thesis.

Table 1. Dates by $^{40}Ar/^{39}Ar$ incremental heating technique of samples from the Lava Mountains.

sample	unit	date (Ma)	Uncertainty (2σ), (± Ma)	date type	MSWD	mineral
LM96-2	Tsd	10.34	0.69	plateau (inc. 3-9)		hornblende
LM96-2	Tsd	7.81	0.14	plateau (inc. 5-9)		biotite
LM96-15	Tv	10.73	0.10	plateau (inc. 7-11)		biotite
LM96-16	Ta	9.54	1.14	plateau (inc. 10-11)		hornblende
LM96-16	Ta	7.82	0.21	plateau (inc. 7-9)		biotite
LM96-17	Tat	10.29	0.78	plateau (inc. 10-11)		hornblende
LM96-17	Tat	8.73	1.58	isochron (inc. 3-11)	1.73	hornblende
LM1132	Tl	6.4	0.1	isochron (inc. 3-9)	0.9	biotite
GFZ-85	Tsr	11.7	0.2	isochron (inc. 4-10)	2.0	sanidine

Notes: $^{40}Ar/^{39}Ar$ dates by the the Cambridge Laboratory for Argon Isotopic Research (CLAIR), MIT. Tsd-Summit Diggings dacite, Tv-other Tertiary volcanic rocks, Ta-Almond Mountain andesite, Tat-Almond Mountain tuff, Tl-Lava Mountains andesite, Tsr-Summit Range dacite. Inc. refers to the increments of the Ar spectrum used to calculate either the isochron or plateau age. MSWD=mean square of weighted deviates for isochron dates.

CHAPTER 3

THE WESTERN LAVA MOUNTAINS VOLCANO

Introduction

The Western Lava Mountains Volcano (WLMV), occupying a broad basin is 9 km in diameter with a moat surrounding a central vent area (CVA) (Fig. 8 and Plate 1). The moat is filled with inward dipping volcanic breccia and pyroclastic rocks. The CVA is formed by coalescing flow-banded andesite and dacite plugs and dikes (Fig. 8 and Plate 1).

The moat around the CVA is filled by Almond Mountain moat deposits, which consist of block-and-ash, rock avalanche, sandstone and conglomerate and debris flow units. These deposits probably represent the explosive destruction/collapse of volcanic domes in the CVA. Breccia locally contains bombs of andesite of up to four meters in diameter. Throughout the CVA Almond Mountain dacite flows are found interbedded with the breccias. Flows are one to three meters thick and dip inward towards the CVA. To the west and north of the CVA lapilli tuff is interbedded with the breccia or occurs near the contact between the breccia and the CVA. Lapilli tuff and Almond Mountain breccias and flows occupy three channels to the west, northwest and northeast of the CVA. An ash-flow tuff (Tat) crops out at the base of the Almond Mountain volcanic section. This tuff appears to thicken to the east and may have erupted from vents in the

eastern Lava Mountains. The Lava Mountains andesite appears to be filling the moat zone between the CVA and rim of the caldera.

The Central Vent Area

Irregularly shaped plugs and dikes that represent the roots of volcanic domes comprise the central vent area (Fig. 8). Plugs and dikes are variably altered and rock varies in color from yellow to purple to dark gray. The degree of alteration corresponds in a general way to unit age as determined by crosscutting relationships. Older more highly altered rocks (yellow dacite) are usually less resistant to erosion and form a gently rolling subdued topography. Younger intrusive rocks (purple to dark gray) are less altered and stand out as steep sided ridges and conical peaks.

The mineralogy of all intrusive rocks is similar regardless of age or degree of alteration. Large (up to 5 mm) blocky plagioclase and blade shaped hornblende characterize the rock. Although mineralogy is similar in all intrusive phases, grain size is variable. Plagioclase may vary from < 1 mm to 1 cm in size, for example. The matrix in highly altered rocks is bleached yellow to white and veined with quartz, calcite, sulfides and barite. In addition, plagioclase is altered to sericite or clay minerals and mafic phases are heavily oxidized. In less altered rocks, matrix is granular to glassy and phenocrysts are fresh in appearance.

Yellow dacite (Tay) is the most voluminous unit in the CVA and is probably composed of many overlapping intrusions. My mapping defined a two km diameter funnel shaped intrusion defined by concentric inward dipping flow banding (Fig. 8 – dashed circle). A paucity of flow banding in other areas prevented the location of other

centers. Plagioclase is the dominant phenocryst phase in the yellow dacite with hornblende subordinate. The matrix is yellow to greenish-yellow and in thin section is composed of calcite, sericite, cryptocrystalline clay minerals chlorite and rare epidote.

Purple dacite (Tap) mainly forms dikes and plugs that stand topographically higher than the yellow dacite. Just west of the Steam Well in the area of petroglyphs (Fig. 8 – point A), a purple dacite dike intrudes yellow dacite. This dike is discontinuous, but can be traced nearly three km to the northeast. Northeast and North-south striking dikes of purple dacite cut both yellow dacite and the Bedrock Springs Formation (Fig. 8 – point B). Here the dikes are narrow (5-10 m) and relatively short (100 m to 0.8 km; columnar jointing is common with columns oriented normal to dike walls. Plugs or necks of purple dacite have funnel shape as indicated by steep inward dipping foliation. One of the most impressive plugs forms a steep-sided peak (Fig. 8 – point C). Flow banding is represented by jointing parallel to phenocryst alignment and color banding, and dips steeply inward. Purple dacite is relatively unaltered compared to yellow dacite. Rocks of purple dacite dikes and plugs sometimes have a fine-grained glassy matrix that rings like glass when struck with a hammer.

Within the CVA, dikes and plugs cut exposures of Bedrock Springs Formation (BSF). Although altered to brick red arkosic sandstone near contacts, the BSF is usually white to gray in color and contains clasts of Atolia-type granite ($\leq$ 5 cm in size) in a coarse matrix of quartz and feldspar (1 to 3 mm). No volcanic clasts were identified in the BSF in exposures within the CVA. Interbedded with sandstone are thin beds (0.5 m) of gray massive limestone. Veins and vugs of calcite are scattered throughout the limestone, but except for occasional animal burrows, no fossils were observed. A broad

northeast-striking antiform in BSF is defined by west dips (20 to 40 degrees to the west-southwest) in the western part of the CVA and east dips in the northwestern CVA (Fig. 8).

Rocks of the CVA intrude volcaniclastic and pyroclastic rocks of the moat. Intrusive relationships are well-displayed on the east side of the CVA (Fig. 8 – point D). Smith (1964) mapped the CVA – moat contact in this area as a northeast striking fault, however, my mapping indicated an intrusive relationship between CVA and moat rocks.

Stratigraphy and Origin of Moat Units

The moat is filled with volcaniclastic and pyroclastic rocks of the Almond Mountain volcanic section. A representative section of the moat rock is on the western side of the CVA (Fig. 8 – point E). At this locality, a pyroclastic flow lies directly on conglomerate of the BSF. This 4 m thick tuff is poorly welded. Inclusions of andesite and/or dacite (plagioclase, hornblende and/or pyroxene phenocrysts) typify the tuff. The tuff is white with phenocrysts of sanidine and biotite (2-3 mm). Cuspate glass shards and 0.5-2 cm pumice clasts were observed on fresh surfaces. Above the tuff is a breccia roughly 10 m thick with poorly-sorted, angular clasts of plagioclase-hornblende bearing dacite ranging from 5 to 30 cm in size. No evidence of hot emplacement, such as bombs, gas escape pipes or welding which would indicate pyroclastic flow, was observed. This resulted in the interpretation that it was a debris flow. Above this is a fluvial layer (7-8 m thick) locally exhibiting cross stratification, which is overlain by 10-15 m of breccia that grades upward into a coarser breccia (50-70 m thick) with 0.5-4 m clasts. Many of these clasts have smooth surfaces broken by micro-columnar joints. The clasts commonly

display radial fractures that extend from the core of the clast to near the surface. Clasts commonly have a very fine-grained (vitric?) rind characterized by columnar joints (1 to 2 cm across each column) that extend 2-3 cm from the surface of the clast to the core. Concentric flow banding, vesicle trains and color bands occur in some clasts.

The breccia containing these clasts may be analogous to the block-and-ash deposits produced by dome collapse at a number of volcanoes worldwide. Excellent examples occur at Unzen, Japan, Colima, Mexico, Augustine, Alaska, and the Soufriere Hills volcano, Montserrat (West Indies) (Robin et al., 1990; Stoopes et al., 1992; Newhall and Voight, 1998; Siebert, 1998; Cole et al., 1998). In these examples, domes collapse due to gravitational failure resulting from oversteepened slopes, ground motion due to earthquakes and/or dome growth. Collapse can also occur when magma rises into the near surface faster than it can degas. Volatile overpressure can trigger dome collapse when gas pressure exceeds lava strength. Alteration, cracks and pore fluid pressure within cracks can appreciably weaken lava strength. Gas rich solidified lava and spines with solid crusts and molten interiors along with solid blocks of dome rock comprise the collapsing material. As the material moves down slope, the escape of trapped gas from breaking vesicles quickly contributes a volatile phase. This gas phase becomes the transporting medium and blocks are supported and moved as a solid-gas suspension (a block-and-ash deposit). Large, hot blocks cool during transport, but are not appreciably broken. Gas suspension and plastic behavior of the blocks (due to elevated temperature) prevent extensive breakage. Radial fractures, columnar joints and concentric interior patterns reflect cooling in the block-and-ash deposit after dome collapse. Based on the similarities between block-and-ash deposits at the analog volcanoes, we interpret the

upper parts of the Almond Mountain breccia (containing large blocks) as a block-and-ash flow deposit produced by the collapse of domes in the CVA.

Interbedded locally with the breccia or occurring at the contact of moat rock with the domes of the CVA are exposures of lapilli rich tuff. This tuff is poorly welded and contains sanidine and biotite phenocrysts. Large pumice clasts (lapilli sized 1-20 cm) and clasts of andesite and dacite characterize the tuff. Locally, zones of breccia (20 m wide by 4 m thick) containing clasts up to 1 m in size are entrained within the tuff. The tuff occupies channels, the most prominent of which is just north of Klinker Mountain (Fig. 8 – point E). Within this 1.5-km wide channel, five lapilli tuff flows have a total thickness of about 100-m. Flows are interbedded with bomb-bearing breccia. Lapilli tuff flows at the base of the channel are thin (5-10 m) and outcrops are tightly bounded by channel margins. Outcrop width increases up section; the highest flow in the section has the greatest thickness and outcrop area. A second channel occupied by lapilli tuff and Almond Mountain andesite occurs south of Klinker Mountain (Fig. 8 – point G). The channels represent the only escape routes for pyroclastic material to areas outside of the WLMV.

Also interbedded with breccia, but stratigraphically higher than lapilli tuff, are flows of Almond Mountain andesite. Flows occur both to the east and west of the central vent complex. Flows are 1-4 m thick and have brecciated upper surfaces. Commonly, agglomerate composed of welded andesite clasts, occurs between flows. Flows are porphyritic with plagioclase and hornblende as dominant phenocrysts. Flow banding or platy jointing occurs locally at the base and middle of some flows. Flows dip towards the

central vent complex in all areas. In the west, flows are both oxidized and converted to propylite (feldspars are extensively replaced by sericite and calcite).

Moat breccia in the Brown's Ranch Fault zone is highly altered, bleached and locally sheared, producing poorly exposed soft outcrops that vary in color from white to purple (Fig. 8 – point H). Smith (1964) mapped most of these exposures as tuff, but was uncertain about this identification. My examination of this area indicated that most of the exposures are highly altered Almond Mountain breccia. In most exposures, breccia clasts are visible, but alteration has changed the color of both clasts and matrix to a white to gray color, making identification of breccia clasts difficult. I was unable to confirm the presence of tuff or lapilli tuff in this area.

Moat deposits pinch out rapidly against the Bedrock Springs Formation, especially in the west and northwestern part of the WLMV (Fig. 8 – point I). In the northwestern WLMV, a 300-m thick section of the Almond Mountain volcanic section pinches to less than 5 m in a lateral distance of about 2-km. Along the western side of the WLMV the contact between Bedrock Springs and moat deposits dips 50 degrees to the east. Although the Almond Mountains/Bedrock Springs contact is not well exposed to the north or east of the CVA, moat deposits in all areas dip toward the CVA. The rapid pinch out of moat deposits, the steep dip of the Bedrock Springs – moat contact and the inward dip of moat units suggest that moat deposits are filling a basin.

An important question is whether the moat basin existed before deposition of moat deposits or is a structural basin or volcanic crater produced during eruptions that created the WLMV. A pre-WLMV caldera can probably be ruled out because evidence of large magnitude explosive volcanism either during Bedrock Springs or early Almond

Mountain time is lacking. Volcanic units exist in the upper part of the BSF, but they are dacite and andesite breccia and block-and-ash deposits and a thin tuff unit similar to those in the Almond Mountain section (Smith et al., submitted). While these units are the products of explosive eruptions, their volume is too small to result in caldera collapse. The basal pyroclastic flow of the Almond Mountain section may have resulted in caldera collapse, but this tuff appears to thicken to the east and probably has a source outside the WLMV in the eastern Lava Mountains (Smith et al., submitted). Another possibility is that the depression represents an unfilled Bedrock Spring basin. Although the moat basin lies entirely within the inferred limits of the deposition of the Bedrock Springs Formation (Smith, 1964, Fig. 9), subsequent folding of the BSF probably reversed the topography of the basin producing a structural and topographic high, thus ending basin infilling. Therefore, it is unlikely that the moat deposits represent the filling of a topographic depression remaining at the end of Bedrock Spring time. Formation of the basin during or after the eruption of WLMV lavas is also a possibility. In this scenario, the volcano collapsed due to eruption of the lapilli tuff or by gravity loading of the CVA. Although lapilli tuff is locally thick, it is unlikely that this unit has enough volume to account for a 9-km diameter crater. Gravity loading is another, but highly speculative possibility. The CVA forms an 8-mgal positive gravity anomaly in the center of the WLMV. Perhaps higher density intrusive rocks in the CVA were isostatically unsupported causing the sagging of the CVA and surrounding moat.

The origin of the Almond Mountain basin is still an unsolved problem. I prefer models that require basin formation prior to Almond Mountain deposition. This preference is based on the field observation that the moat deposits lapped against a

preexisting topographic wall in the northwestern and western parts of the WLMV. The origin of the basin, however, is unknown.

Gravity Survey and Geology

The "Golden Valley Complete Bouguer Gravity" map covering the entire Lava Mountains was completed by the U.S. Navy's Geothermal Office (Fig. 9). On this map, the CVA is displayed as a gravity high. The moat zone occupied by Almond Mountain breccia and tuff is a gravity low. The gravity data suggests that the deepest part of the moat is just northeast of Klinker Mountain. There is an 8-mgal difference between the CVA and the center of the gravity low. There is an especially steep gradient between the Trona Road and the gravity low (13 mgals in 3 km). This gradient in part reflects the western wall of the 9 km diameter basin and in part the difference in density between the high density Rand Schist to the west and lower density volcanic rocks to the east. Channels occupied by Almond Mountain breccia, flows and tuffs, roughly corresponds to elongated gravity lows. Exposures of Atolia Quartz Monzonite and Rand Schist produce gravity highs to the north, west and east of the Lava Mountains. The Brown's Ranch Fault zone is displayed as a northeast trending gravity gradient (7 mgals in 1-2 km) with higher gravity values to the west and lower to the east. Most of the southern part of the eastern Lava Mountains is a gravity low. This low appears to continue uninterrupted to the south into the Cantil Valley. The origin of this gravity low is unknown. It may reflect accumulations of tuff or of basin sediment.

Structural Control of the Western Lava Mountains Volcano

Faulting may have indirectly controlled the location of volcanic vents. Most of the volcanoes in the Lava Mountains are located on the axes or flanks of folds related to northwest directed compression during sinistral displacement (Smith, 1964 and 1991) (Fig. 10). In addition to the volcanic vents mapped by Smith (1964), I observed that the vent zone of the Western Lava Mountains volcano lies along the axis of a topographic and structural high that may have formed by folding. Furthermore, vents of Summit Diggings andesite are aligned E-W, close to the axis and on the southern flank of the Dome Mountain anticline (Fig. 10). These observations suggest that the axial region of folds, areas subject to extensional stresses, may have served to localize vent areas.

Evolution of the WLMV

The following is my interpretation of the evolution of the WLMV:

1. Deposition of the Bedrock Springs Formation occurred in a basin adjacent to the Garlock Fault. Folding related to the left-lateral movement on the Garlock Fault produced a northeast striking antiform at the site of the WLMV (Fig. 10). Folding may have continued during and after the deposition of the Almond Mountain volcanic section (Smith, 1964).
2. The first volcanic activity related to the WLMV may be recorded as block-and-ash and pyroclastic flow units interbedded with arkosic conglomerate in the upper part of the BSF.

3. A period of erosion followed the deposition and folding of the BSF. A 9-km wide topographic depression was produced during this time. The origin of the depression remains unknown.
4. The basal tuff of the Almond Mountain section erupted from a source to the east of the WLMV at 10.29 Ma and flowed to the west across the site of the WLMV (Fig. 11).
5. The WLMV formed between 10.29 and about 9.54 Ma by the eruption of numerous domes in the CVA. Some of the domes collapsed and produced debris flow breccias, block-and-ash and lapilli tuffs that filled a moat developed between the domes and the wall of the 9-km diameter depression (Fig. 12). Alteration and mineralization of CVA rocks probably occurred at this time.
6. After a period of quiescence (9.54-6.4 Ma) the CVA remained a topographic high and the moat a topographic low.
7. At 6.4 Ma, a part of the moat was filled with flows of Lava Mountains andesite (Fig. 13).
8. After 6.4 Ma the altered rocks of the CVA were preferentially eroded, leaving the Lava Mountains andesite to cap the topographically high ridges about the CVA.
9. Between 10.29 and the present, the Lava Mountains were separated from the El Paso Mountains by nearly 40 km of motion on the Garlock Fault (Smith et al., submitted).

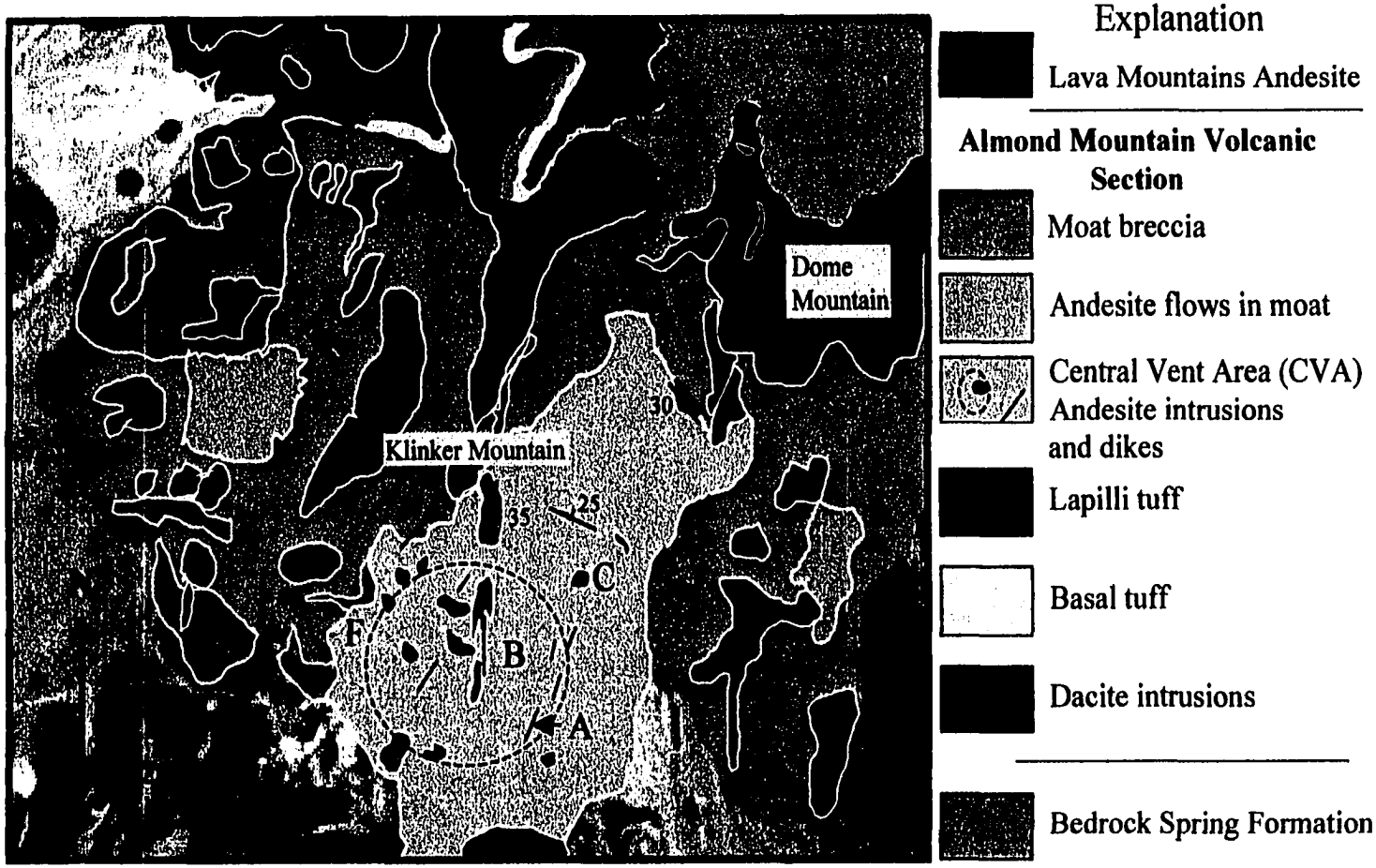

Figure 8. Geological index map of the Western Lava Mountains volcano. Letters indicate locations mentioned in the text. Dikes in CVA shown by lines, plugs of "purple" dacite in dark gray, "yellow" dacite in light gray, vent area in yellow" dacite shown by dashed line.

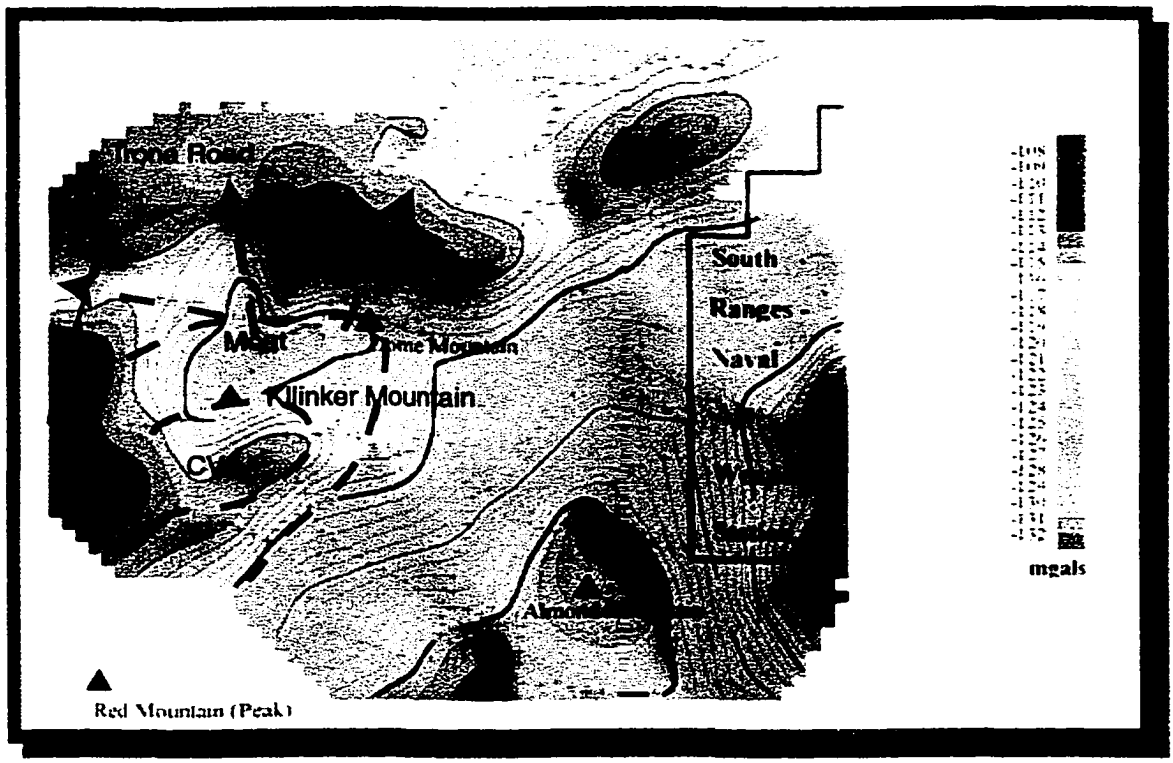

Figure 9. Complete Bouguer Gravity Map of the Lava Mountains. Reduction density is 2.67 gm/cc; contour interval 1 mgal. Gravity survey by Allen Katzenstein, U.S. Navy Geothermal Project Office, China Lake, California. Approximate location of moat and central vent area (CVA) of the WLMV are shown by dashed lines. Dashed arrows indicate approximate location of channels (see text for details).

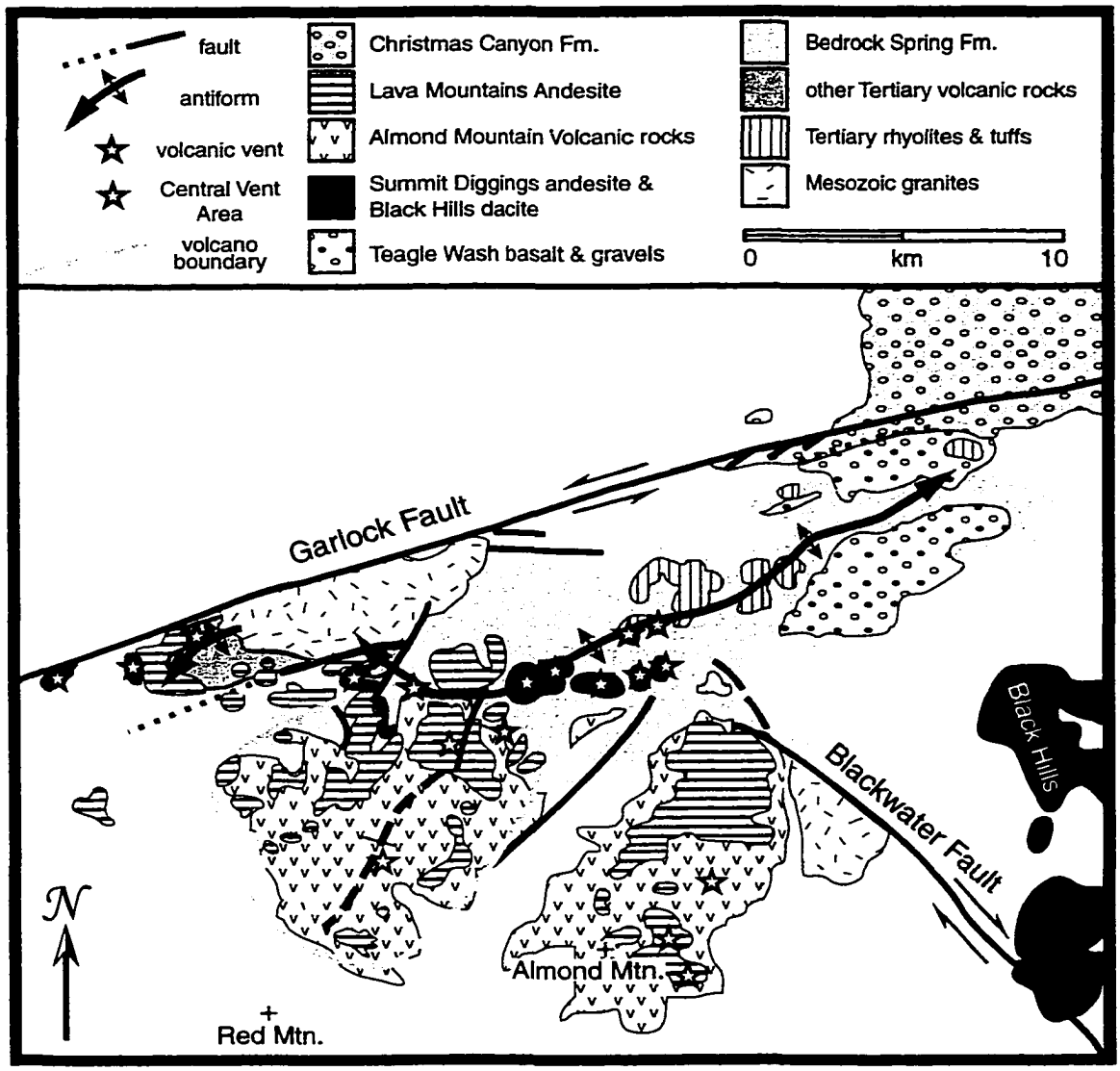

Figure 10. Geological map of the Lava Mountains showing locations of major folds (red lines), the WLMV (yellow line and stars) and other vents in the Lava Mountains (green stars).

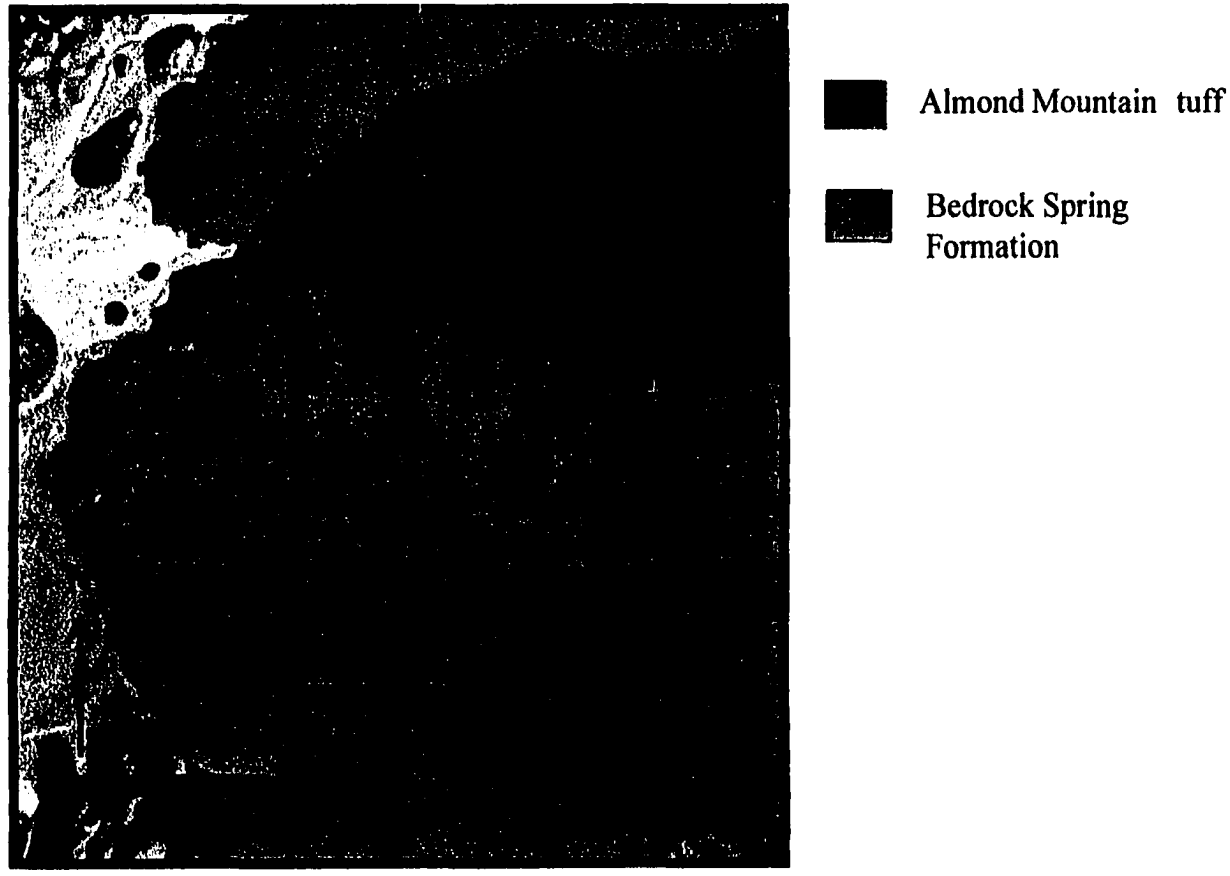

Figure 11. Evolution of the WLMV (10.29 Ma): Basal tuff of the Almond Mountain section erupted from a source to the west of the WLMV and flowed east across the northern part of the Bedrock Spring basin. Area of the map is same as that of Figure 8 and Plate 1.

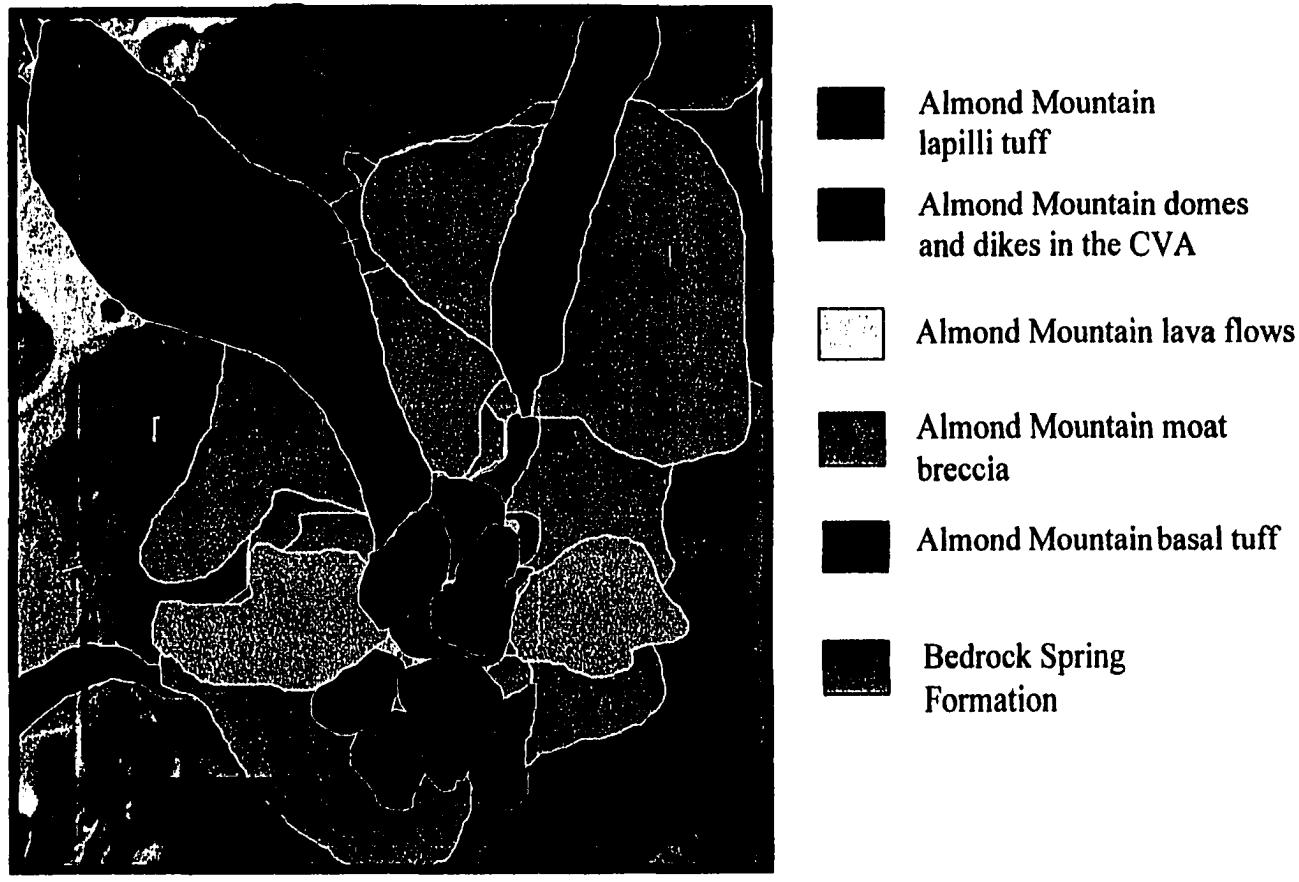

Figure 12. Evolution of the WLMV (9.54-10.29 Ma): Dacite domes formed the CVA. Debris from dome destruction formed in a moat zone about the central vent. Lapilli tuff escaped from the WLMV through three channels. Area of the map is same as that of Figure 8 and Plate 1.

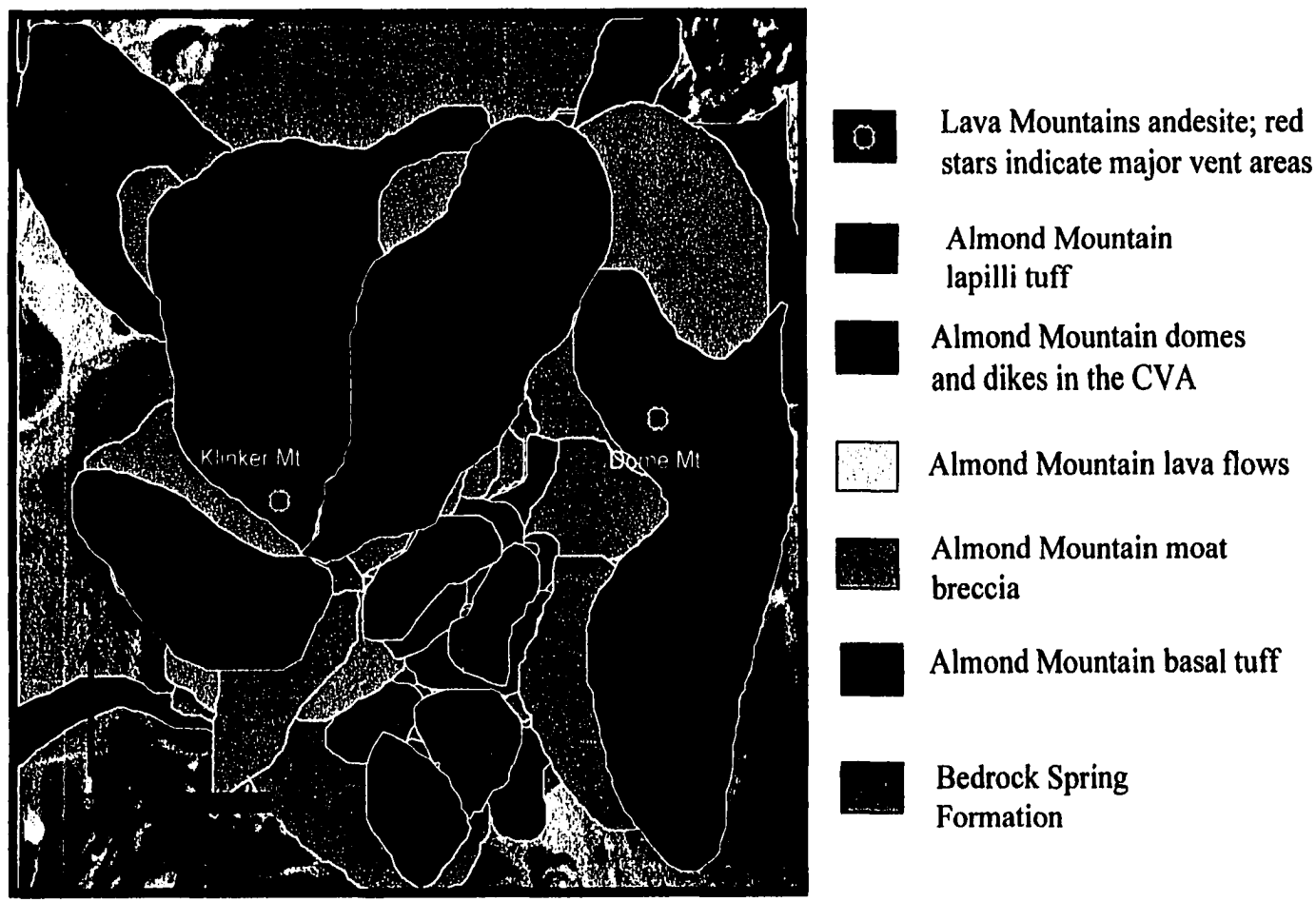

Figure 13. Evolution of the WLMV(6.4 Ma): From sources at Klinker and Dome Mountains, Lava Mountains andesite flowed into the moat zone (green colors) about the CVA. Area of the map is same as that of Figure 8 and Plate 1.

CHAPTER 4

GEOCHEMISTRY

Geochemical Techniques

Seventy-one samples were collected and analyzed for major oxides and trace elements by X-ray fluorescence spectrometry at the Rock Chemistry Laboratory, UNLV. Rare-earth element (REE) and other selected trace element analyses for 69 samples were analyzed at the GeoAnalytical Laboratory at Washington State University by ICP-MS. The Isotope Geochemistry Laboratory at the University of Kansas provided radiogenic isotopic analyses (Sm/Nd, Rb/Sr, and Pb systems) of 41 samples. The Cambridge Laboratory for Argon Isotopic Research (CLAIR), MIT dated six samples using the $^{40}Ar/^{39}Ar$ step heating technique (Tables 1, and 2, Appendix I).

All geochemical analyses were performed on whole rock samples. Each sample was ground into chips (~0.5 cm^2) of fresh, unweathered rock using the Braun jaw crusher equipped with tungsten carbide jaws. Then 50-70 ml of the chips were powdered for 2 minutes in a Bico shatter box composed of tungsten carbide rings and bowl. Major and trace element analyses were performed on powdered samples by making fused glass disks. Each disk was prepared by mixing 1.7000 g of sample, 8.5000 g of lithium tetraborate ($Li_2B_4O_7$), and 0.274 -0.3 g of ammonium nitrate (NH_4NO_3). All reagents were measured to ± 0.0005 g. Then each sample mixture was placed in a gold-platinum (Au/Pt) crucible and heated at 1100° C for 30 minutes. Samples were poured into an

Au/Pt mold and left to cool on a hot plate (250° C) until the glass disk could be removed from the mold. Each disk was stored in a desiccator prior to analysis. Calibration of the Rigaku 3030 X-ray spectrometer was based on internal standards (AGV-1, MA-N, BE-N, STM-1, DNC-1 for major oxides and G-2, GH, BE-N, SCo-1 for trace element analyses). United States Geologic Survey standards (GA and MAG-1) were run as unknowns and compared to published values (Govindaraju, 1994). Rare-earth elements were analyzed using an Inductively Coupled Plasma Mass Spectrometer (ICP-MS) at Washington State University. Isotope (Sm/Nd, Rb/Sr and U/Pb) analyses were conducted at University of Kansas Isotope Geochemistry Laboratory, using methods described in Feuerbach et al. (1993).

Results

Volcanic rocks of the Lava Mountains Andesite, Almond Mountain volcanic section and Summit Diggings andesite comprise most of the volcanic section in the Lava Mountains. These rocks (the main group) are calc-alkaline andesites and dacites that define a compositionally similar magma type (Fig. 5). Only the Teagle Wash basalt, rhyolite tuffs (Tt) in the northeast part of the Lava Mountains and in the eastern Summit Range and andesite enclaves in Lava Mountains Andesite have compositions different from this main group (Fig. 5). The largest chemical differences in the main group are a five-wt. % (62 to 67 wt. %) variation in SiO_2 and 1.5 wt. % in MgO (1.5-3.0 wt. %). Other elements (TiO_2, Al_2O_3, K_2O and P_2O_5) show little variation, MgO, FeO and CaO decrease slightly with increasing SiO_2, and Na_2O displays a small increase (Fig. 6). Although showing some scatter, trace elements are remarkably similar. Cr and Ni show

the largest change with Cr increasing from 15 to 50 ppm as Ni increases from 10 to 67 ppm. Rare-earth patterns have smooth slopes from about 100x chondrite abundances for La to between 4 and 8x chondrite for Lu. Ce/Yb varies between 30 and 58 (Fig. 14). Primitive mantle normalized element distribution diagrams have peaks at Ba, Pb, Sr, and K and troughs at Nb-Ta, P and Ti (Fig. 15). Nb/La ranges between 0.3 and 0.5. Isotopic ratios are also remarkably similar. $^{87}Sr/^{86}Sr$ is 0.7065±0.0002, ε_{ND} –1 to –3 (Fig. 16), and $^{206}Pb/^{204}Pb$ 19.1 to 19.3.

The Lava Mountains Andesite contains enclaves that average 5 cm in size with some as large as 30 cm. The enclaves are sub-angular to rounded with generally sharp margins. They are fine-grained and glassy and contain hornblende and feldspar phenocrysts. Acicular crystals of apatite are abundant in the matrix. The enclaves have 58 wt. % SiO_2, 4 to 6 wt. % less silica than their host rocks, and are higher in TiO_2, FeO, MgO, CaO, P, rare-earth elements, Sr, Sc, Cr and Ni and lower in Rb when compared to their host rock and the Almond Mountain volcanic section (Figs. 5, 6 and 14). Isotopic ratios are nearly identical to Lava Mountains, Almond Mountain and Summit Diggings samples (Fig. 16).

Low SiO_2 (51 wt. %) and high MgO (6.3 wt. %), FeO (11 wt. %) and CaO (10 wt. %) characterize the Teagle Wash basalts (Fig. 6). Rare-earth elements are similar to other Lava Mountains rocks except for elevated concentrations of heavy rare-earth elements (Figure 14). Teagle Wash basalt is similar to OIB, but has a mild "arc-like" chemistry with troughs at Nb and Rb, elevated Y, Yb and Lu and a peak at Pb (Fig. 17). $^{87}Sr/^{86}Sr$ is lower (0.7054) and ε_{ND} (1.2-1.7) and $^{206}Pb/^{204}Pb$ (19.2) higher than andesites of the Almond Mountain and Lava Mountains sections (Fig. 16).

Although felsic volcanic rocks are common in the Lava Mountains, rocks with SiO_2 greater than 70 wt. % are rare. Tuffs in the "Other Upper Pliocene (?) Volcanics (Tt)" and a tuff in the eastern Summit Range are the only rhyolites in the Lava Mountains area (Fig. 5).

Volcanism in the Lava Mountains (11.7 to 5.8 Ma) occurred during sinistral motion along the Garlock Fault. The only other major Tertiary volcanic field cut by the Garlock Fault lies to the east in the Eagle Crags area (Sabin, 1994; Monastero et al., 1997) (Fig. 1). Here volcanism clearly preceded faulting, and in contrast to the Lava Mountains, volcanic rocks vary in composition from basalt to rhyolite and show considerable chemical variability. The source of Lava Mountains magma, its subsequent evolution, and the control of the Garlock Fault on magma emplacement remain important questions.

Nature of Lithosphere

Models to explain the petrogenesis of the Lava Mountains andesitic and dacitic magmas must account for the unique makeup of the lithosphere in the western Mojave Desert. Studies by Glazner and O'Neil (1989) and Miller et al. (2000) indicate that lithospheric structure changes from west to east across the Mojave Desert. In the west at the longitude of the Lava Mountains an underthrust accreted Mesozoic schist complex (the Rand-Pelona-Orocopia schists-POR) lies beneath a complex of Mesozoic granitoids. Lithospheric mantle is not present or is very thin in this area and POR schists may lie directly on asthenospheric mantle. Miller et al. (2000) also suggest that a thin wedge of Farallon-plate crust and mantle may exist beneath POR schist at the longitude of the Lava

Mountains, but the existence of this layer is uncertain. East of the Lava Mountains the lithospheric character becomes more typical of the southern Great Basin and Colorado River extensional corridor with North American crust lying on subcontinental lithospheric mantle (Bradshaw et al., 1993). Potential sources for the Lava Mountains magmas, therefore, include a combination of Mesozoic granitoids, POR schists and asthenospheric mantle. Based on the discussion above, subcontinental lithospheric mantle can be ruled out as a source for Lava Mountains volcanic rocks.

POR schists vary in composition from metabasalt to metagraywacke. Metabasalt is interlayered with metagraywacke and varies in thickness from millimeters to several hundred meters (Dawson and Jacobson, 1989). Albite, chlorite, amphibole and epidote are dominant minerals. POR mafic rocks were divided into three chemical groups by Dawson and Jacobson (1989). Groups 1 and 2 resemble mid-ocean ridge basalt (MORB) and group 3 is similar to alkali basalt. Group 3 rocks only crop out in the Orocopia Mountains nearly 200 km south of the Lava Mountains and thus are not pertinent to this study. Based the analysis of two samples, metabasalt has ε_{Nd} of 9-11 and $^{87}Sr/^{86}Sr$ 0.7028 to 0.7045 (Miller et al., 1996). The metabasalts probably represent remnants of subducted oceanic crust, but the tectonic environment, protolith age, and emplacement history are controversial (Dawson and Jacobson, 1989; Miller et al., 1996). Except for two isotopic analyses, no chemical data is available for the metagraywackes. Two samples of metagraywacke have ε_{Nd} between –6 and –8 and $^{87}Sr/^{86}Sr$ between 0.707 and 0.710 (Miller et al., 1996) (Fig. 18).

Atolia quartz monzonite to granodiorite (70 Ma) comprise much of the Mesozoic granitoids in the vicinity of the Lava Mountains (Smith, 1964). Atolia granitoid has

$^{87}Sr/^{86}Sr$ of 0.7085 to 0.724 and $^{206}Pb/^{204}Pb$ of 19.5 to 19.6. Trace element data is limited but Nd varies from 3-33 ppm, Sr from 10 to 800 ppm, La from 15-47 ppm and Nb between 3 and 14 ppm (Glazner, 1989; Glazner and O'Neil, 1989).

Petrogenetic Model

Determining the source and evolutionary history of the Lava Mountain volcanic rocks is a significant problem. Uncertainties regarding the structural makeup of the lithosphere, compositional heterogeneity, and a poor geochemical database for lithospheric samples contribute to this problem. Because of these uncertainties, models must be qualitative. With these concerns in mind, I suggest a three-stage model for the evolution of Lava Mountain volcanic rocks.

The first stage involves the partial melting of asthenospheric mantle peridotite to produce basaltic magma. Peridotite is a reasonable source rock that can produce basalt after as little as 0.1% partial melting (McKenzie, 1985; Asmeron et al. 2000). Furthermore, anhydrous peridotite is commonly found as xenoliths in alkali basalt from the western Mojave Desert area (Wilshire et al., 1988). Considering the absence of lithospheric mantle in this area, asthenospheric mantle is the only rock type that can be melted to produce basalt without assuming very large amounts of anatexis.

After this partial melting event, basalt magma rose into the lower lithosphere and interacted with the POR schists to produce Teagle Wash-type mafic magmas (stage 2). The melt fraction of rising magma need not be large. In fact, Asmeron et al. (2000) have shown that magma representing only 0.1% partial melts can rise through the lithosphere. Small amounts of contamination (1-10%) of low $^{87}Sr/^{86}Sr$ and high ε_{Nd} asthenospheric

melts with a mixture of metabasalt and metagraywacke of the Rand Schist which has higher $^{87}Sr/^{86}Sr$ and lower ε_{Nd} would produce basalt magmas with the isotopic signature of the Teagle Wash basalt (Fig. 19). The arc-like trace-element pattern of the Teagle Wash basalt may also be explained by adding metagraywacke to asthenospheric basalt, since graywacke contains rock clasts of arc magmatic rocks (Dawson and Jacobson, 1989).

Teagle Wash magma rose to the boundary between the underthrust POR schists and the granitoid upper crust (stage 3). This boundary may be a major crustal density barrier. Seismic reflection data indicates that the granitoid upper layer with a density of about 2.6 g/cc lies on POR rocks with densities between about 2.8 to 3.1 g/cc at a depth of about 20 km (Malin et al., 1995). Assuming that the rising mafic magma had a composition similar to that of Teagle Wash basalt, its calculated density is 2.95-2.98 g/cc using the method of Bottinga and Weill (1970). Magmas with this composition and density would ascend until reaching their density compensation level, which in this case is just below or at the contact between granitoid rocks and Rand Schist. Magma trapped at this 20-km density barrier will rise as soon as it evolves by assimilation-fractional crystallization processes to a density less than that of the overlying host rock (less than 2.6 g/cc). This density or less is achieved as soon as SiO_2 becomes greater than about 60-wt. %. The resulting magma would correspond to the composition of Lava Mountains andesite and dacite. Contamination of magma with Atolia-type upper crust probably occurred at or just above the density barrier. Crustal contamination is indicated by disequilibrium textures in Almond Mountain volcanic rocks, the Summit Diggings andesite and the Lava Mountains Andesite. These textures include abundant embayed

quartz xenocrysts mantled by fine-grained clinopyroxene and large (up to 1 cm) zoned plagioclase crystals containing glass inclusions and embayed margins.

Quantitative modeling of the processes that occur at the density barrier is difficult, because magmas with compositions between the parent (Teagle Wash basalt) and the Lava Mountains dacites are trapped at the barrier. These compositions never reach the surface and cannot be sampled. Furthermore, the composition of the Teagle Wash basalt itself was most probably modified by crustal contamination. The P_2O_5/K_2O ratio is a good index of crustal contamination (Carlson and Hart, 1987; Wilson, 1989). Crustal rocks have ratios of about 0 and mantle derived melts >0.4. Samples with $P_2O_5/K_2O <$ 0.4 have been subjected to crustal contamination. Teagle Wash basalts have ratios of 0.35-0.3. Crustal contamination is also evident by mixing curves between Teagle Wash basalt and granitoid upper crust on the ε_{Nd} vs. SiO_2 diagram (Fig. 19).

The only hint of the nature of the fractional crystallization process that occurs at the density barrier can be inferred by the presence of andesite enclaves within Lava Mountain Andesite host rocks. The enclaves probably represent less evolved compositions that existed prior to or contemporaneously with Lava Mountains Andesite. Fractional crystallization (10 to 30%) of hornblende and plagioclase may have changed Cr and Ni from greater than 100 ppm to less than 50 (Fig. 20) and SiO_2 contents from 58 to about 65 wt. % (enclave composition to host composition). Rapid rise of evolved and buoyant magmas through the crust to the surface without additional significant chemical evolution is suggested by the restricted range of chemistry of these rocks. Rapid rise may have been promoted by coeval strike-slip faulting that resulted in the fracturing and folding of the upper crust.

An important question is the number of times this sequence of events occurred. The first and second episodes of magmatism are separated by about 0.5 Ma, but the second and third by as much as 3 Ma. It is unlikely that a magma body could survive in the upper crust for a period of 0.5 m.y; we suggest, therefore, that this sequence of events occurred at least three times in much the same manner.

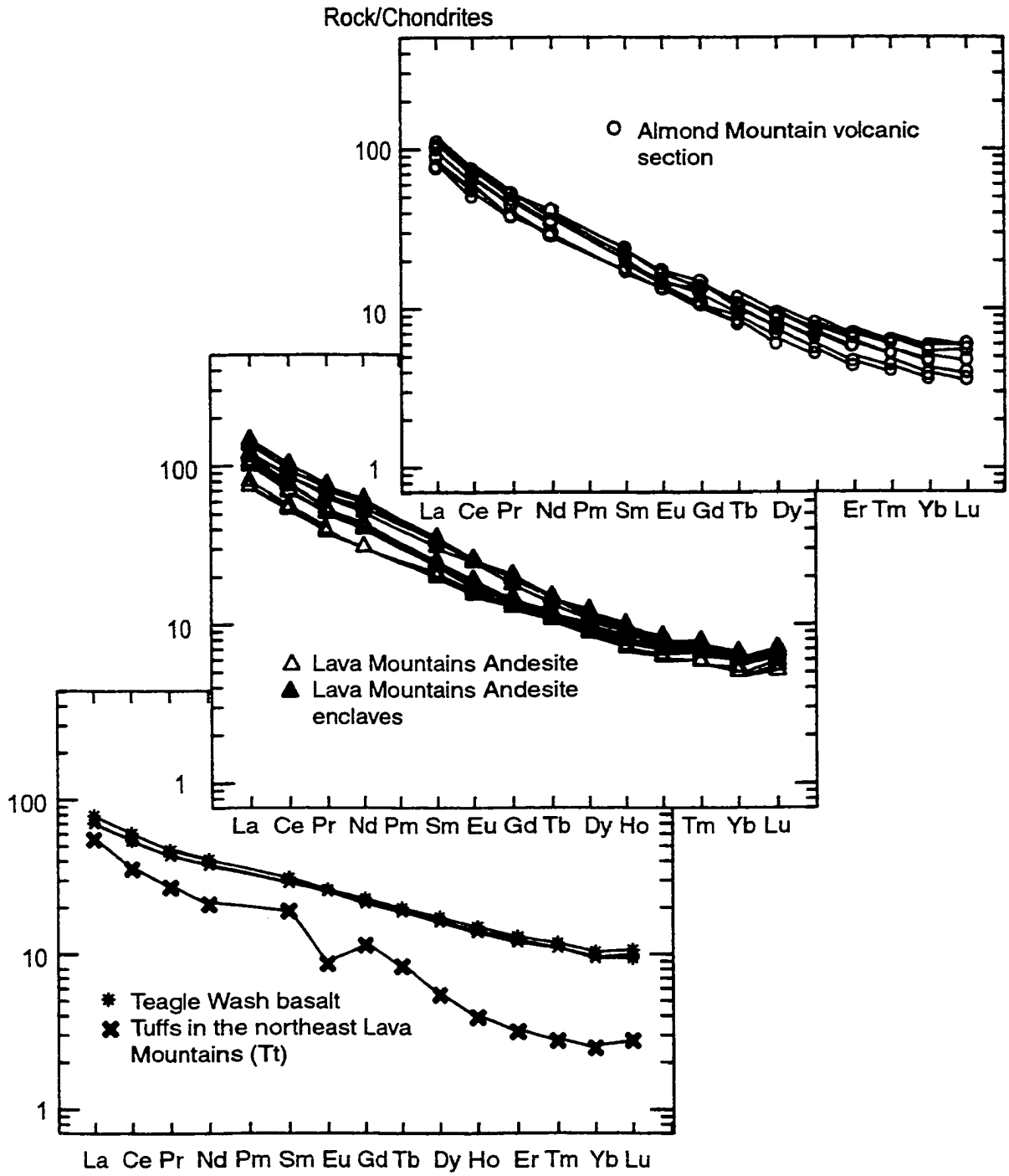

Figure 14. Rare-earth element diagrams for volcanic rocks in the Lava Mountains. Chondrite compositions from Sun and McDonough (1989).

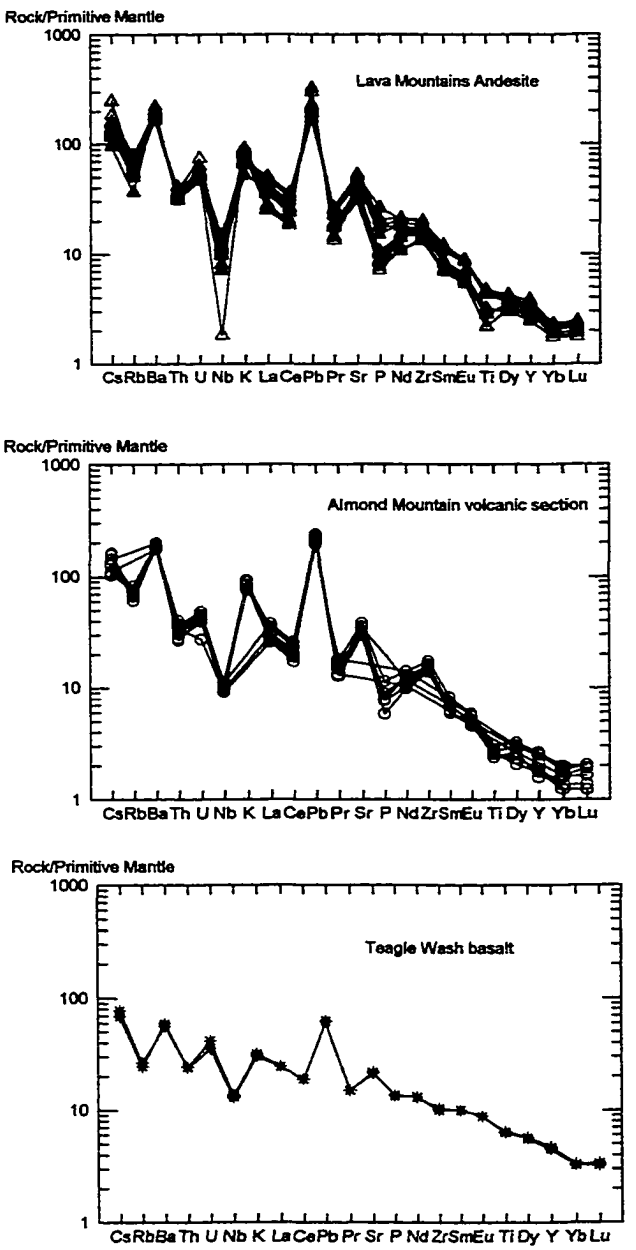

Figure 15. Primitive mantle normalized element diagrams for volcanic rocks in the Lava Mountains. Primitive mantle compositions from Sun and McDonough (1989).

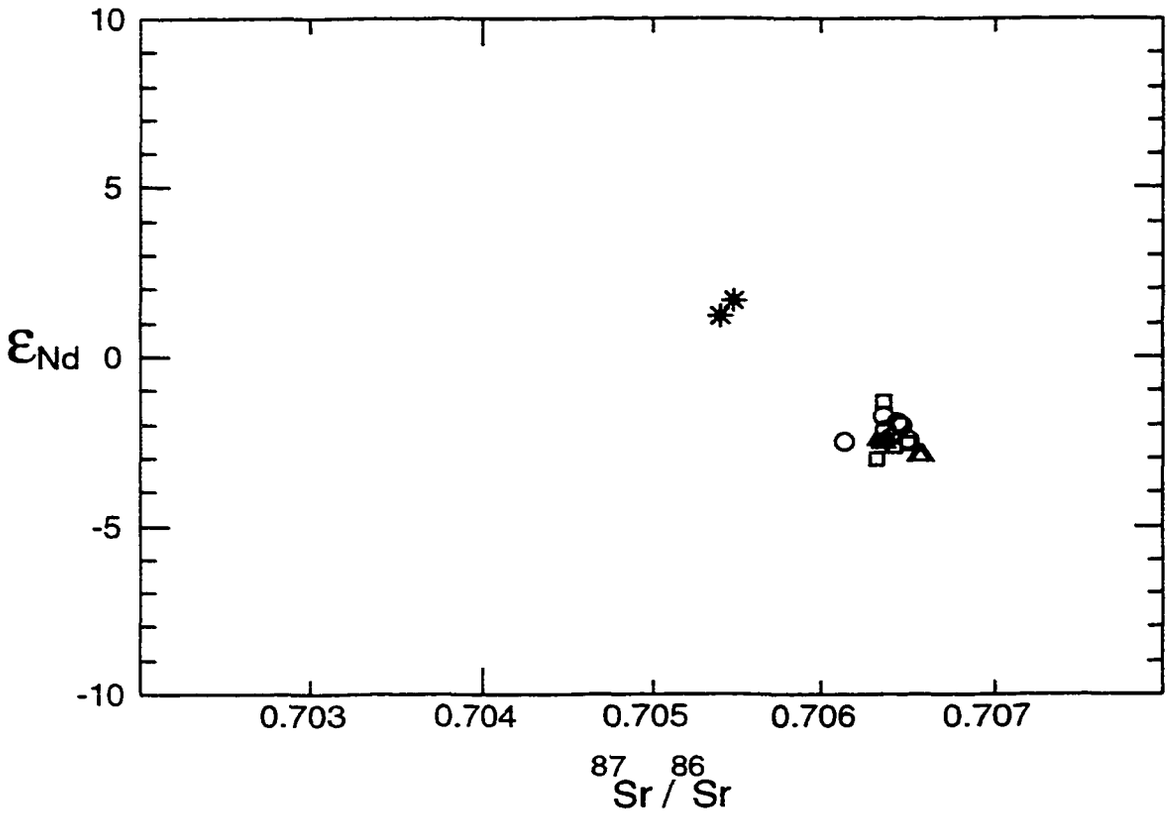

Figure 16. Epsilon Nd vs. initial Sr plot for Lava Mountains volcanic rocks. Symbols are defined on figure 5.

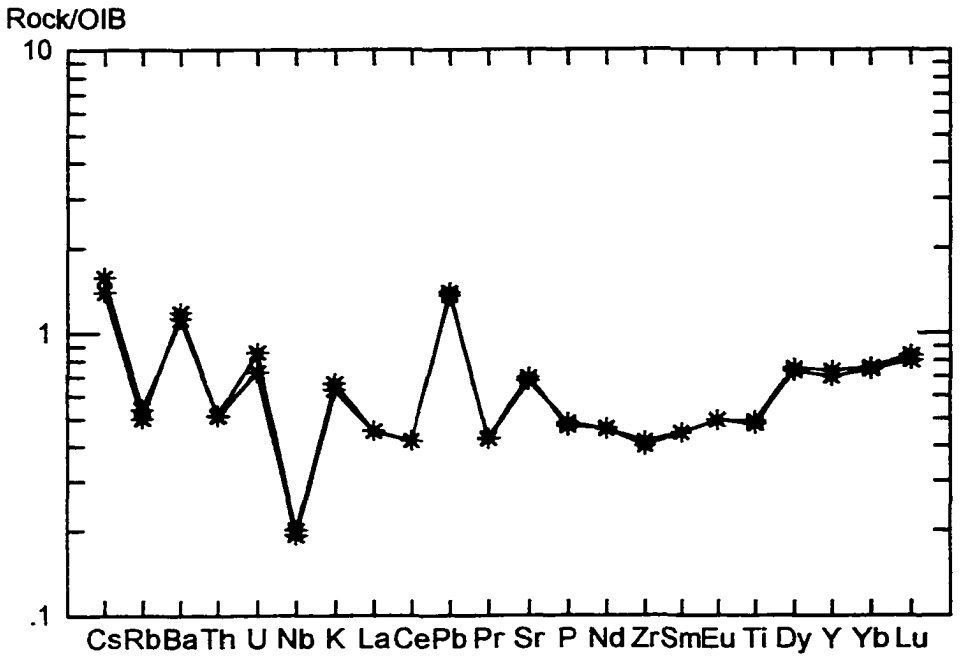

Figure 17. Ocean island basalt (OIB) normalized element diagram for the Teagle Wash basalt. OIB compositions from Sun and McDonough (1989).

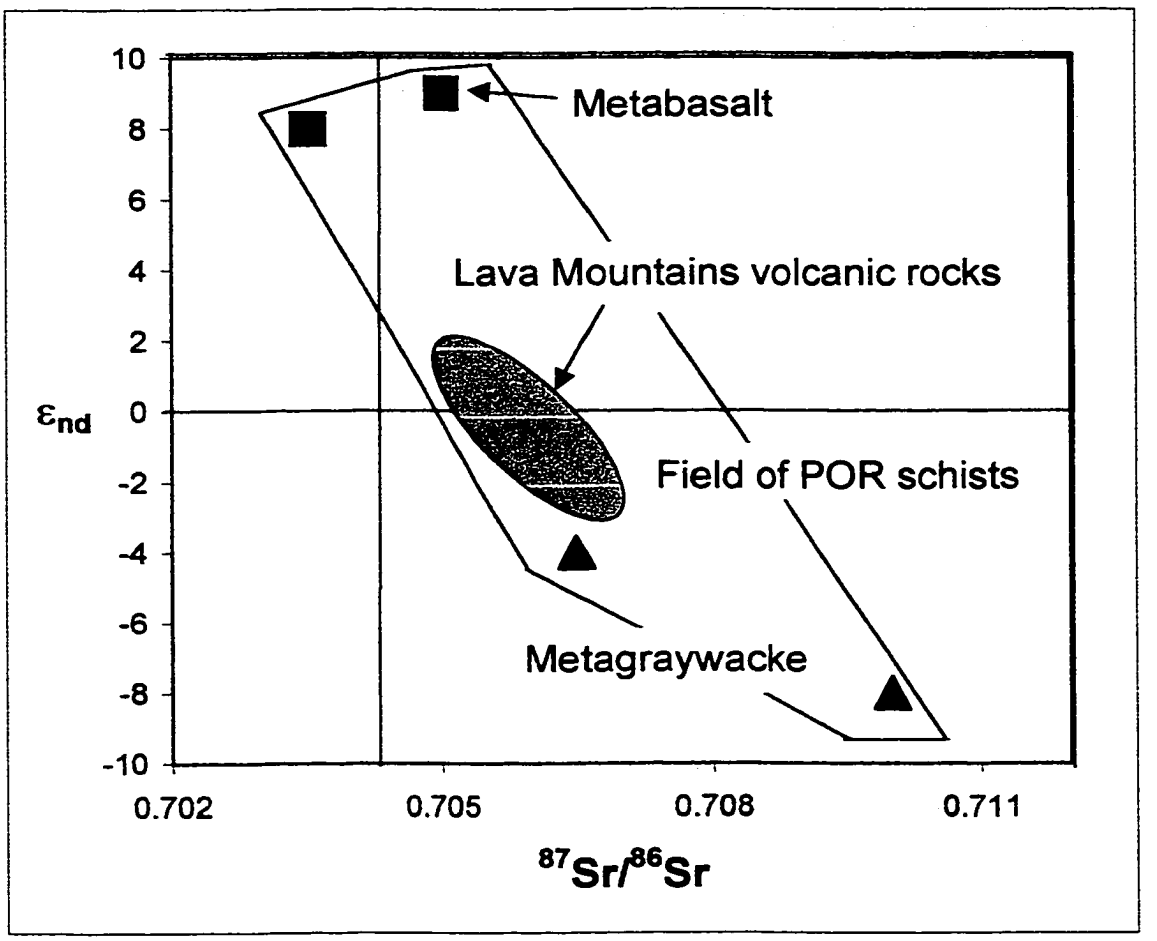

Figure 18. ε_{nd} vs. $^{87}Sr/^{86}Sr$ plot showing the field of Pelona-Orocopia-Rand (POR) schists. Lava Mountain rocks and metabasalt and metagraywacke from the Rand Schist. POR data from Miller et al. (1996).

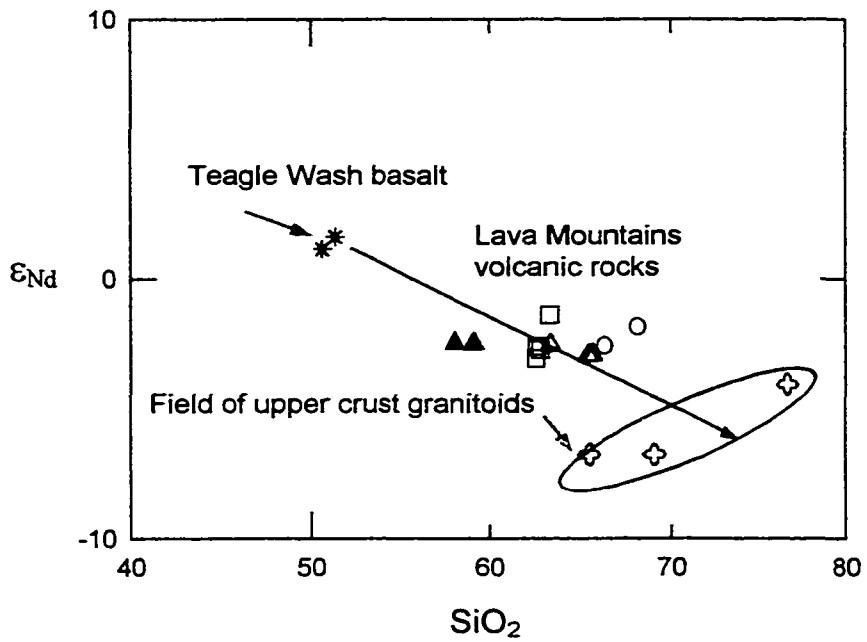

Figure 19. ε_{Nd} vs. SiO_2 plot showing that Lava Mountains volcanic rocks lie on a hypothetical mixing curve between Teagle Wash basalt and upper crustal granitoids. All data from Table 2. Symbols defined on Figure 5.

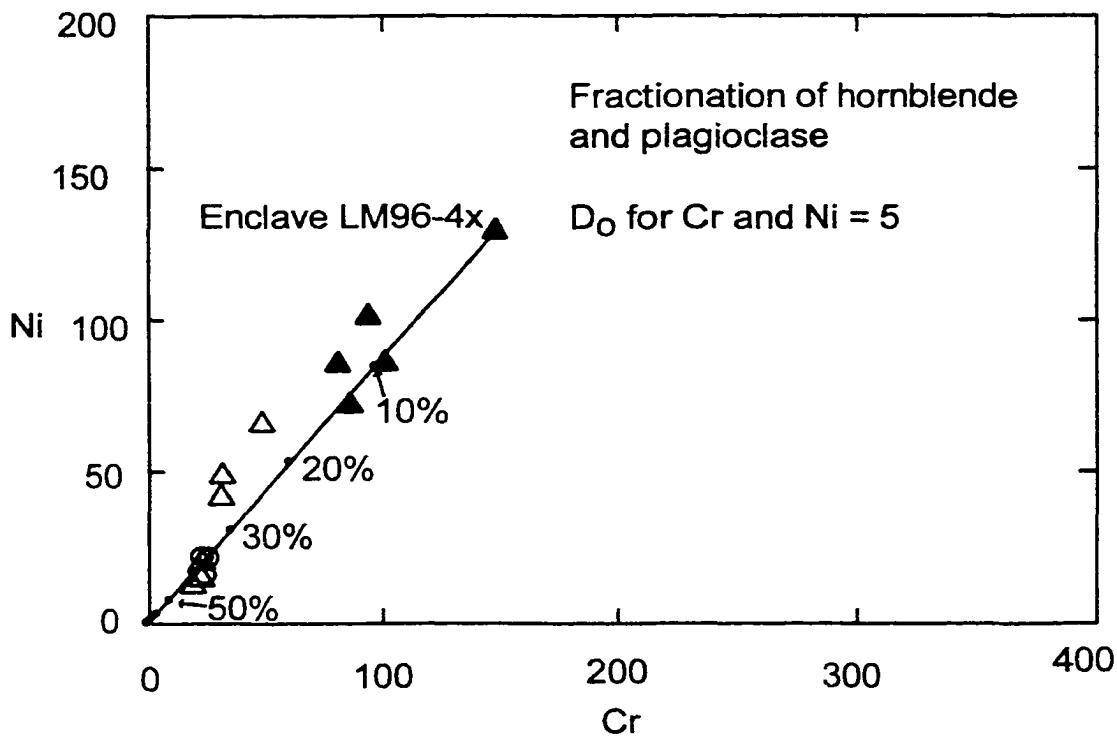

Figure 20. Fractional crystallization model showing evolution of Lava Mountains volcanic rocks from a magma with the composition of enclave LM96-4x. Ni and Cr concentrations in ppm.

Table 2. Sr, Nd, and Pb isotope ratio and trace element analyses

sample no.	$^{87}Sr/^{86}Sr_i$	Sm	Nd	$^{147}Sm/^{144}Nd$	$^{143}Nd/^{144}Nd$	ε_{Nd}	Pb	$^{206}Pb/^{204}Pb$	$^{207}Pb/^{204}Pb$	$^{208}Pb/^{204}Pb$
Lava Mountains Andesite										
LM96-4	0.706373	3.645	21.02	0.10484	0.512503	-2.53	14.28	19.236	15.700	38.969
LM96-4x	0.706386	4.721	26.90	0.10609	0.512507	-2.44	12.04	19.233	15.696	38.980
LM96-6	0.706586	2.946	15.45	0.11528	0.512483	-2.92	19.60	19.189	15.695	39.002
LM97-26	0.706570	3.643	20.16	0.10922	0.512486	-2.90	14.83	19.183	15.661	38.870
LM97-28x	0.706327	4.813	26.57	0.10951	0.512508	-2.48	12.37	19.190	15.659	38.850
Almond Mountain Volcanic rocks										
LM96-7	0.706137	3.128	12.67	0.14923	0.512505	-2.54	11.68	19.211	15.676	38.897
LM96-8	0.706371	2.598	20.57	0.07636	0.512538	-1.80	12.69	19.269	15.702	38.989
LM96-17	0.706592	2.564	14.48	0.10702	0.512528	-2.09	17.33	19.237	15.671	38.911
LM98-46	0.706513	2.920	16.13	0.10942	0.512504	-2.50	13.65	19.197	15.658	38.838
LM98-K1	0.706543	2.366	12.55	0.11398	0.512494	-2.76	n.d.	19.203	15.655	38.896
LM98-K2	0.706386	2.836	15.31	0.11206	0.512502	-2.54	13.60	19.212	15.658	38.851
LM98-K4	0.706381	2.451	13.57	0.10919	0.512519	-2.21	13.05	19.220	15.663	38.870
LM98-K6	0.706468	3.107	17.82	0.10539	0.512526	-2.07	14.02	19.496	15.913	39.510
LM98-K8	0.706643	2.552	14.62	0.10552	0.512549	-1.67	n.d.	19.222	15.684	38.916
LM98-K11	0.706449	3.140	18.07	0.10506	0.512532	-1.95	13.36	19.112	15.556	38.496
LM98-K12	0.706344	2.953	16.16	0.11045	0.512507	-2.44	13.42	19.204	15.666	38.856
LM98-K13	0.706453	2.346	12.75	0.11127	0.512495	-2.74	n.d.	19.219	15.666	38.873
Teagle Wash basalt										
LM96-13	0.705407	4.294	18.88	0.13749	0.512698	+1.17	4.27	19.288	15.677	38.943
LM96-14	0.705475	4.286	19.02	0.13621	0.512723	+1.65	4.47	19.270	15.671	38.904
Dove Spring Formation, member 4 basalt										
LM98-K19	0.705337	3.185	13.265	0.14518	0.512739	2.00	n.d.	19.316	15.672	38.970
Summit Diggings andesite										
LM96-2	0.706372	3.844	22.04	0.10543	0.512563	-1.35	14.78	19.178	15.663	38.860
LM96-11	0.706514	2.810	14.08	0.12072	0.512501	-2.58	14.46	19.161	15.650	38.871
LM96-12	0.706426	3.098	15.79	0.11866	0.512495	-2.69	21.76	19.143	15.639	38.827

Table 2,
continued

sample no.	$^{87}Sr/^{86}Sr_i$	Sm	Nd	$^{147}Sm/^{144}Nd$	$^{143}Nd/^{144}Nd$	ε_{Nd}	Pb	$^{206}Pb/^{204}Pb$	$^{207}Pb/^{204}Pb$	$^{208}Pb/^{204}Pb$
LM97-21	0.706328	3.048	16.19	0.11380	0.512477	-3.04	12.86	19.210	15.667	38.881
Black Hills dacite										
LM97-37	0.706761	4.496	23.58	0.11528	0.512448	-3.60	14.52	19.175	15.638	38.874
LM98-44	0.706635	2.003	9.974	0.12141	0.512488	-2.83	18.68	19.190	15.649	38.860
LM98-45	0.706687	2.474	12.42	0.12046	0.512510	-2.40	20.27	19.216	15.681	38.957
Summit Range dacite										
LM97-29	0.706134	3.230	16.52	0.11822	0.512629	-0.08	19.96	19.208	15.661	38.892
Dove Spring Formation, member 2 tuff										
LM98-K14	0.706951	1.2455	6.278	0.11448	0.512702	1.30	n.d.	19.146	15.644	38.806
LM98-K16	0.707125	0.7514	3.614	0.12572	0.512640	0.08	n.d.	n.d.	n.d.	n.d.
LM98-K17	0.707260	0.8901	4.041	0.13317	0.512797	3.14	3.58	19.193	15.649	38.890
other Tertiary volcanic rocks										
LM96-15	0.705942	2.895	15.23	0.11495	0.512703	+1.37	16.67	19.180	15.664	38.854
LM96-18	0.705360	4.869	23.05	0.12773	0.512710	+1.49	11.64	19.157	15.647	38.945
LM97-19	0.706565	2.871	17.18	0.10101	0.512460	-3.25	20.71	19.028	15.638	38.798
LM97-31	0.708809	2.640	9.747	0.16377	0.512591	-0.84	15.37	19.225	15.679	39.141
LM97-32	0.704075	3.619	15.78	0.13867	0.512876	+4.78	4.25	19.023	15.607	38.714
LM97-36	0.708750	n.d.	n.d.	n.d.	n.d.	n.d.	4.52	19.399	15.690	39.202

Notes: Isotopic analyses by isotope dilution performed at the Isotope Geochemistry Laboratory, University of Kansas.

CHAPTER 5

CORRELATION ACROSS THE GARLOCK FAULT

Concepts and Basics

Various estimates have been made concerning the initiation of displacement on the Garlock Fault, ranging from 10-9 Ma (Loomis and Burbank, 1988) to > 17 Ma (Monastero et al., 1997). Volcanism in the Lava Mountains covered a range from 11.7 Ma to 6.4 Ma and thus occurred contemporaneously with displacement along the Garlock Fault. The proximity of the Lava Mountains volcanic centers to the Garlock Fault allow units to be traced across the fault and gives the opportunity to better understand and constrain movement during the Tertiary Period.

Units similar in age to those in the Lava Mountains have been located in the El Paso Mountains in the Miocene Dove Springs Formation (Loomis and Burbank, 1988). I use geochemistry to test three correlations. (1) A thin tuff (10 m thick) in the lower part of member 5 in the Dove Spring Formation was dated at 10.4±1.6 Ma (fission track date, Cox and Diggles, 1986). In the Lava Mountains the basal ash-flow of the Almond Mountain section is 10.29±0.78 Ma and a lapilli tuff in the lower middle part of the same section is between 10.29 and 9.54 Ma. Potentially, both tuffs are candidates for correlation with the member 5 tuff in the Dove Spring Formation, El Paso Mountains. (2) Member four of the Dove Springs Formation was dated between 11.5 and 10.5 Ma

(Loomis and Burbank, 1988) and includes a layer of basalt that could be corollary to the Teagle Wash Basalt of the Lava Mountains. (3) The last correlation to be made in this thesis is between the tuff found in the northeastern Lava Mountains and the tuff of member two of the Dove Springs Formation. Loomis and Burbank (1988) dated this member to be between 13.3 and 12.5 Ma using the fission track technique. Also, conglomerate clasts in the eastern Lava Mountains are characteristic of lithologies found in the El Paso Mountains.

Evidence and Specifics

I have found three correlations possible between the Lava Mountains and the El Paso Mountains which demonstrates that they were adjacent to one another during the late Miocene. These are (1) correlation of the Teagle Wash basalt and basalt boulders in a conglomerate below the Teagle Wash basalt with the basalt in member four of the Dove Springs Formation, (2) Correlation of lapilli tuff in the Almond Mountain section with the tuff of member five of the Dove Springs Formation, and (3) correlation the tuff found in the northeastern Lava Mountains with tuffs of member 2 of the Dove Springs Formation.

The member four basalt composed of two flows (Tdb2 and Tdb3, Loomis and Burbank, 1988) is fine-grained and vesicular and contains phenocrysts of olivine and plagioclase (Loomis and Burbank, 1988). This mineralogy is also typical of the Teagle Wash Basalt. Chemistry of the member four basalt is similar to the Teagle Wash Basalt at all levels (major elements to isotopes). Isotopic ratios of $^{206}Pb/^{204}Pb$ range from 19.2 to 19.3 and $^{87}Sr/^{86}Sr$ for both is 0.7054 ± 0.0001, demonstrating the similarity of the two

units. These similarities lead to the conclusion that the member 4 basalt in the Dove Springs formation correlates with the Teagle Wash Basalt in the Lava Mountains.

The source of fine-grained, vesicular basalt boulders in Quaternary deposits in the Lava Mountains and in the conglomerate beneath the Teagle Wash basalt is controversial. Smith (1964 and 1991) suggested that they originated to the southeast in the Black Hills and Carter (1980 and 1982) thought they might represent Black Mountain basalt from the northern El Paso Mountains (Fig. 3). Geochemical data clearly indicate that neither one of these possibilities is tenable. Dark colored volcanic rocks in the Black Hills, thought to be basalt by Smith (1964 and 1991), is fine- to medium-grained, flow-banded hornblende dacite with between 63.4 to 64.8 wt % SiO_2 and 1.71 to 2.55 wt % MgO. It is therefore too felsic to correlate with the basalt boulders in the Lava Mountains. Black Mountain basalt from the El Paso Mountains is too low in SiO_2 (48.3 to 49.1 wt %) and too high in Al_2O_3 (15.5 to 17 wt %) to correlate with the basalt boulders (51 wt % and 14.5 wt % respectively). The chemistry of a basalt boulder in the conglomerate beneath the Teagle Wash basalt is almost identical to the basalt in member four of the Dove Springs Formation (Fig. 4). Therefore, I conclude that the basalt boulders originated in the El Paso Mountains and are correlative with basalt flows of member four of the Dove Spring Formation.

In the lower part of member 5 of the Dove Springs Formation is a thin tuff (10 m thick), dated at 10.4 ± 1.6 Ma (fission track date, Cox and Diggles, 1986). The basal ash-flow tuff of the Almond Mountain section in the Lava Mountains is 10.29 ± 0.78 Ma. A lapilli tuff in the lower middle part of the same section is between 10.29 and 9.54 Ma. Both are potentially candidates for correlation with the member 5 tuff of the Dove

Springs Formation in the El Paso Mountains. Rare-earth element plots show that the member 5 tuff is similar to the basal and lapilli tuffs in the Almond Mountain section (Fig. 21), except for a difference in the higher heavy rare-earth element abundances of the member 5 tuff. Similar chemistry is also notable on a Th vs. La plot where the member 5 tuff falls close to the field of the basal and lapilli tuffs of the Almond Mountain section (Fig. 22). From these observations it is suggested that the member 5 tuff can be correlated to the tuffs of the Almond Mountain volcanic section.

Tuffs in member 2 thin to the north and form prominent cliffs in Red Rock Canyon in the western El Paso Mountains. Dated at 11.8 to 15.1 Ma (fission track dates, Loomis and Burbank, 1988), these tuffs are older than the tuffs of the Almond Mountain volcanic section. Geochemistry also disallows a correlation between these two units. A rhyolitic tuff found in the northeastern Lava Mountains (mapped as Tt by Smith, 1964) may correlate with member 2. This is based on similarities in trace element chemistry. Member 2 tuffs and Tt share low Ba, P, Ti and Zr and high Rb, Th, and U and negative Eu anomalies (Fig. 23). Based mainly on geochemistry, the tuff of the northeastern Lava Mountains may correlate with member 2 tuffs of the Dove Springs Formation in the El Paso Mountains.

History of Deposition across the Garlock Fault

Based on the previous correlations, it is suggested that the El Paso Mountains lay to the north of the Lava Mountains between about 10.3 and 11.6 Ma. Prior to this, they were northeast of the site that was to become the Lava Mountains. Sediments were transported south and deposited into the Bedrock Springs basin (unit immediately below

the Almond Mountain volcanic section) and volcanic units from the Lava Mountains migrated north into the El Paso Mountains area. There is now 32-40 km separation between the two mountain ranges, indicating a displacement rate of about 3.1-3.8 mm/yr. This rate is less than the average Holocene rate of 6-8 mm/year (McGill and Sieh, 1993) and the Pleistocene rate of 7 mm/year (Carter, 1987). It is similar to the average displacement rate of 3.5 mm/year (Monastero et al. 1997) obtained from a total offset of 64 km in about 17 Ma. This information leads to the following depositional history across the Garlock Fault (Fig. 24).

1. Member 2 of the Dove Spring Formation and tuffs in the northeastern Lava Mountains erupted (Fig. 24a).
2. Fanglomerate fans from the El Paso Mountains washed across the Garlock Fault into the Bedrock Springs basin. The fans contain clasts and slide blocks of Mesozoic basement rocks and boulders of basalt (first flow) from member 4 of the Dove Springs Formation. Member 4 basalt flows erupted from sources in the El Paso Mountains and flowed south through the channels cut into the fan. Inclusion of the basalt boulders in the fanglomerate and the overlying basalt require that the fan formed between the eruption of the two flows of member 4 basalt (11.6 to 10.4 Ma). Distinctive clast types, specifically hornblende quartz diorite, indicate that the fan may have originated at the mouth of Mesquite Canyon in the El Paso Mountains (Carter, 1982, 1987 and 1994) (Fig. 24b).
3. Pyroclastic flows from the western Lava Mountains crossed the Garlock Fault at about 10.3 Ma and are now found in the western El Paso Mountains in

member 5 of the Dove Springs Formation. This requires that the two ranges remained in contact at this time (Fig. 24c).

4. The Lava Mountains and El Paso Mountains separated after 10.3 Ma due to sinistral motion on the Garlock Fault. Faulting also resulted in the counterclockwise rotation of the El Paso Mountains (Loomis and Burbank, 1988) and folding in the Lava Mountains (Smith, 1964). Events 4 and 5 may have occurred simultaneously (Fig. 24d).
5. Sediment transport reversed in Quaternary time and sandstone accumulated north of the Garlock Fault in the Christmas Canyon basin. Ash from eruptions of the Yellowstone Caldera accumulated in the upper part of the Christmas Canyon Formation at about 602 ka (Gansecki et al., 1998). Gravels, including member 4 basalt clasts traveled north and deposited on the sandstone facies of the Christmas Canyon Formation. These gravels produced the conglomerate facies as described by Smith (1964). This represents the second reworking of the basalt boulders of the Teagle Wash basalt and the basalt of member 4 of the Dove Springs Formation (Fig. 24e).

Smith's (1964) interpretation that the conglomerate in the northeast and the overlying Teagle Wash basalt are Quaternary in age is resolved by this model. A similar suggestion was made by Carter (1994), but inferred that metamorphic rocks slid into the Bedrock Springs Formation as intact blocks and subsequent erosion left these block as topographic highs after which they were incorporated into the Christmas Canyon conglomerates.

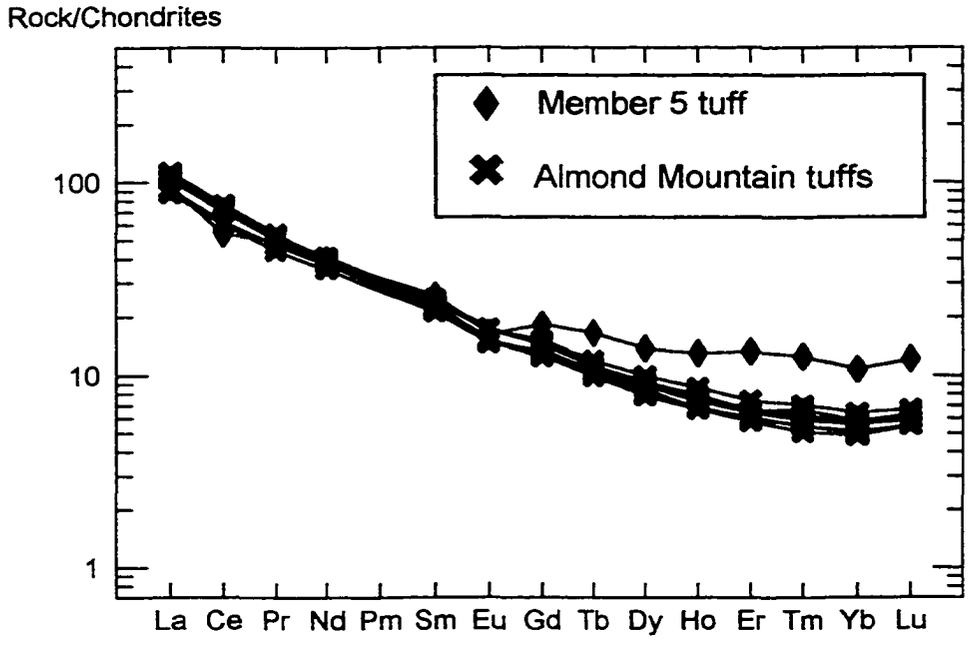

Figure 21. Chondrite normalized element diagram showing correlation between the member 5 tuff in the El Paso Mountains with the Almond Mountain tuffs. Chondrite compositions from Sun and McDonough (1989).

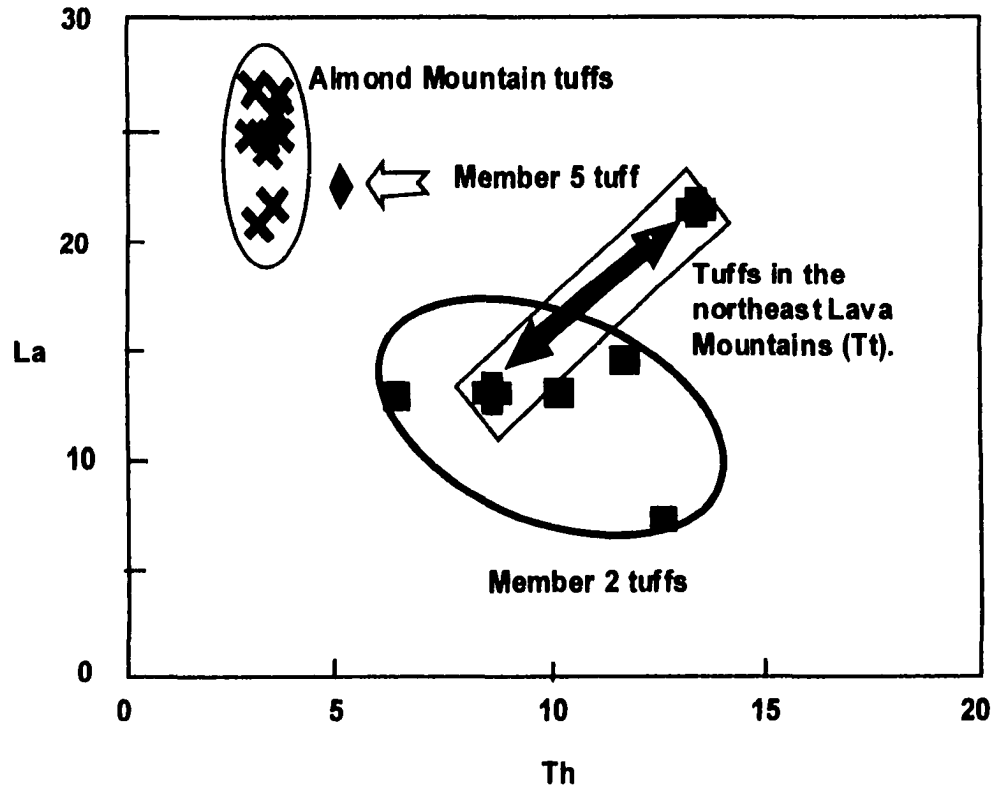

Figure 22. La vs. Th plot summarizing the correlations between tuffs in the Lava and El Paso Mountains. La and Th concentrations in ppm.

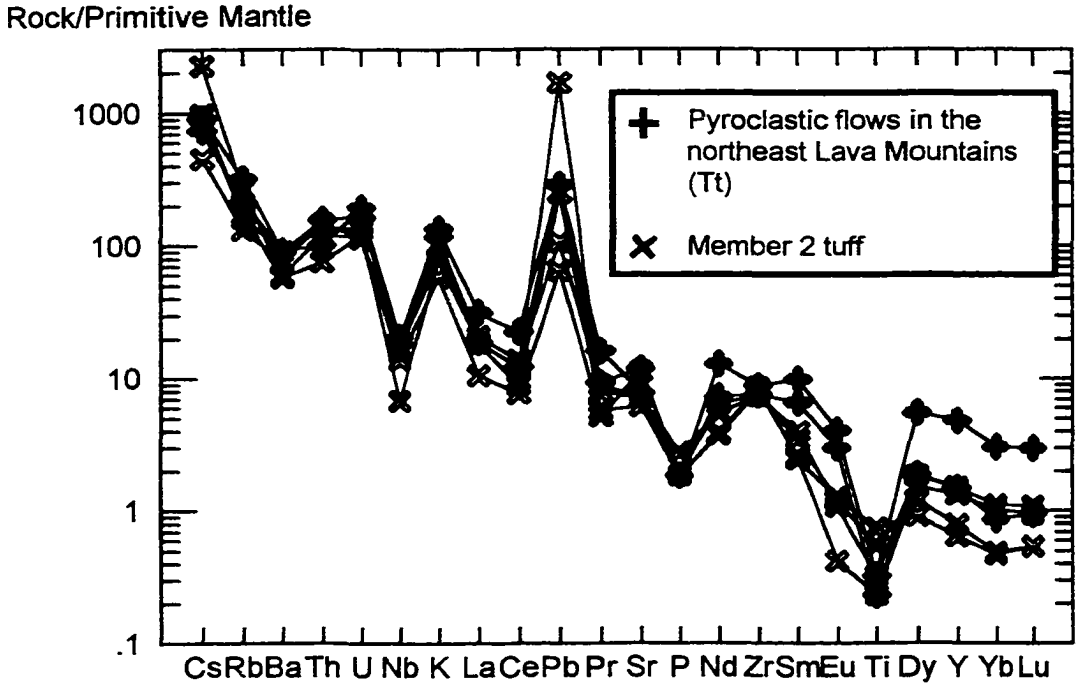

Figure 23. Primitive mantle element diagram showing correlation between pyroclastic flows in the northeast Lava Mountains (Tt) and the member 2 tuff in the El Paso Mountains. Primitive mantle compositions from Sun and McDonough (1989).

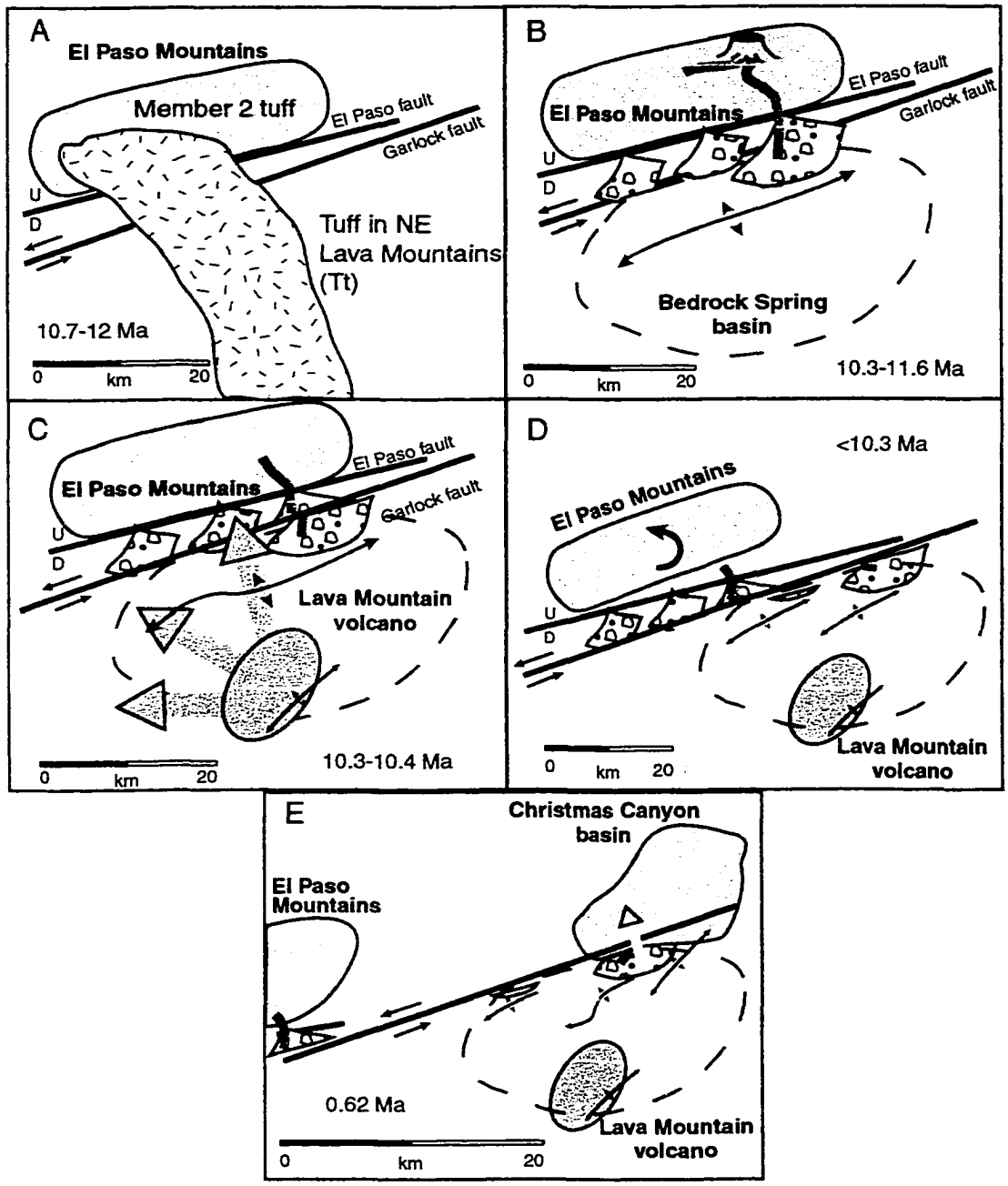

Figure 24. Summary of the history of eruption and deposition across the Garlock Fault (see text for details).

CHAPTER 6

CONCLUSIONS

This thesis covered several aspects of volcanism in the Lava Mountains along and to the south of the Garlock Fault in the Mojave Desert, southern California. The Garlock Fault, a major northeast striking, left-lateral fault has about 64 km of sinistral displacement and some localized dip-slip displacement. First, a new stratigraphy was developed based on the work of G.I. Smith (1964) and updated by findings in the field and from a volcanological viewpoint. Based on this new information, a stratigraphy and unit description was developed for the newly discovered Western Lava Mountains Volcano. While several vent areas exist, it has been shown that a crater/caldera existed with a moat containing outflow units of the volcano.

Geochemistry from assorted volcanic units has allowed a petrogenetic model to be formulated. This model includes the fractionation and lithospheric contamination of an asthenospheric melt at and below a density barrier formed by granitoids overlying POR schists. The limited geochemical data on the schists make this model difficult to quantify, but based on the current models of the subsurface structure in the area, this model appears to be a reasonable one.

Finally, based on the stratigraphy and geochemistry, correlations were attempted across the Garlock Fault between the Lava Mountains and the El Paso Mountains. The El Paso Mountains lie north of the Garlock Fault and roughly 40 km west of the Lava

Mountains. Three units were correlated across the fault. These correlations demonstrate that between 10.3 and 11.6 Ma, the El Paso Mountains lay to the north and directly across the Garlock Fault from the Lava Mountains and that a total of 32-40 km movement of the fault occurred since 10.3 Ma, which implies a displacement rate of about 3.1-3.8 mm/yr.

REFERENCES CITED

Asmerom, Y., Cheng, H., Thomas, R., Hirschmann, M, and Edwards, R.L., 2000, Melting of the Earth's lithospheric mantle inferred from protactinium-thorium-uranium isotopic data: Nature, v. 406, p. 293-296.

Bottinga, Y. and Weill, D.F., 1970, Densities of liquid silicate systems calculated from partial molar volumes of oxide components: American Journal of Science, v. 269, p. 169-182.

Bradshaw, T. K., Hawkesworth, C. J. and Gallagher, K., 1993, Basaltic volcanism in the southern Basin and Range: No role for a mantle plume: Earth and Planetary Science Letters, v. 116, p. 45-62.

Carlson, R.W., and Hart, W.K., 1987, Crustal genesis on the Oregon Plateau: Journal of Geophysical Research, v. 92, p. 6191-6206.

Carter, B.A., 1980, Quaternary displacement on the Garlock Fault, California: in Fife, D.L. and Brown, A.R., eds., Geology and Mineral Wealth of the California Desert: South Coast Geological Society Guidebook: Dibblee Volume: South Coast Geological Society, Santa Ana, p. 457-466.

Carter, B.A., 1982, Neogene displacement on the Garlock Fault, California: Transactions of the American Geophysical Union, v. 63, no. 45, p. 1124.

Carter, B.A., 1987, Quaternary fault-line features of the central Garlock Fault, Kern County, California: Geological Society of America Centennial Field Guide-Cordilleran Section, p. 133-135.

Carter, B.A., 1994, Neogene offsets and displacement rates, central Garlock Fault, California: in Geological Society of America Cordilleran Section Guidebook, San Bernardino, California, p. 348-356.

Cole, P. D., Calder, E. S., Sparks, R. S. J., and Young, S., 1998, Gravitational dome-collapse versus fountain collapse pyroclastic flows formed during the current 1995-97 eruption of Soufriere Hills volcano, Montserrat, West Indies: Abstract volume, Colima Volcano-Sixth International Meeting, Universidad de Colima, p.34.

Cox, B. F., and Diggles, M. F., 1986, Geologic map of the El Paso Mountains Wilderness Study area: U. S. Geologic Survey MF-1827, scale 1:24,000.

Davis, G. A. and Burchfiel, B. C., 1973, Garlock Fault: An intracontinental transform structure, southern California: Geological Society of America Bulletin, v. 84, p. 1407-1422.

Dawson, M.R. and Jacobson, C.E., 1989, Geochemistry and origin of mafic rocks from the Pelona, Orocopia and Rand Schists, southern California: Earth and Planetary Science Letters, v. 92, p. 371-385.

Dibblee, T. W. Jr., 1995, Geology of the Summit Diggings area, northern Mojave Desert, and late Cenozoic Lateral Displacement on the Garlock Fault, *in* The Garlock Fault and El Paso Mountains Guidebook, edited by A Pace, D. Seymour, G.

Roquemore, R. Briones, J. Baldwin and L. Lewis, Santa Anna, South Coast Geological Society, p. 88-94.

Feuerbach, D. L., Smith, E. I., Walker, J. D., and Tangeman, J. A., 1993, The role of the mantle during crustal extension: Constraints from geochemistry of volcanic rocks in the Lake Mead area, Nevada and Arizona: Geological Society of America Bulletin, v. 105, p. 1561-1575.

Gansecki, C. A., Mahood, G. A., McWilliams, M., 1998, New ages for the climactic eruptions at Yellowstone; single-crystal $^{40}Ar/^{39}Ar$ dating identifies contamination: Geology, v. 26, p. 343-346.

Glazner, A. F. and O'Neil, J. R., 1989, Crustal structure of the Mojave Desert, California: Inferences from Sr and O isotope studies of Miocene volcanic rocks: Journal of Geophysical Research, v. 94, p. 7861-7870.

Glazner, A. F., 1989, Recycling of continental crust in Miocene volcanic rocks from the Mojave block, southern California: Geological Society of America Memoir 174, p. 147-168.

Govindaraju, K., 1994, 1994 compilation of working values and sample description for 383 geostandards: Geostandards Newsletter, Special Issue, v. 18, 158 p.

Izett, G. A. and Wilcox, R. E., 1982, Map showing localities and inferred distributions of the Huckleberry Ridge, Mesa Falls and Lava Creek Ash beds (Pearlette Family Ash beds) of Pliocene and Pleistocene age in the western United States and southern Canada: USGS Miscellaneous Investigations Series Map I-1325, scale 1:4,000,000

Jacobson, C. E., 1990, The $^{40}Ar/^{39}Ar$ Geochronology of the Pelona schist and related Rocks, Southern California: Journal of Geophysical Research, v. 94, no. B1, p. 509-528.

Le Bas, M. J., Le Maitre, R. W., Streckeisen, A., and Zanettin, B., 1986, A chemical classification of volcanic rocks based on the total alkali-silica diagram: Journal of Petrology, v. 27, p. 745-750.

Loomis, D. P. and Burbank, D. W., 1988, The stratigraphic evolution of the El Paso basin, southern California: Implication for the Miocene development of the Garlock Fault and uplift of the Sierra Nevada: Geological Society of America Bulletin, v. 100, p. 12-28.

Malin, P. E., Goodman, E. D., Henyey, T. L., Li, Y. G., Okaya, D. A. and Saleeby, J. B., 1995, Significance of seismic reflection beneath a tilted exposure of deep continental crust, Tehachapi Mountains, California: Journal of Geophysical Research, v. 100, p. 2069-2087.

McGill, S. and Sieh, K., 1993, Holocene slip rate of the central Garlock Fault in southeastern Searles Valley, California: Journal of Geophysical Research, v. 98, p. 14217-14231.

McKenzie, D., 1985, Th-U disequilibrium and the melting process beneath ridge axes: Earth and Planetary Science Letters, v. 72, p. 81-91.

Miller, J.S., Glazner, A.F., and Crowe, D.E., 1996, Muscovite-garnet granites in the Mojave Desert: relation to crustal structure of the Cretaceous arc: Geology, v. 24, p. 335-338.

Miller, J.S., Glazner, A.F., Farmer, G.L., Suayah, I.B., and Keith, L.A., 2000, A Sr, Nd and Pb isotopic study of mantle domains and crustal structure from Miocene volcanic rocks in the Mojave Desert, California: Geological Society of America Bulletin, v. 112, p. 1264-1279.

Monastero, F. C., Sabin, A. E. and Walker, J. D., 1997, Evidence for post-early Miocene initiation movement on the Garlock Fault from offset of the Cudahy Camp Formation, east-central California: Geology, v. 25, p 247-250.

Newhall, C. and Voight, B., 1998, A survey of precursors to dome collapse: Abstract volume, Colima Volcano-Sixth International Meeting, Universidad de Colima, p. 31.

Robin, C., Komorowski, J-C., Boudal, C. and Mossand, P., 1990, Mixed magma pyroclastic surge deposits associated with debris avalanche deposits at Colima volcanoes, Mexico: Bulletin of Volcanology, v. 52, p. 391-403.

Seibert, Lee, 1998, Repetitive edifice failure at Augustine Volcano, Alaska and other volcanoes: implications for Volcan de Colima Abstract volume, Colima Volcano-Sixth International Meeting, Universidad de Colima, p. 32-33.

Smith, G. I., and Ketner, K. B., 1970, Lateral displacement on the Garlock Fault, southeastern California, suggested by offset sections of similar metasedimentary rocks: U. S. Geological Survey Professional Paper 700-D, p. D1-D9.

Smith, G. I., 1962, Large lateral displacement on the Garlock Fault, California, as measured from offset dike swarm: American Association of Petroleum Geologist Bulletin, v. 46, p. 85-104.

Smith, G. I., 1964, Geology and volcanic petrology of the Lava Mountains, San Bernardino County, California: U. S. Geological Survey Professional Paper 457, 97 p.

Smith, G. I., 1991, Anomalous folds associated with the east-central part of the Garlock Fault, southeastern California: Geological Society of America Bulletin, v. 103, p. 615-624.

Stoopes, G. R., and Sheridan M. F., 1992, Giant debris avalanches from the Colima volcanic complex, Mexico; implications for long-runout landslides (100 km) and hazard assessment: Geology, v. 20, p. 299-302.

Sun, S. –s., and McDonough, W.F., 1989, Chemical and isotopic systematics of oceanic basalts: implications for mantle composition and processes: in A. D. Saunders and M.J. Norry (eds), "Magmatism in the Ocean Basins, Geological Society of London Special Publication 41, p. 313-314.

Wilshire, H. G., Meyer, C. E., Nakata, J. K., Calk, L. C., Shervais, J. W., Nielson, J. E. and Schwartzman, E. C., 1988, Mafic and ultramafic xenoliths from volcanic rocks of the western United States: U. S. Geological Survey Professional Paper 1443, 179 p.

Wilson, M., 1989, Igneous Petrogenesis: London, Uwin Hyman, 466 p.

APPENDIX I

MAJOR ELEMENT OXIDE AND TRACE ELEMENT CONCENTRATIONS

Major element oxide, trace and rare earth element concentrations. Tl, Lava Mountains Andesite; Ta, Almond Mountain Volcanic rocks; Tds, Dove Spring Fm.; Tsd, Summit Diggings andesite; Ttw, Teagle Wash basalt; Tbh, Black Hills dacite; Tv, Tertiary volcanic rocks; Tr; Tertiary rhyolite; Tsr, Summit Range dacite; Td, Tertiary diorite; Tt, Tertiary tuff; Ti, Tertiary intrusive rocks; Tbp, volcanic clast in Bedrock Spring Fm.; Ka, Atolia Quartz Monzonite; Kg, Cretaceous granodiorite; Mzr, Rand Schist; Mzg, Mesozoic granitic rocks.

	Lava Mountains Andesite (Tl)								
Sample	LM96-1	LM96-4	LM96-4X	LM96-5	LM96-6	LM97-20	LM97-23	LM97-23X	LM97-24X
long (°W)	117.425	117.548	117.548	117.437	117.437	117.520	117.520	117.520	117.520
lat (°N)	35.368	35.452	35.452	35.360	35.360	35.437	35.438	35.438	35.438
SiO_2	66.50	63.35	58.09	65.34	65.40	63.65	64.41	58.52	59.20
TiO_2	0.48	0.70	0.92	0.47	0.47	0.69	0.67	0.97	1.02
Al_2O_3	16.86	17.03	15.64	16.52	16.05	16.38	16.57	17.57	17.46
Fe_2O_3T	3.44	4.38	5.78	3.36	3.24	3.94	3.97	5.39	5.17
MnO	0.06	0.06	0.10	0.06	0.06	0.06	0.06	0.09	0.09
MgO	1.60	2.78	4.77	1.54	1.51	2.41	2.36	4.12	4.62
CaO	3.88	4.65	6.43	3.80	4.14	4.34	4.43	6.76	6.58
Na_2O	4.27	4.18	3.49	4.07	4.03	3.82	4.14	3.75	3.80
K_2O	2.42	2.31	1.54	2.50	2.57	2.68	2.66	2.13	2.14
P_2O_5	0.19	0.23	0.39	0.15	0.18	0.23	0.19	0.45	0.38
LOI	0.86	0.82	0.50	2.27	1.82	1.76	1.45	1.56	1.35
Total	100.6	100.5	97.7	100.1	99.5	99.9	100.9	101.3	101.8
Rb	40.8	33.6	23.0	39.6	40.8	48.7	40.9	35.0	37.0
Th	2.70	2.63	2.57	2.76	3.10	2.64	2.82	2.94	3.03
Ba	1273	1246	1532	1323	1303	1395	1409	1364	1331
Sr	843	783	1101	763	787	802	775	1103	1111
La	17.46	25.19	28.18	18.82	17.19	25.53	27.19	34.54	32.78
Ce	32.9	46.54	52.98	34.66	32.18	46.57	47.29	62.65	58.08
Pr	3.68	5.19	6.15	3.93	3.66	5.14	5.19	7.22	7.00
Nd	14.4	19.76	24.09	15.34	14.47	19.52	20.51	29.01	28.56
Sm	3.2	3.85	4.73	3.27	3.05	3.68	3.80	5.33	5.41
Eu	0.96	1.11	1.44	0.94	0.90	1.01	1.06	1.47	1.50
Gd	2.72	2.93	3.69	2.78	2.65	2.89	2.97	4.14	4.22
Tb	0.41	0.41	0.51	0.42	0.40	0.40	0.41	0.56	0.56
Dy	2.3	2.21	2.74	2.38	2.30	2.19	2.29	3.03	3.14
Ho	0.45	0.40	0.51	0.47	0.45	0.40	0.42	0.56	0.57
Er	1.2	1.03	1.26	1.25	1.15	1.04	1.06	1.39	1.36
Tm	0.18	0.15	0.15	0.17	0.18	0.15	0.15	0.20	0.19
Yb	1.08	0.86	1.02	1.14	1.07	0.86	0.91	1.14	1.12
Lu	0.17	0.13	0.17	0.18	0.17	0.14	0.15	0.18	0.18
Y	12.5	11.1	16.0	13.3	12.5	11.4	13.4	15.1	16.7
Cs	1.95	1.11	0.75	1.92	1.96	1.21	1.21	0.95	1.06
Nb	8.58	8.49	10.08	7.65	7.78	7.09	1.28	5.02	10.50
Hf	4.32	3.69	3.51	3.37	3.29	3.93	4.04	3.91	3.80
Zr	213	168	190	147	151	195	206	227	219
Sc	6.2	9.0	14.8	6.4	6.3	8.0	8.6	12.8	13.3
Cr	23.1	48.5	147	19.2	22.8	30.9	31.4	86.0	101
Ni	20.2	65.6	129	12.5	14.7	41.5	48.5	71.8	85.6

	Lava Mountains Andesite (Tl)					*Almond Mountain Volcanic rocks (Ta)*			
Sample	LM97-25X	LM97-26	LM97-27	LM97-28X	LM97-47	LM96-7	LM96-8	LM96-16	LM96-17
long (°W)	117.520	117.527	117.527	117.548	117.478	117.440	117.542	117.555	117.538
lat (°N)	35.438	35.448	35.447	35.452	35.425	35.365	35.428	35.428	35.432
SiO_2	58.57	65.65	64.47	59.14	64.1	66.33	68.16	65.39	62.23
TiO_2	0.95	0.63	0.61	1.02	0.62	0.59	0.57	0.56	0.64
Al_2O_3	17.09	16.45	15.68	17.00	17.4	16.75	16.86	16.60	16.46
Fe_2O_3T	5.49	3.72	3.70	5.56	3.82	3.46	3.37	3.29	3.68
MnO	0.07	0.05	0.05	0.07	0.06	0.06	0.02	0.04	0.09
MgO	3.80	1.98	1.88	4.26	2.01	1.62	0.250	1.61	1.98
CaO	6.46	3.85	3.86	6.34	4.20	3.90	3.48	4.05	3.62
Na_2O	3.94	4.21	3.91	3.97	3.65	3.75	4.14	4.27	2.63
K_2O	1.96	2.60	2.74	2.06	2.32	2.78	2.69	2.49	3.07
P_2O_5	0.57	0.19	0.16	0.32	0.22	0.19	0.13	0.17	0.17
LOI	1.78	1.63	2.14	1.25	3.30	1.63	0.76	1.54	5.44
Total	100.7	101.0	99.5	101.0	101.7	101.0	100.4	100.0	100.0
Rb	31.6	47.4	49.1	31.5	50.1	38.5	42.3	48.2	61.5
Th	2.67	2.81	2.74	2.64	3.45	2.26	2.58	2.37	2.99
Ba	1433	1295	1288	1208	1141	1283	1343	1277	1247
Sr	1064	663	638	977	713	642	625	743	736
La	32.09	23.90	23.80	28.26	24.84	20.95	18.47	17.77	24.99
Ce	58.05	43.13	42.32	53.13	42.54	37.49	34.52	30.28	45.68
Pr	6.89	4.85	4.81	6.36	4.91	4.20	3.53	3.53	4.95
Nd	27.67	18.86	19.02	25.97	18.96	16.57	13.34	13.78	19.13
Sm	5.23	3.59	3.72	5.17	3.71	3.31	2.63	2.65	3.58
Eu	1.50	0.99	0.98	1.47	1.01	0.98	0.78	0.83	1.01
Gd	4.01	3.04	3.03	4.11	3.06	2.74	2.06	2.23	3.02
Tb	0.55	0.43	0.45	0.56	0.43	0.39	0.29	0.31	0.42
Dy	2.85	2.45	2.59	3.01	2.47	2.16	1.51	1.71	2.36
Ho	0.53	0.45	0.48	0.54	0.48	0.42	0.29	0.31	0.45
Er	1.30	1.16	1.22	1.39	1.17	1.05	0.71	0.76	1.10
Tm	0.18	0.17	0.18	0.18	0.17	0.15	0.10	0.11	0.17
Yb	1.02	1.02	1.08	1.13	1.02	0.93	0.61	0.66	0.99
Lu	0.16	0.17	0.17	0.17	0.16	0.15	0.09	0.10	0.16
Y	17.6	16.7	14.1	17.2	15.3	11.6	8.05	8.48	12.57
Cs	0.96	1.26	0.91	1.01	1.44	1.22	1.26	0.84	3.69
Nb	8.04	5.65	6.86	6.86	8.29	7.84	7.44	6.51	9.52
Hf	3.71	4.30	4.27	3.77	4.16	3.67	3.60	3.76	4.30
Zr	224	201	206	208	193	156	157	181	204
Sc	11.6	7.0	6.6	12.7	7.0	7.0	6.2	7.0	6.8
Cr	81			93.3		23.4	24.6	26.1	27.4
Ni	85.3	29.5	25.7	101		22.0	16.0	21.5	26.6

Almond Mountain Volcanic rocks (Ta)

Sample	LM97-22	LM97-38	LM98-46	LM98-48	LM98-K1	LM98-K2	LM98-K4	LM98-K6	LM98-K7
long (°W)	117.533	117.507	117.438	117.477	117.558	117	117	117.555	117.560
lat (°N)	35.445	35.385	35.375	35.425	35.408	35	35	35.427	35.428
SiO_2	63.54	66.88	61.0	63.5	63.05	64.20	66.49	64.20	65.05
TiO_2	0.58	0.55	0.56	0.67	0.56	0.60	0.51	0.51	0.47
Al_2O_3	16.42	16.37	16.8	17.2	16.66	16.56	16.17	15.56	15.40
Fe_2O_3T	3.51	3.29	3.82	4.33	3.47	3.53	3.12	3.04	2.69
MnO	0.06	0.05	0.19	0.07	0.04	0.06	0.05	0.05	0.04
MgO	2.14	0.89	1.44	1.98	1.34	1.76	0.88	1.18	1.07
CaO	3.80	3.37	4.23	4.38	3.82	3.77	3.10	3.40	2.84
Na_2O	3.27	3.58	3.06	4.14	3.00	3.84	3.56	3.24	2.98
K_2O	3.07	2.70	2.32	2.30	2.94	2.44	2.66	2.77	2.80
P_2O_5	0.20	0.18	0.05	0.25	0.18	0.18	0.16	0.19	0.16
LOI	3.42	2.13	8.20	1.11	4.95	3.07	3.29	5.32	6.51
Total	100.0	100.0	101.8	99.9	100.0	100.0	100.0	99.4	100.0
Rb	68.6	52.1	41.4	46.1	76.8	57.0	44.3	52.8	55.8
Th	3.32	3.38	3.38	3.13	3.01	2.86	2.92	3.07	3.41
Ba	1080	1348	1140	1283	1192	1296	1380	1533	1445
Sr	737	627	706	797	654	783	664	609	576
La	24.41	23.88	21.89	24.01	17.99	20.29	18.09	25.67	24.82
Ce	44.22	41.75	37.99	43.91	33.54	36.52	33.31	45.28	44.15
Pr	4.91	4.60	4.51	4.91	3.89	4.11	3.61	4.95	4.89
Nd	19.24	17.39	17.62	18.99	14.84	15.69	13.94	18.96	17.72
Sm	3.81	3.08	3.37	3.62	2.94	3.11	2.76	3.59	3.51
Eu	1.01	0.86	0.85	0.99	0.81	0.83	0.77	0.94	0.89
Gd	3.11	2.57	2.76	2.97	2.52	2.72	2.20	2.78	2.63
Tb	0.45	0.35	0.40	0.42	0.40	0.38	0.34	0.39	0.37
Dy	2.54	1.93	2.26	2.36	2.20	2.17	1.91	2.22	2.04
Ho	0.49	0.37	0.42	0.45	0.43	0.42	0.36	0.40	0.38
Er	1.23	0.94	1.07	1.14	1.14	1.10	0.93	1.06	0.96
Tm	0.18	0.13	0.16	0.16	0.16	0.15	0.13	0.15	0.13
Yb	1.09	0.78	0.97	0.97	0.99	0.93	0.81	0.91	0.83
Lu	0.17	0.12	0.15	0.15	0.16	0.15	0.14	0.15	0.14
Y	13.58	7.18	9.30	12.00	12.57	11.50	9.63	11.60	10.14
Cs	1.95	0.81	1.29	1.26	3.09	1.00	0.86	1.12	1.08
Nb	9.07	6.86	7.20	7.16	6.30	6.87	6.52	7.88	6.44
Hf	3.98	3.93	4.00	3.82	3.12	3.75	3.44	4.60	4.11
Zr	186	173	181	193	160	183	163	209	200
Sc	7.3	6.2	7.7	7.6	6.8	6.9	5.8	7.6	4.5
Cr	31.4	108	45		24.0				
Ni	29.9	250	234						

	Almond Mountain Volcanic rocks (Ta)						*Dove Spring Fm. (Tds)*		
Sample	LM98-K8	LM98-K9	LM98-K10	LM98-K11	LM98-K12	LM98-K13	LM98-K14	LM98-K15	LM98-K16
long (°W)	117.560	117.560	117.560	117.558	117.440	117.438	117.978	117. 980	117.982
lat (°N)	35.428	35.428	35.428	35.427	35.375	35.378	35.370	35.352	35.363
SiO_2	65.02	65.31	64.85	64.50	61.97	66.47	69.80	66.20	71.16
TiO_2	0.47	0.49	0.51	0.55	0.60	0.53	0.07	0.12	0.16
Al_2O_3	15.34	15.76	16.06	15.45	16.69	16.64	12.16	14.02	12.18
Fe_2O_3T	2.67	2.85	2.94	3.44	3.71	3.33	0.92	3.07	2.98
MnO	0.04	0.04	.04	0.06	0.05	0.06	0.05	0.05	0.06
MgO	0.96	1.32	1.21	1.23	1.58	1.11	0.45	0.35	0.47
CaO	3.23	3.14	3.03	3.63	3.65	3.75	0.90	1.51	0.91
Na_2O	2.98	2.79	2.47	3.81	2.05	4.33	2.98	2.70	1.93
K_2O	3.20	2.78	2.60	3.09	2.48	2.53	2.36	3.08	2.38
P_2O_5	0.20	0.17	0.17	0.22	0.22	0.17	0.04	0.06	0.04
LOI	5.89	5.35	6.12	4.02	7.01	1.08	9.94	8.85	7.25
Total	100.0	100.0	100.0	100.0	100.0	100.0	99.7	100.0	99.5
Rb	53.7	51.4	48.7	53.4	49.5	53.4	103	169	110
Th	3.29	3.52	3.46	3.02	3.10	2.92	11.66	10.11	6.38
Ba	1445	1423	1323	1552	1173	1531	633	418	398
Sr	589	592	588	650	762	675	150	150	129
La	24.77	26.54	25.18	26.81	20.88	20.97	14.42	12.99	12.73
Ce	43.36	47.04	46.43	47.13	37.00	36.73	24.71	21.86	15.89
Pr	4.82	5.17	4.95	5.07	4.21	4.02	2.17	1.58	1.43
Nd	18.29	18.54	18.40	19.24	16.6	15.67	8.67	7.42	5.19
Sm	3.34	3.43	3.43	3.61	3.24	2.96	1.76	1.55	1.08
Eu	0.87	0.88	0.89	1.01	0.86	0.83	0.18	0.20	0.21
Gd	2.59	2.57	2.68	2.96	2.72	2.55	1.56	1.29	0.85
Tb	0.38	0.38	0.39	0.42	0.39	0.37	0.26	0.18	0.13
Dy	2.04	1.99	2.17	2.29	2.26	2.13	1.35	0.88	0.67
Ho	0.39	0.38	0.38	0.43	0.43	0.39	0.25	0.14	0.12
Er	0.99	1.01	1.01	1.08	1.10	1.02	0.62	0.30	0.27
Tm	0.14	0.14	0.14	0.15	0.16	0.14	0.09	0.04	0.04
Yb	0.86	0.85	0.87	0.95	0.95	0.83	0.54	0.24	0.23
Lu	0.14	0.14	014	0.15	0.16	0.13	0.08	0.04	0.04
Y	10.69	10.59	12.30	12.20	10.95	6.76	6.76	3.54	2.91
Cs	1.08	1.21	1.05	1.14	1.31	0.80	7.57	17.85	7.74
Nb	6.28	6.67	7.18	7.56	6.89	5.75	4.84	11.30	11.84
Hf	4.25	4.23	4.46	4.46	3.80	3.38	2.68	2.91	2.71
Zr	195	197	207	212	181	166	83	82	95
Sc	4.7	5.0	5.2	5.6	7.3	7.0	1.6	3.6	3.7
Cr									
Ni									

	Dove Spring Fm. (Tds)			*Summit Diggings andesite (Tsd)*					*Ttw*
Sample	LM98-K17	LM98-K18	LM98-K19	LM96-2	LM96-3	LM96-11	LM96-12	LM97-21	LM96-13
long (°W)	117.978	117.975	117.982	117.547	117.543	117.620	117.617	117.532	117.413
lat (°N)	35.363	35.423	35.383	35.448	35.448	35.445	35.458	35.440	35.497
SiO_2	70.53	42.46	52.20	63.32	63.32	62.63	62.82	62.58	50.62
TiO_2	0.06	0.43	1.44	0.72	0.70	0.59	0.60	0.64	1.37
Al_2O_3	11.90	8.67	15.05	16.85	17.50	16.92	17.41	17.22	14.41
Fe_2O_3T	0.66	2.61	10.27	4.43	4.41	4.57	4.77	3.87	10.98
MnO	0.03	0.07	0.15	0.06	0.07	0.05	0.09	0.03	0.15
MgO	0.39	1.52	6.22	3.09	2.99	2.54	2.74	1.72	6.87
CaO	1.28	21.18	8.92	4.73	4.81	4.80	5.07	4.07	9.85
Na_2O	2.74	1.25	2.50	4.11	4.21	4.05	3.98	4.34	2.77
K_2O	1.73	1.28	0.58	2.29	2.16	2.16	2.17	2.62	0.91
P_2O_5	0.04	0.23	0.29	0.22	0.23	0.21	0.19	0.19	0.30
LOI	11.29	20.28	2.37	1.49	1.49	2.52	1.38	1.23	1.38
Total	100.7	100.0	100.0	101.3	101.9	101.0	101.2	98.5	99.6
Rb	83.6	50.6	17.3	38.4	32.4	64.5	65.4	52.1	16.7
Th	12.50	4.98	2.97	2.72	2.53	6.79	6.54	1.96	2.04
Ba	531	503	390	1263	134	1019	1039	1189	393
Sr	239	343	343	798	810	1025	1011	713	446
La	7.25	22.57	17.13	26.00	25.09	16.06	17.51	18.01	16.68
Ce	13.68	33.14	33.13	48.14	45.74	29.28	32.18	32.71	33.41
Pr	1.43	4.74	3.82	5.36	5.15	3.44	3.71	3.74	4.11
Nd	5.07	18.61	16.14	20.60	19.80	14.08	14.90	15.02	1.64
Sm	1.14	3.95	4.65	4.09	4.02	2.81	3.21	3.04	4.44
Eu	0.07	0.95	1.46	1.18	1.15	0.97	0.99	0.89	1.48
Gd	1.10	3.75	4.70	3.12	3.04	2.69	2.86	2.60	4.36
Tb	0.19	0.62	0.76	0.44	0.43	0.41	0.42	0.37	0.70
Dy	1.11	3.51	4.79	2.39	2.32	2.19	2.41	2.11	4.10
Ho	0.21	0.74	0.89	0.44	0.44	0.45	0.46	0.39	0.78
Er	0.56	2.21	2.22	1.11	1.07	1.16	1.21	0.99	1.97
Tm	0.08	0.32	0.30	0.16	0.15	0.16	0.17	0.14	0.28
Yb	0.50	1.84	1.90	0.96	0.95	1.02	1.06	0.88	1.60
Lu	0.07	0.31	0.28	0.15	0.14	0.17	0.17	0.14	0.24
Y	2.97	24.23	22.79	12.00	11.60	7.73	12.71	11.23	20.36
Cs	3.57	2.99	0.27	1.23	1.06	2.26	5.16	0.85	0.61
Nb	9.85	7.82	11.01	8.19	8.45	5.89	5.23	6.03	9.26
Hf	2.55	2.63	2.95	3.82	3.74	2.91	2.97	3.56	2.69
Zr	90	101	107	174	176	161	172	180	116
Sc	1.4	7.7	24.7	9.4	9.1	10.7	10.7	6.5	23.3
Cr			203	51.4	44.2	48.9	38.9	19.1	322
Ni			93.4	57.6	53.0	55.8	34.8	9.5	138

	Teagle Wash basalt (Ttw)			*Black Hills dacite (Tbh)*			*Tv*		*Tr*
Sample	LM96-14	LM99-50	LM99-59	LM97-37	LM98-44	LM98-45	LM96-15	LM97-18	LM97-19
long (°W)	117.413	117.401	117.431	117.322	117.298	117.298	117.573	117.540	117.500
lat (°N)	35.497	35.502	35.445	35.352	35.333	35.333	35.453	35.451	35.428
SiO_2	51.32	52.38	52.74	63.44	64.08	63.8	68.42	62.04	71.31
TiO_2	1.40	1.39	1.39	0.60	0.64	0.61	0.44	1.16	0.26
Al_2O_3	14.54	15.16	15.18	17.21	17.26	17.5	15.75	19.50	15.76
Fe_2O_3T	11.08	11.10	11.23	4.35	4.40	4.25	2.76	2.42	2.20
MnO	0.15	0.15	0.20	0.07	0.07	0.07	0.05	0.06	0.06
MgO	6.31	6.83	6.28	1.71	2.55	2.37	0.47	0.35	0.39
CaO	10.05	9.70	12.78	5.28	4.44	5.17	3.06	5.42	2.28
Na_2O	2.78	2.72	2.53	3.80	4.20	4.04	3.53	3.73	4.15
K_2O	0.96	1.01	0.31	2.20	2.25	2.37	3.05	2.81	3.29
P_2O_5	0.29	0.31	0.19	0.22	0.20	0.27	0.14	0.25	0.07
LOI	1.53	1.12		1.97	0.85	1.15	2.76	4.42	0.96
Total	100.4	101.9	100.7	100.9	101.7	101.6	100.4	102.2	100.7
Rb	15.5	18.3	22.77	47.2	57.2	56.2	92.1	87.0	67.7
Th	2.05	3.09		5.15	6.09	5.78	6.55	7.11	2.84
Ba	413	443		1579	1227	1195	1042	652	1594
Sr	459	457	462	885	996	1008	456	374	527
La	16.68	18.67		24.81	15.66	14.95	20.37	25.19	24.35
Ce	33.35	36.96		41.83	29.12	28.00	34.58	47.85	41.23
Pr	4.12	4.46		5.19	3.41	3.28	3.73	5.44	4.38
Nd	17.76	19.06		20.49	13.58	13.06	14.06	21.55	15.89
Sm	4.44	4.74		4.02	2.76	2.68	2.90	5.13	2.77
Eu	1.48	1.51		1.10	0.86	0.79	0.74	1.52	0.69
Gd	4.48	4.67		3.82	2.68	2.43	2.64	4.87	2.41
Tb	0.71	0.74		0.55	0.39	0.36	0.42	0.80	0.35
Dy	4.19	4.39		3.24	2.18	2.16	2.51	4.81	2.16
Ho	0.80	0.85		0.63	0.43	0.40	0.47	0.96	0.41
Er	2.04	2.14		1.63	1.13	1.02	1.31	2.63	1.10
Tm	0.28	0.30		0.23	0.15	0.15	0.20	0.39	0.17
Yb	1.63	1.76		1.36	0.92	0.92	1.27	2.47	1.10
Lu	0.25	0.27		0.21	0.16	.015	0.20	0.39	0.19
Y	21.3	21. 9		19.2	8.3	10.7	14.4	26.2	12.9
Cs	0.54	095		2.13	3.12	1.94	2.79	3.10	1.28
Nb	9.63	9.75	8.53	6.48	5.67	5.38	11.84	13.52	8.36
Hf	2.74	2.89		3.42	3.15	3.01	3.63	5.22	4.4
Zr	112	107	106	176	166	171	152	211	183
Sc	24.4	24.2		8.4	9.2	9.1	4.4	14.8	1.2
Cr	338	349	331	27.5	32.0	30.0	21.0	29.5	11.1
Ni	148	154	133	175			15.7	18.0	7.2

	Tsr	*Kg*	*Tr*	*Td*	*Mzg*	*Mzg*	*Ka*	*Tr*	*Ti*
Sample	LM97-29	LM97-30	LM97-31	LM97-32	LM97-33	LM97-34	LM97-35	LM97-36	LM98-40
long (°W)	117.603	117	117	117	117.268	117.365	117.527	117	117.577
lat (°N)	35.463	35	35	35	35.356	35.338	35.460	35	35.405
SiO_2	67.89	65.47	75.63	54.58	68.76	76.64	69.08	75.26	65.41
TiO_2	0.42	0.87	0.06	1.63	0.32	0.07	0.62	0.20	0.64
Al_2O_3	15.34	17.16	14.30	17.41	16.60	13.27	15.75	14.08	16.77
Fe_2O_3T	2.84	4.18	0.71	8.19	2.69	0.41	3.29	0.71	3.44
MnO	0.07	0.06	0.04	0.14	0.11	0.03	0.05	0.001	0.04
MgO	0.479	1.45	0.075	4.05	0.755	0.046	0.797	0.204	1.57
CaO	4.87	4.39	0.69	7.13	4.13	0.47	2.78	0.23	4.00
Na_2O	4.03	3.62	3.42	3.96	4.24	3.58	3.60	2.69	3.26
K_2O	3.36	2.69	4.46	1.49	2.08	4.86	3.42	4.36	2.78
P_2O_5	0.13	0.24	0.02	0.27	0.12	0.03	0.05	0.02	0.22
LOI	2.77	0.41	0.49	2.76	0.63	0.22	1.13	1.44	3.18
Total	102.2	100.5	99.9	101.6	100.4	99.6	100.7	99.2	101.3
Rb	94.7	68.0	205	31.7	49.0	262	105	173	79.6
Th	8.58	8.39	15.0	3.48	2.96	26.8	11.2	14.6	4.24
Ba	887	1358	389	394	1034	62	998	871	12.67
Sr	559	819	87.9	385	556	72	562	95	784
La	21.77	46.96	13.40	17.20	16.9	15.02	31.63	38.17	26.96
Ce	37.56	79.81	23.16	32.45	27.30	10.91	57.62	65.35	48.14
Pr	4.12	8.62	2.53	3.86	2.87	0.61	6.15	6.72	5.41
Nd	15.81	32.64	9.71	16.20	10.33	1.59	23.03	23.34	20.27
Sm	3.29	6.25	3.09	4.19	2.09	0.22	4.42	4.65	3.74
Eu	0.71	1.50	0.36	1.51	0.68	0.07	1.03	0.52	0.92
Gd	2.96	4.28	3.85	4.45	1.91	0.16	3. 15	3.90	3.22
Tb	0.47	0.57	0.79	0.74	0.30	0.02	0.41	0.62	0.45
Dy	2.82	2.87	5.16	4.66	180	0.13	2.16	3.75	2.60
Ho	0.57	0.49	1.06	0.94	0.36	0.03	0.38	0.75	0.48
Er	1.54	1.15	2.89	2.54	1.08	0.08	091	2.10	1.25
Tm	0.23	0.16	0.43	0.36	0.17	0.02	0.13	0.32	0.18
Yb	1.43	0.92	2.78	2.35	1.20	0.13	0.78	2.08	1.14
Lu	0.22	0.14	0.42	0.36	0.22	0.03	0.13	0.33	0.16
Y	18.7	9.87	27.3	27.6	5.12		5.88	13.2	9.3
Cs	5.18	1.12	2.58	0.53	2.50	5.00	1.58	5.41	2.03
Nb	4.86	13.91	14.72	14.86	8.16	2.19	11.75	12.78	8.58
Hf	3.60	5.33	3.45	3.80	2.70	2.78	4.80	5.34	4.32
Zr	171	253	70.9	178	124	57.1	198	181	213
Sc	4.8	5.6	1.3	24.2	3.9	1.5	4.0	2.6	6.7
Cr				86.7			30.0		
Ni	15.3	12.3	12.6	43.3	9.3	4.9	319	14.1	

	Tv	*Tt*	*Tbp*	*Tt*	*Mzr*	*Tv*	*Tds*
Sample	LM98-49	LM99-51	LM99-53	LM99-54	LM99-57	LM99-58	RRC970704-a
long (°W)	117	117.405	117.440	117.442	117.650	117.601	
lat (° N)	35	35.504	35.445	35.467	35.387	35.467	
SiO_2	73.81	70.36	64.26	72.65	49.12	75.46	52.36
TiO_2	0.44	0.07	0.61	0.06	1.61	0.27	1.25
Al_2O_3	15.41	13.47	16.78	14.99	14.37	12.99	14.9
Fe_2O_3T	0.49	1.33	3.77	1.09	11.23	1.18	11.0
MnO	0.002	0.02	0.04	0.03	0.20	0.03	0.02
MgO	0.02	0.29	1.28	0.53	6.58	0.35	8.11
CaO	2.34	1.06	4.24	1.01	12.78	0.34	9.08
Na_2O	3.74	2.83	1.05	2.89	2.53	1.03	2.64
K_2O	3.11	4.06	2.59	3.67	0.31	7.20	0.03
P_2O_5	0.14	0.04	0.18	0.04	0.19	0.07	0.02
LOI	1.12	5.44	1.33	3.05	2.84	2.65	
Total	100.6	99.0	99.1	100.0	101.8	101.5	99.4
Rb	90.2	204	29.3	135	7.6	194	5.0
Th		13.3	2.63	8.58	0.21	8.10	2.15
Ba		623	1246	640	30	400	235
Sr	475	164	795	251	293	268	366
La		21.57	23.02	13.09	4.14	20.76	12.44
Ce		40.31	41.86	21.74	11.81	35.71	26.84
Pr		4.46	4.59	2.56	1.94	3.61	3.50
Nd		17.43	17.93	9.78	10.72	12.92	14.61
Sm		4.36	3.48	2.90	4.16	2.60	3.50
Eu		0.68	1.00	0.50	1.55	0.52	1.17
Gd		4.23	2.80	2.34	5.52	2.14	3.83
Tb		0.71	0.39	0.31	1.06	0.34	0.68
Dy		4.05	2.16	1.38	7.05	1.99	3.60
Ho		0.74	0.40	0.22	1.52	0.39	0.70
Er		1.79	1.02	0.52	4.12	1.06	1.89
Tm		0.25	0.14	0.07	0.59	0.15	
Yb		1.49	0.84	0.42	3.61	0.97	1.64
Lu		0.22	0.14	0.07	0.57	0.16	0.25
Y	16.9	21.80	11.29	6.72	39.94	11.48	19.39
Cs		7.24	0.21	5.80	0.51	9.90	0.49
Nb	18.0	13.25	7.02	14.68	2.44	7.92	8.9
Hf		3.41	3.81	2.83	2.63	3.10	2.43
Zr	161	98	174	84	92	122	99
Sc		1.8	6.6	1.6	49.0	9.9	21.6
Cr			25.2		351		215
Ni					82.6		117

Major element oxides and trace elements (Rb, Sr, Y, Zr, Cr, Ni) by XRF analysis were done at the Rock Chemistry Laboratory, University of Nevada, Las Vegas. Other trace and rare earth elements by ICP-MS analysis were done at the GeoAnalytical Laboratory, WSU.

VITA

Graduate College
University of Nevada, Las Vegas

Deborah L. Keenan

Local Address:
1555 E. Rochelle, Apt. 143
Las Vegas, Nevada 89119

Degrees:
Bachelor of Science, in Geology, 1996,
Old Dominion University, Norfolk, Virginia

Master of Science, Geology, 2000
University of Nevada, Las Vegas

Publications:

Rees, M.N., Smith, E.I., Duebendorfer, E.M. and Keenan, D.L., 1998, Cambrian marginal basin rifting and subduction recorded in the Ellsworth-Whitmore Mountains Terrane, West Antarctica: *in* Special Abstracts Issue, Gondwana 10: Event Stratigraphy of Gondwana, Journal of African Earth Sciences, v. 27, no. 1A, p. 151-153.

Rees, M.N., Smith, E.I., Keenan, D.L., and Duebendorfer, E.M., 1999, Cambrian Magmatic Rocks of the Ellsworth Mountains, West Antarctica: Antarctic Journal of the United States, Review 1997, v. 32, no. 5, p. 3-5.

Smith, E.I., Sánchez, A., Keenan, D.L., and Monastero, F.C., 1999, Stratigraphy and geochemistry of volcanic rocks in the Lava Mountains, California: implications for the Miocene development of the Garlock Fault: Geological Society of America Abstracts with Programs, v. 31, no. 7, p. 262.

Smith, E.I., Sánchez, A., Keenan, D.L., Monastero, F.C., 2000, Stratigraphy and Geochemistry of Volcanic Rocks in the Lava Mountains, California; Implications for the Miocene Development of the Garlock Fault: *in* Allen Glazner, J.D. Walker and John Bartley, Geologic Evolution of the Central Mojave Desert and Southern Basin and Range; Geological Society of America Special Paper (In press).

Thesis Title:

The Geology and Geochemistry of the Lava Mountains, Mojave Desert, California: Implications for the Miocene Development of the Garlock Fault

Thesis Examination Committee:

Chairperson, Dr. Eugene I. Smith, Ph.D.
Committee Member, Dr. Michael L. Wells, Ph.D.
Committee Member, Dr. Terry Spell, Ph.D.
Graduate Faculty Representative: Dr. Steven Lepp, Ph.D.

Plate 1

35° 27' 30"

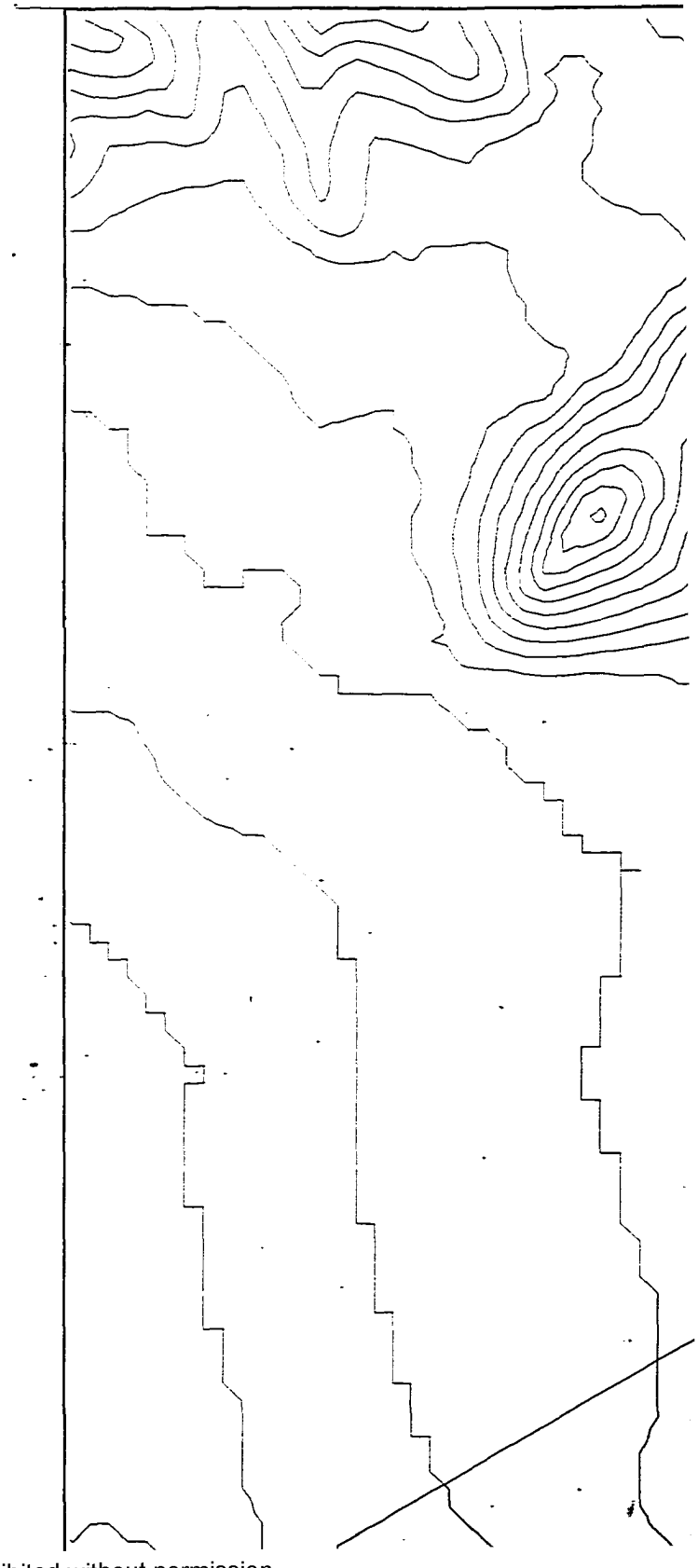

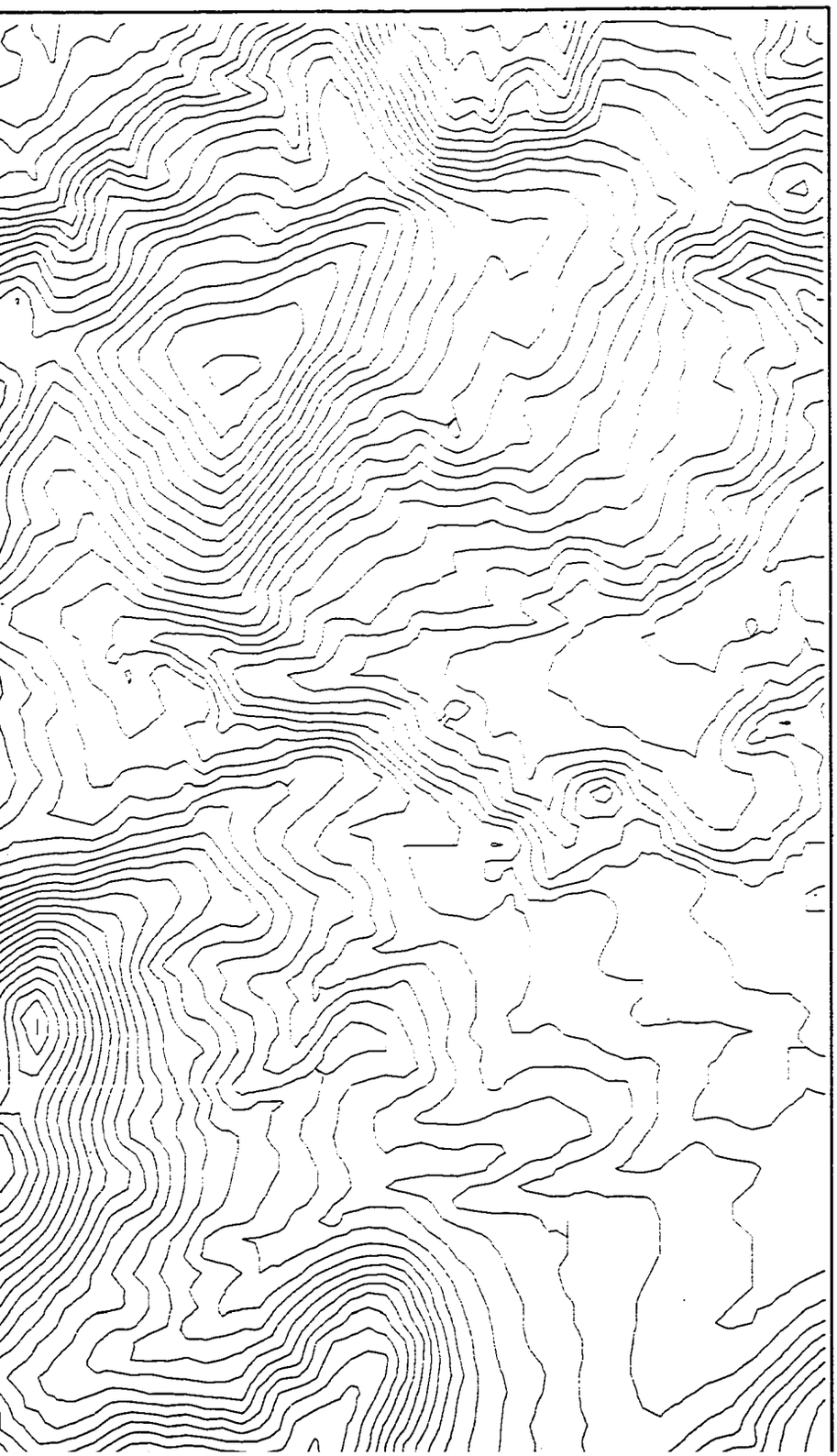

Geologic Map

Debo

Quaternary

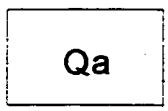

Qa

Quaternary aluvium and fanglomer

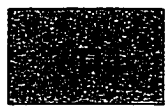

Lava Mountains andesite. Andesi
Porphy
Age 5.8

Almond Mountain volcanic rocks (

Map of the Western Lava Mount

by

eborah L. Keenan and Eugene I

Description of Map Units

fanglomerate deposits

e. Andesite flows that cap mesas and locally cascade over escarpments. Porphyritic plagioclase, hornblende andesite. Locally brecciated at base. Age 5.8-6.4 Ma.

nic rocks (9.5-10.29 Ma).

Mountains, California

gene I. Smith

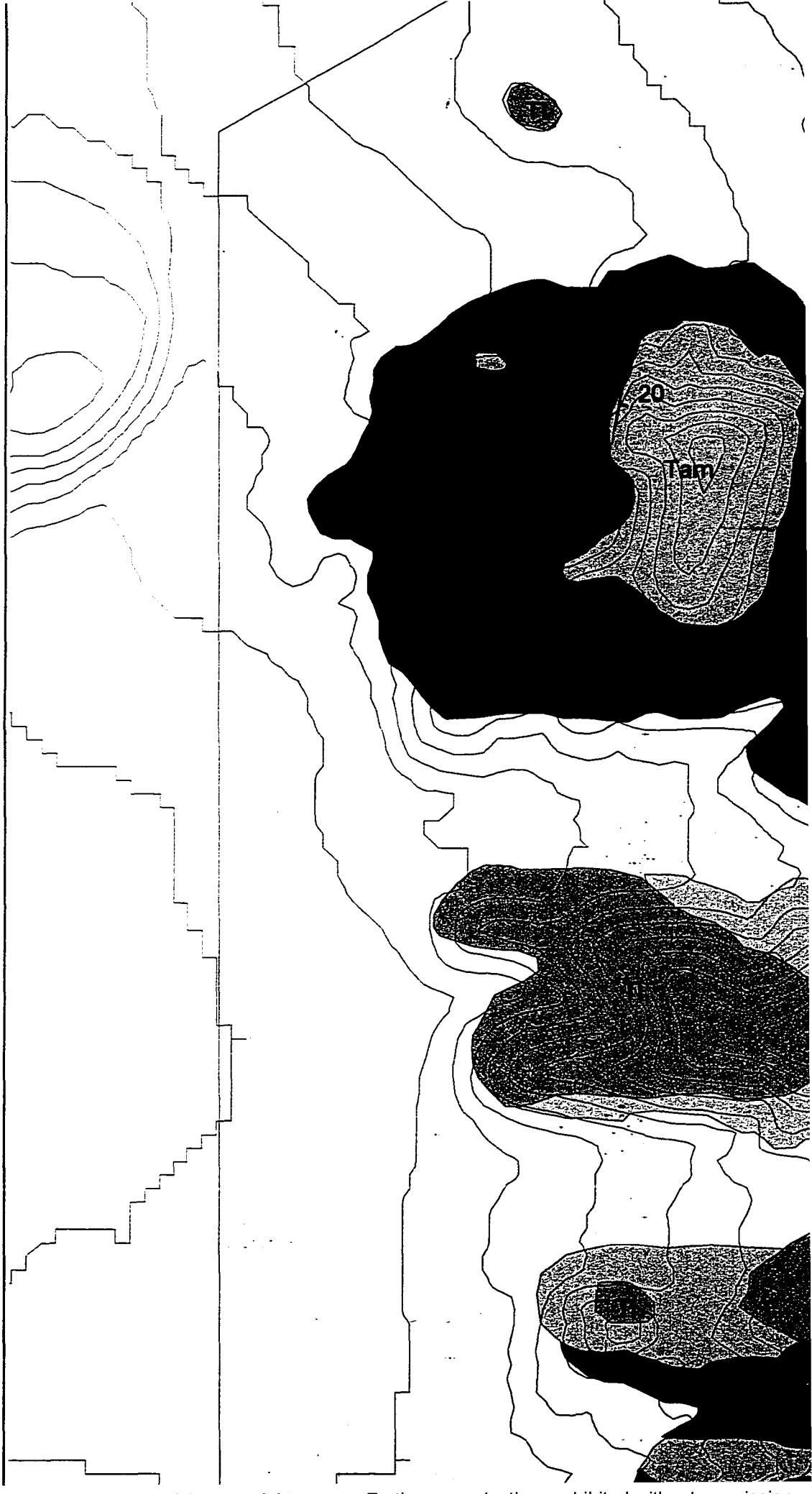

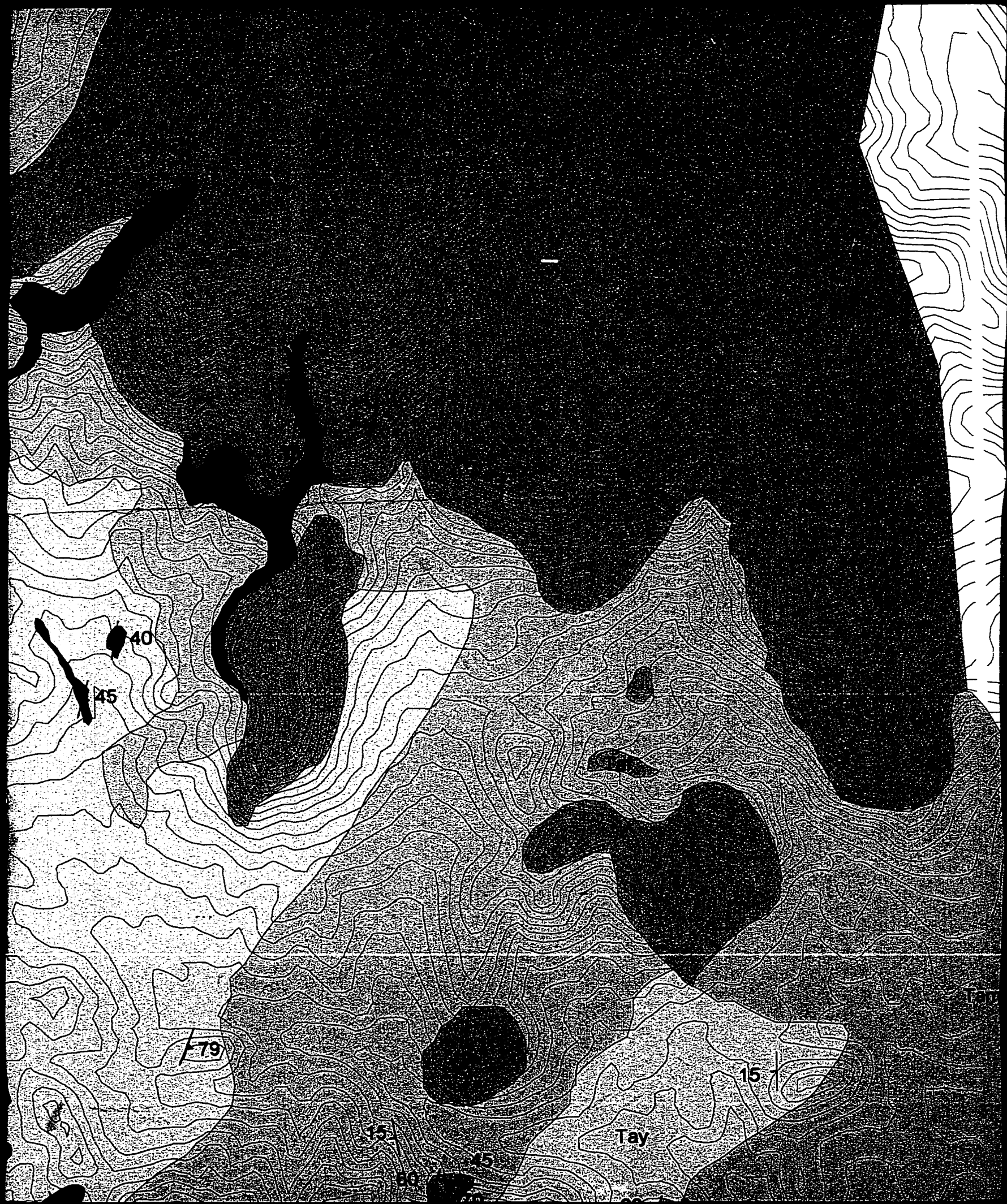

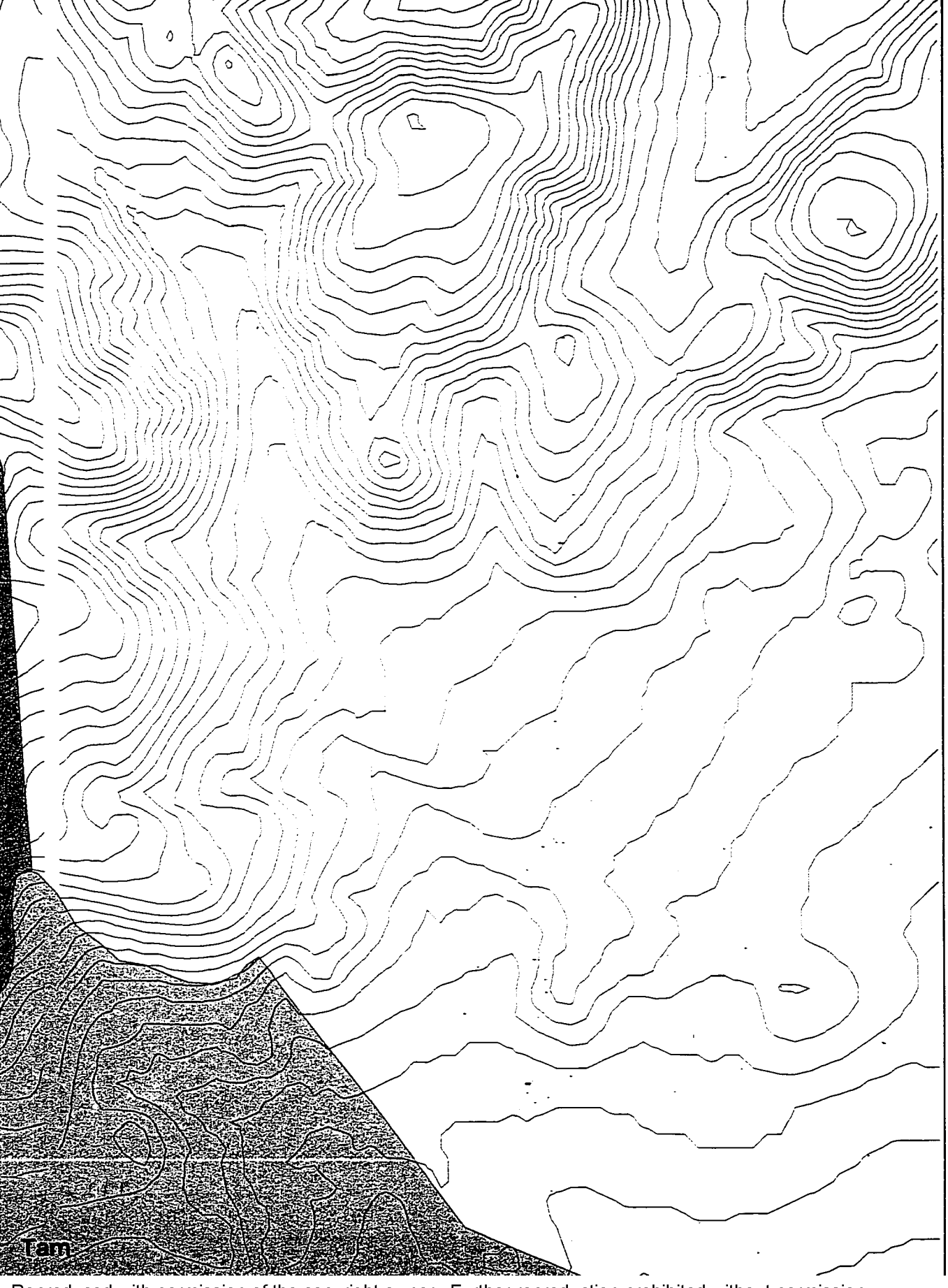

Tertiary

Almond Mountain volcanic ro

Rocks of the Central

Purple dacite

Form
Porp
In pla

Fine-grained dacite

Fine-

Yellow dacite

Form
Porp
calci
Prob
interl

Rocks of the moat

Tam

Moat deposits

Block
centr
the c

Pyroclastic units

In
zo
ar
wi
pu

Bedrock Spring Formation

A
"A
ir

Ages 9.5-10.1 Ma.

Mountain volcanic rocks (9.5-10.29 Ma).

Rocks of the Central Vent Complex

Purple dacite Forms dikes and plugs that intrude yellow dacite and moat rocks. Porphyritic with large (0.5 mm) blocky plagioclase and blade-shaped hornblende. In places matrix is vitric and flow banded.

Fine-grained dacite Fine-grained dacitic plugs that intrude rocks of the central vent complex and moat.

Yellow dacite Forms gently rolling topography in the central vent area of the Western Lava Mountains vo Porphyritic with phenocrysts of plagioclase and subordinate hornblende. Matrix is altered calcite, sericite, cryptocrystalline clay minerals, chlorite and rare epidote. Locally flow ban Probably represents the subvolcanic roots of a volcanic dome complex. Also includes dac interbedded with moat deposits to the east and west of the central vent complex.

Rocks of the moat of the Western Lava Mountains volcano

Moat deposits Block and ash and volcaniclastic deposits. Clasts of dacite up to 4 m. Rocks dip inward to central vent complex and may represent the erosion and explosive destruction of domes o the central vent complex.

Pyroclastic units Includes a dacitic pyroclastic flow at the base of the section that is 4 m thick. Poorly we zonation. Inclusions of andesite and/or dacite typify the tuff. Phenocrysts of sanidine and biotite. Cuspate shards and 0.5-2 cm pumice clasts. Also includes dacitic lapilli tuf with moat breccia. Poorly welded containing phenocrysts of sanidine and biotite. Cont pumice clasts (1-20 cm) and clasts of andesite and dacite.Thickness up to 100 m in cha

k Spring Formation Arkosic sandstone and conglomerate containing some siltstone and limestone. Clasts "Atolia-type" granite; matrix consists of coarse feldspar and quartz. Near contacts with intrusive rocks, sandstone is brick red in color.

We acknowle
the funding fo

ed hornblende.

mplex and moat.

stern Lava Mountains volcano.
lende. Matrix is altered to
pidote. Locally flow banded.
nplex. Also includes dacite flows
vent complex.

4 m. Rocks dip inward toward
e destruction of domes of

t is 4 m thick. Poorly welded without
henocrysts of sanidine
includes dacitic lapilli tuff interbedded
nidine and biotite. Contains large
kness up to 100 m in channels.

e and limestone. Clasts are mainly
uartz. Near contacts with

We acknowledge the U.S. Navy's Geothermal Project Office for providing the funding for this project. We especially thank Francis C. Monastero (Navy GPO) for his interest and support. We thank Alexander Sanchez

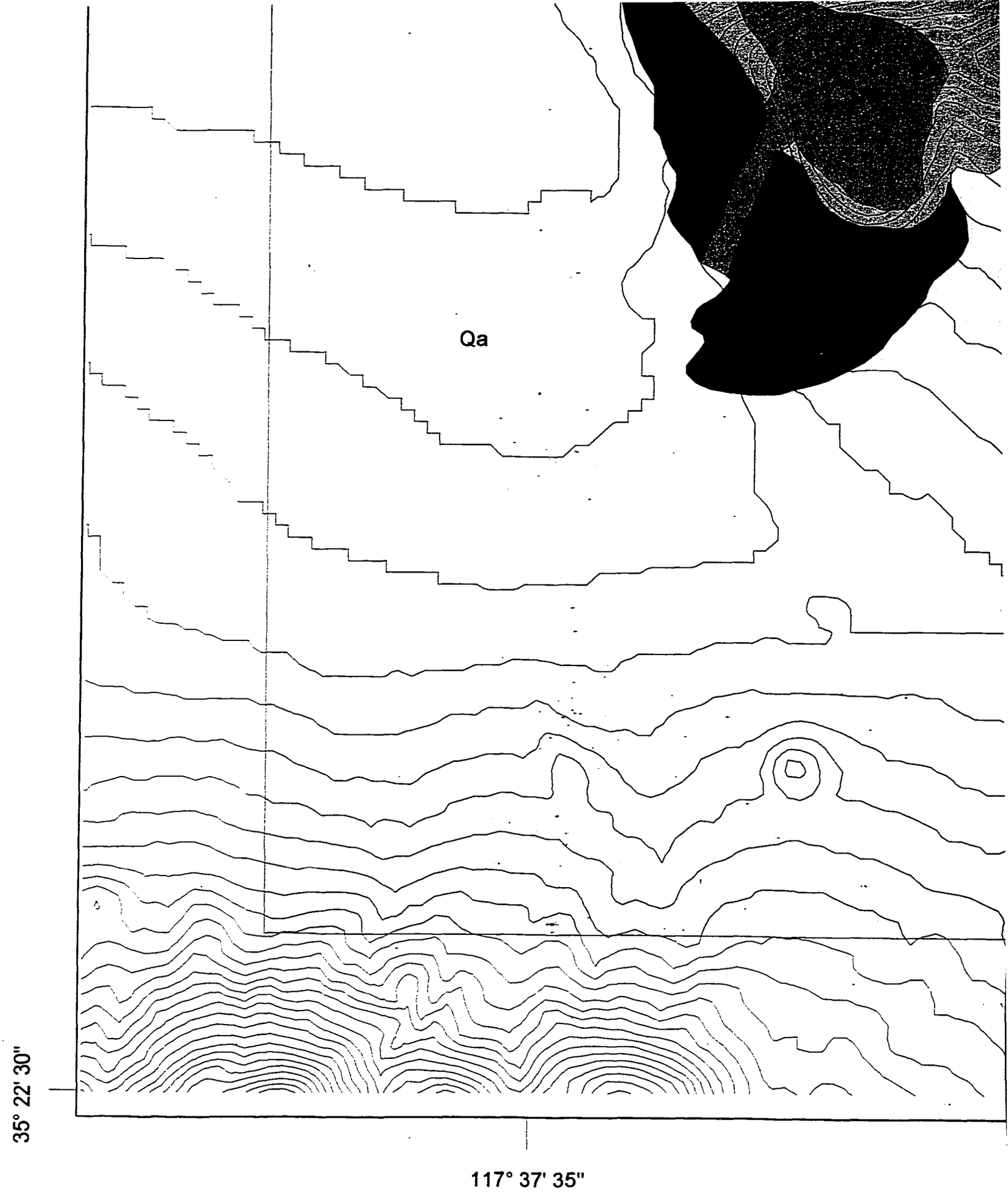

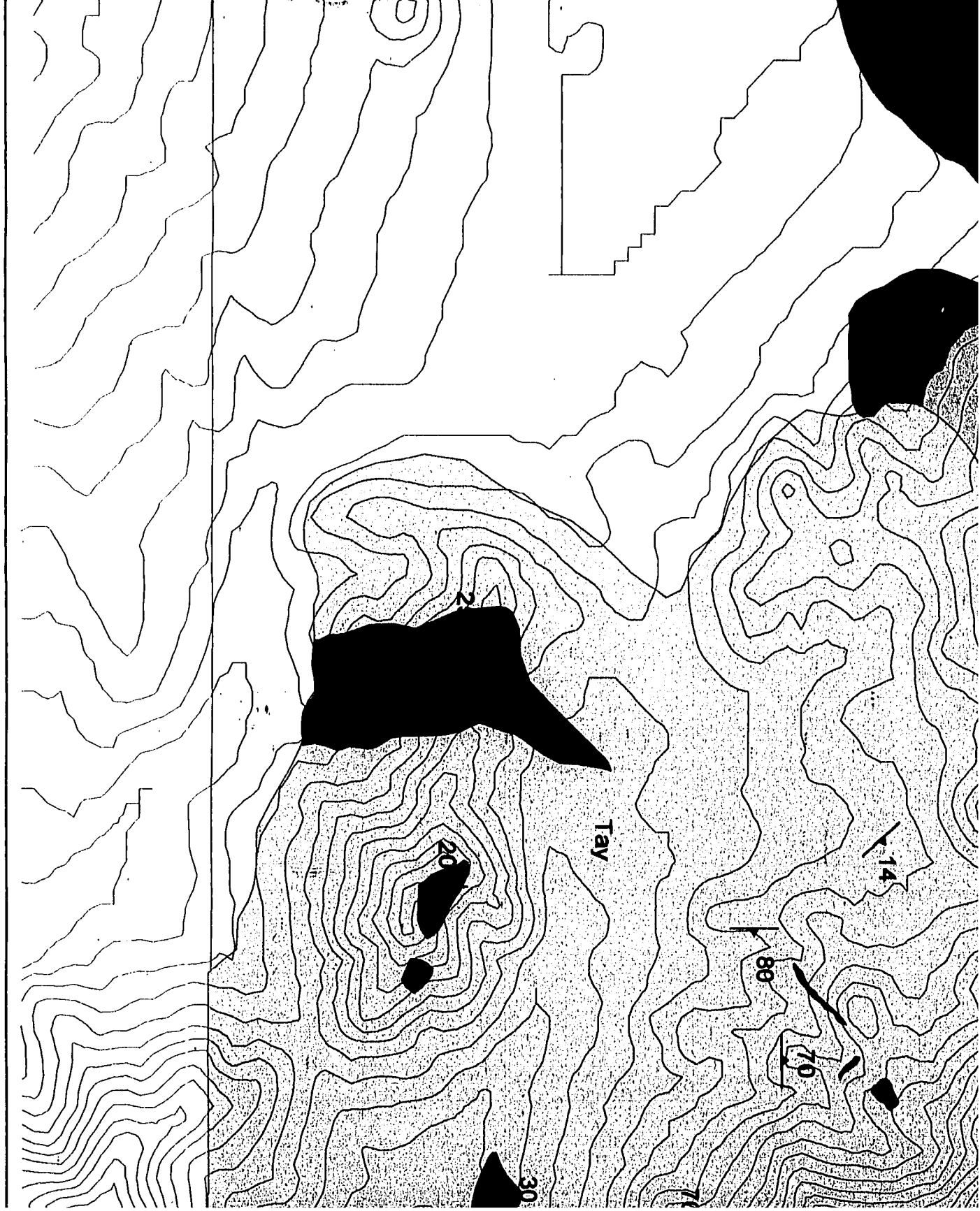

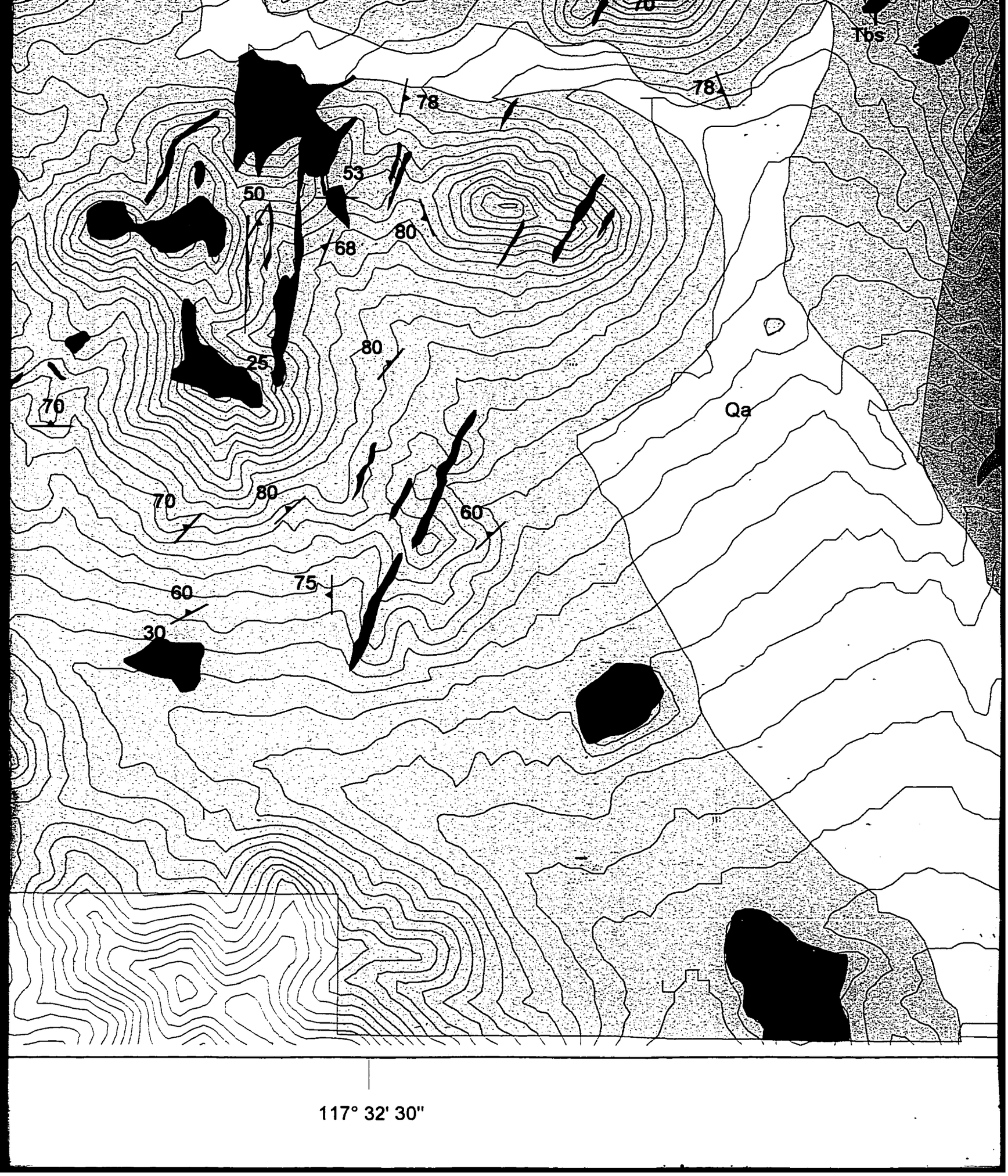

117°

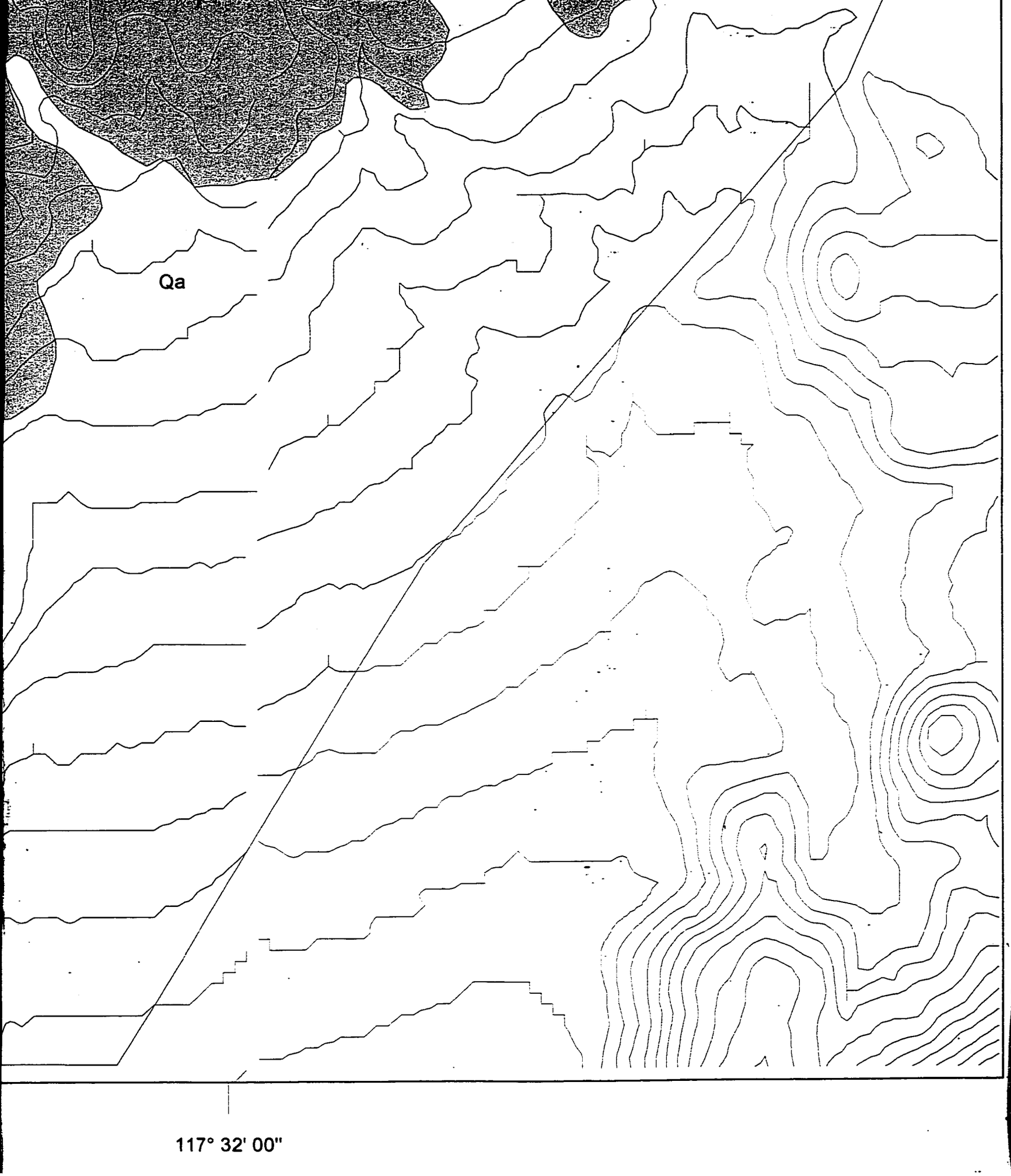

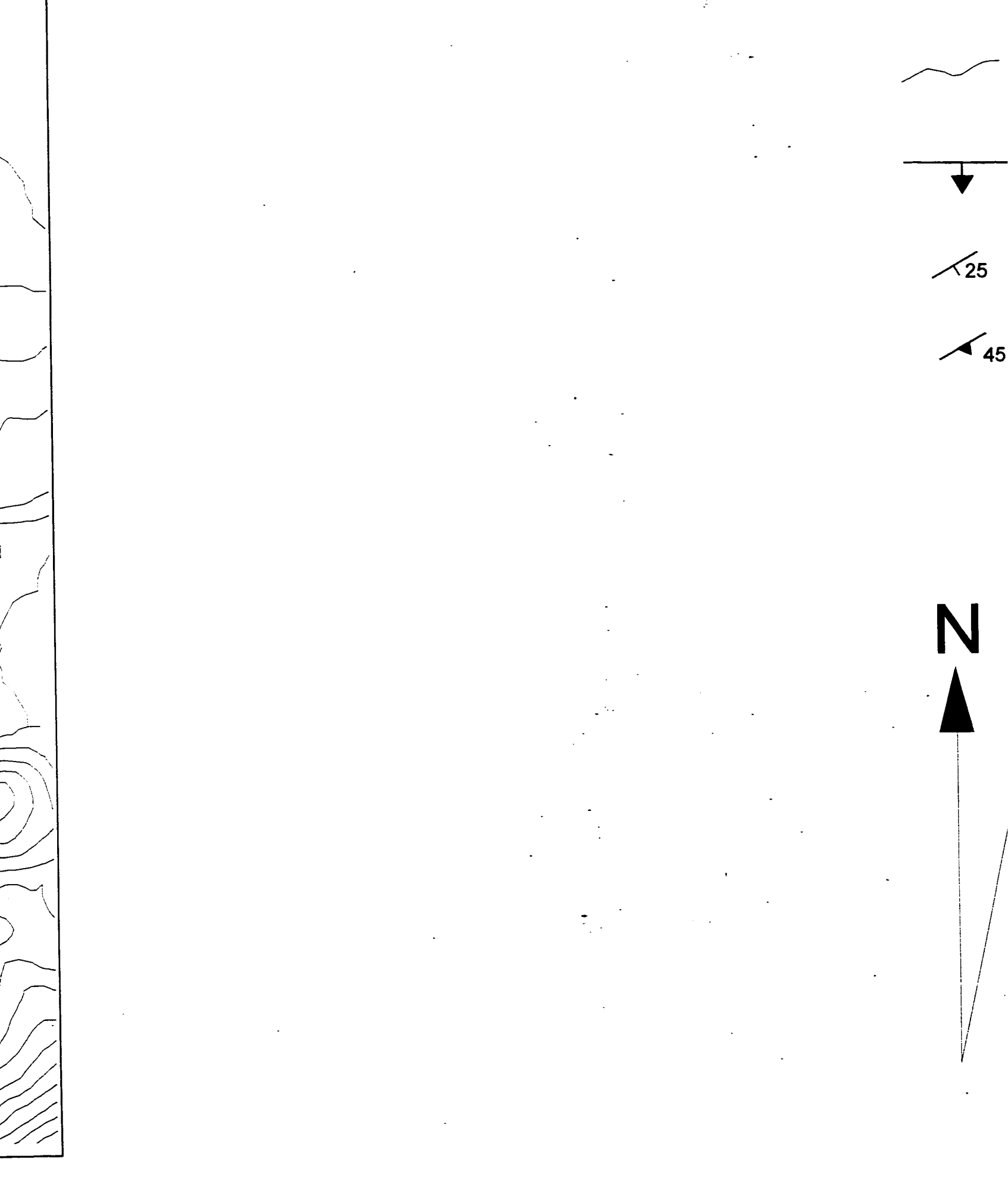

intrusive rocks, sandstone is brick red in color.

Contact

Normal Fault

Arrow on downthrown side.

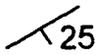

Strike and dip of beds

Strike and dip of flow banding in domes, intrusions and flows.

Cor

S

0

0

We acknowledge the U.S. Navy's Geothermal Project Office for prov the funding for this project. We especially thank Francis C. Monaste (Navy GPO) for his interest and support. We thank Alexander Sanc for his contributions to this map. The 2000 UNLV Winter field camp (Ilsa Schiefelbein (teaching assistant), Jeff Churchill, Terri Waggone Charlene Wakefield, Travis West and Becki Kubart) also contributec this map. Doug Walker (University of Kansas), John Van Hoesen, a Rik Orndorff (UNLV) helped in the production of the map.

Contour interval 20 feet.

Scale 1:12,000

0 mile 1

0 kilometer 1

Ve acknowledge the U.S. Navy's Geothermal Project Office for providing he funding for this project. We especially thank Francis C. Monastero Navy GPO) for his interest and support. We thank Alexander Sanchez or his contributions to this map. The 2000 UNLV Winter field camp lisa Schiefelbein (teaching assistant), Jeff Churchill, Terri Waggoner, Charlene Wakefield, Travis West and Becki Kubart) also contributed to his map. Doug Walker (University of Kansas), John Van Hoesen, and Rik Orndorff (UNLV) helped in the production of the map.

t.

1

September 2000

1